Hydroxamic acids interactions with metals in aqueous and micellar media: a mechanistic study of complexation reactions and metallacrown formation

Maria Rosa Beccia

UNIVERSITÀ DI PISA
Dipartimento di Chimica e Chimica Industriale

Scuola di Dottorato "Galileo Galilei"

Hydroxamic acids interactions with metals in aqueous and micellar media: a mechanistic study of complexation reactions and metallacrown formation

Ph.D. Thesis

Maria Rosa Beccia

Supervisor

Prof. Fernando Secco

External Supervisors

Prof. Begoña García Ruiz
Universidad de Burgos, Spain

Prof. Maria Amelia Santos
Universidade Técnica de Lisboa, Portugal

Discussed January 31, 2012

Acknowledgements

I would like to thank all the people that have supported me during the last three years as a Ph.D. student and without whom all this work would not have been possible.

My deepest gratitude is to my supervisor, Prof. Fernando Secco, whose advice, support and patience have been fundamental for the completion of this thesis. I am grateful to him for having taught me how to do research.

Part of this thesis has been performed in collaboration with the University of Burgos (Spain), under the guidance of Prof. Begoña García Ruiz. I am deeply grateful to her for constructive and always pleasant discussions and for heartily receiving me in her laboratory, together with Prof. J. M. Leal.

I would also like to thank Prof. Marcella Venturini for her continuous encouragement and presence all along these years. This work owes her much.

I want to express my gratitude to Dr. Tarita Biver for her constant help, her continuing enthusiasm, and for her trust in my abilities, that motivated me to do this research.

I am grateful to the *Investigación Desarrollo y Innovación* Center of Burgos University, where part of the experiments was performed. In particular, I acknowledge the help and guidance of Dr. J. Delgado Tajadura in using FAB-MS and FTIR techniques.

I am also thankful to Dr. M. Tegoni, from University of Parma, for the synthesis of the (S)-α-alaninehydroxamic acid and for useful discussions on metallacrowns.

I am grateful to the members of the jury for having accepted to evaluate this work and the referees for their interest and useful comments.

Many friends have walked beside me during these years. Their support and care helped me overcome setbacks and stay focused on my work. I would especially thank Sabriye, Tommaso, Rebeca, Natalia and María, who shared with me the amazing experience of being a Ph.D. student.
To Pierre, for his presence and attentions, *un grand merci*.

Finally I want to thank my brother and my parents, who have trust in me. They have always stimulated me to stay open-minded and to do my best.

Contents

List of Schemes

List of Figures

List of Tables

Preface

This thesis is focused on the different aspects of hydroxamic acids coordination, in particular on their ability to give rise to metal complexes of different stoichiometry and geometry. An in depth analysis of the binding mechanisms is carried out with the help of complementary approaches, ranging from classical spectrophotometry to a more peculiar kinetic analysis by fast techniques.

Hydroxamic acids have a high binding affinity to a range of transition metal ions, particularly Fe(III), and are ligands ubiquitous in coordination chemistry and chemical biology. They have been widely employed as chelating agents for a long time and studies of their metal complexes still attract great attention. Since the possible biological activity of hydroxamic acids must be correlated with the formation of their metal complexes, interest in these systems has increased extensively over the past decade. Furthermore, hydroxamic acids can be used in extractive metallurgy as flotation agents, because of their ability to form very stable chelates with various metal ions. Hence, studies on hydroxamic acids metal complexes formation and dissociation reactions are object of vast interest, as they conduct to the comprehension of the involved microscopic mechanisms and to the evaluation of their physical and chemical requirements.

In this context this thesis focuses on the equilibria and mechanisms involved in this class of complexation reactions mainly in aqueous solution, but also in micellar media. Reactions of some hydroxamic acids with three relevant and common cations in biological, industrial and environmental fields are investigated. In particular, examples of three different modes of coordination of hydroxamic acids with metal ions are reported and analyzed: from mononuclear complexes (Ni(II)) to supramolecular compounds (Cu(II)), passing through a dinuclear complex (Fe(III)). The hydroxamic acids taken into account are salicylhydroxamic acid (SHA), benzohydroxamic acid (BHA) and (S)-α-alaninehydroxamic acid (Alaha).

This study is mainly based on a combination of kinetic and thermodynamic methods in order to analyze the investigated systems in different perspectives.

In this thesis a new method is developed that enables the evaluation of the separate contributions to the equilibrium and rate parameters in the aqueous and micellar phase (Nickel-SHA system). Furthermore, the formation of a dinuclear complex (M_2L) in

aqueous solution, formed by the reaction of Fe(III) with SHA, is demonstrated for the first time. Such a complex provides the rationale for the building of supramolecular structures as metallacrowns, whose self-assembly mechanism is also worked out in this thesis work, together with metallacrowns host-guest solution equilibria (Copper-Alaha and Copper-Lanthanum-Alaha systems). Special attention is also paid to the complex speciation of the Fe(III) ion in aqueous solution. In particular, the non negligible contribution of the Fe(III) trimer is proved and its structure is clarified.

This thesis, together with putting into light the richness of hydroxamic acids coordination mechanisms, reveals the importance of a complementary approach, based on both kinetics and thermodynamics, for the treatment of complex systems involved in multiple equilibria.

CHAPTER 1
Introduction

Transition metals compounds are concerned with a number of research fields with vast applications and have proven to be a nearly ideal touchstone for many of the models that have been developed to understand structure and bonding. The scope of coordination chemistry of transition metal ions is indeed very broad and interdisciplinary. Some of the important types of coordination compounds occur in biological systems (for example, heme and chlorophyll). There are also significant applications of metal complexes that involve their use as catalysts and their formation provides the basis for several techniques in analytical chemistry. Because of the relevance of this area, study of complexation reactions is essential for many related fields of chemistry.

When forming a complex, ligands selection is a critical consideration, as they influence the reactivity of the central atom, including ligand substitution rates, the reactivity of the ligands themselves and redox reactions. In the wide area of coordination chemistry, reactions of nitrogen-oxygen donor ligands (polyamines, hydrazines, hydroxylamines and their derivatives) represent an interesting section of research since the complexes formed can act as aqueous phase catalysts. Moreover, since such reactions are an archetype of metal-ligand interactions in biological systems, they are used as models for bioinorganic processes.

Hydroxamic acids represent an example of O- or N- (in the case of aminohydroxamic acids) donor chelators. These compounds, whether naturally occurring or synthetic, are an important family of organic bioligands (Kehl, 1982; Santos, 1998). Indeed, they are able to coordinate metal ions with very high affinity (Albrecht-Gary and Crumbliss, 1998). Their ability to act as metal chelators constitutes the basis of (i) their use as flotation agents in extractive metallurgy and (ii) their employment in many biological applications. Hydroxamic acids are intimately associated with the uptake or removal of iron from the body (Raymond, 1990). On top of that, in recent years it has become evident that these weak acids possess other types of biological activities (Zamora et al., 1995; Arnold et al., 1998). Their role as potent and selective inhibitors of a range of metalloenzymes is of special interest in inorganic chemistry because the biological activities of hydroxamic acids have been mainly attributed to their complexing properties toward transition-metal

ions (Marmion et al., 2004). As a result, the transition-metal complexes of hydroxamic acids are frequently used as bioinorganic model compounds to investigate enzymatic interactions and binding properties. Metal complexes of hydroxamic acids were also found to play an important role in living systems as constituents of antibiotics (Okada et al., 1988), growth factors (Burt et al., 1981), tumor inhibitors (Duan et al., 2002) and cell-division factors (Byers et al., 1967; Kurzak et al., 1992). Therefore, there is continuing interest in studying hydroxamic acids metal complexes formation and dissociation reactions, in order to develop theories about why and how these reactions occur and to examine their physical and chemical requirements.
In this context this thesis focuses on the equilibria and mechanisms involved in this class of complexation reactions, that is the detailed manner in which they proceed, with emphasis on the number and nature of the steps involved, on the depiction of each reaction intermediate, activated complex or transition state, on the derivation of thermodynamic and kinetic parameters.

In particular, a deeper look has been taken into versatility of hydroxamic acids chelation modes with metal ions. Hence, this study starts from the analysis of the mechanism of formation of a mononuclear complex (Ni(II)/Salicylhydroxamic acid), passing through investigation of a dinuclear complex (Fe(III)/Salicylhydroxamic acid), ending, finally, with the examination of the process of formation of supramolecular compounds (metallacrowns), based on hydroxamic acids metal chelation.

In the first part of this work, the influence and the catalytic effect of micellar media on hydroxamic acids complexation reactions have been investigated. Most of hydroxamic acids biological activity is related to their ability to form very stable chelates with metal ions. Furthermore, the stability and hydrophobicity of their resulting metal complexes opens prospects for using them as membrane carriers. Indeed, hydrophobic ligands, once bound to a metal, facilitate the transport of the latter across the cell membranes (Buzatu and Darie, 2003). For instance, microorganisms produce low molecular weight chelating agents, called siderophores, that incorporate a hydroxamate group and can solubilize iron from the environment by complexing and transporting it into the cells (Neilands, 1976). Thus, the knowledge of the equilibria and mechanisms of metal complexes formation and dissociation reactions in hydrophobic bulk could be, and it is, of great biological and chemical interest. Moreover, studying hydroxamic acids complexations in micellar

medium exhibits interesting applications in the field of metal extraction, as there is continuing attention in developing efficient methods for the selective separation and recovery of metal ions from wastewaters or precious metals, even at very low concentration, so that the water can be recycled and the metals reused. Among a wide number of separation methods, surfactant-based separation processes (Scamehorn et al., 1989; Gazzaz and Robinson, 2000; Tondre, 2000; Mulligan et al., 2001) have been shown to be a promising alternative in the removal of heavy metals from wastewater streams. In this context, a mechanistic study of Ni(II) interaction with salicylhydroxamic acid, SHA, (Scheme 1.1) and an investigation on the surfactant effect have been performed in this thesis work and are reported in Chapter 3.

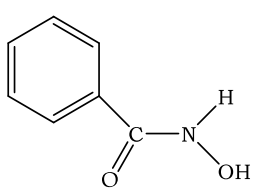

BHA

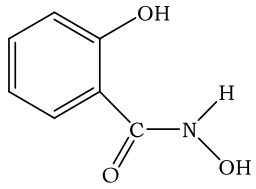

SHA

Scheme 1.1 *Representation of benzohydroxamic acid, BHA and salicylhydroxamic acid, SHA.*

The second part of this thesis is centered on the use of hydroxamic acids metal complexes as precursors of an important family of supramolecular compounds, the metallacrowns (MCs), provided with interesting recognition properties (Kurzak et al., 1991; Pecoraro et al., 1997; Gibney et al., 2002; Careri et al., 2003; Mezei et al., 2007).

Metallacrowns are self-assembled metallamacrocycles and can be considered the inorganic analogues of crown ethers (Pecoraro et al., 1997; Mezei et al., 2007). They contain a metal-ligand coordination framework, which constitutes the metallacrown scaffold and they are characterized by the presence of a core cavity, which may encapsulate a variety of cations or anions. This scaffold is conceptually obtained by replacing the methylene carbons of crown ethers with metal-heteroatom coordination units (Scheme 1.2). Since their discovery in 1989 by Pecoraro and Lah (Lah et al., 1989; Lah and Pecoraro, 1989), the chemistry of MCs largely expanded.

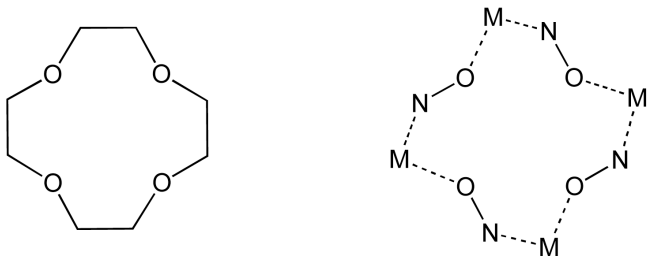

(A) (B)

Scheme 1.2 *Representations of the cavities of the 12-crown-4 (12-C-4, a) and of a 12-metallacrown-4 (12-MC-4, b).*

About twenty years after their discovery, several hundreds of metallacrowns and related host-guest adducts have been characterized, both in solid state and in solution. The number of new MCs and related metallamacrocycles grows every year, together with the number of their newly identified structural, magnetic and optical features, or host-guest capabilities. The devised applications of MCs span from the field of bioinorganic chemistry to that of functional materials for molecular recognition or new frameworks with innovative magnetic and optical properties (Mezei et al., 2007). As regards the metallacrown features of potential biological and environmental relevance, three of them are of main importance: the binding of anions with biological interest (Lim et al., 2007; Tegoni et al., 2009; Jankolovits et al., 2010), the encapsulation of metal ions relevant in diagnostic (Stemmler et al., 1999; Parac-Vogt et al., 2006; Dallavalle et al., 2010) and the encapsulation of metal ions for nuclear waste treatment (Stemmler et al., 1997; Tegoni et al., 2010). The stability of MCs and their formation mechanism are, therefore, key features that must be known for the design of MCs and metallacrown-based materials with functional applications.

In some hydroxamic acids, the presence of secondary coordinating residues at adjacent binding sites opens new perspectives in their coordination chemistry, as they are able to bind more than one metal ion. This is the case of salicylhydroxamate, α- and β-aminohydroxamates, which, in combination with suitable metal ions, are able to give rise to metallacrowns. Salicylhydroxamic acid and β-aminohydroxamic acid were extensively employed during the last decade for the synthesis of the 12-metallacrown-4 complexes (12-MC-4). Salicylhydroxamic acid (SHA), which contains both hydroxymate and phenolate donor atoms, is well suited to the synthesis of these macrocyclic compounds,

particularly in conjunction with highly charged metal ions (for instance Fe(III)). This ligand can, in principle, bind two metal ions, giving rise to a dinuclear, fully deprotonated complex (Scheme 1.3) which constitutes the repetitive unit of an SHA based metallacrown (Pecoraro et al., 1997).

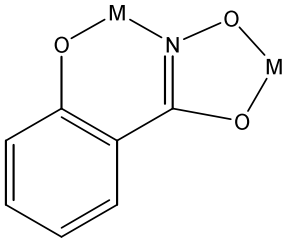

Scheme 1.3 *Representation of a dinuclear complex of salicylhydroxamic acid.*

The structure of such a precursor complex has been hypothesized by Pecoraro et al. (Pecoraro et al., 1997; Gibney et al., 2002; Mezei et al., 2007), but not found experimentally as an isolated entity. A detailed study of such a complex has been performed in this thesis work and is illustrated in Chapter 4. A study of the Fe(III) complex of the parent Benzohydroxamic acid (BHA, Scheme 1.1) is also present in this chapter, in order to compare the chelation capabilities of these ligands, which differ just in a phenol group.

On the other hand, α-aminohydroxamates were employed in the synthesis of both 12-metallacrowns-4 and 15-metallacrowns-5 (15-MC-5, Scheme 1.4), in the latter case using Cu(II) as ring metal and lanthanides(III), calcium(II) or uranyl(VI) as core metal.

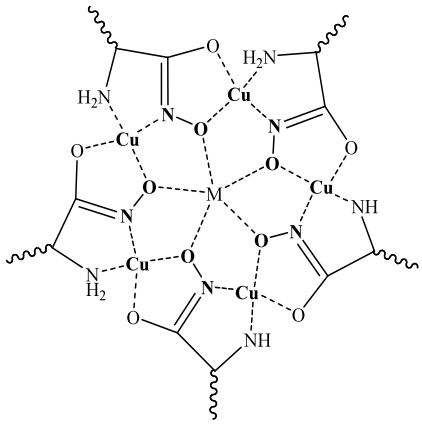

Scheme 1.4 *Representation of a 15-MC-5 of a Copper(II)/(S)-α-alaninehydroxamate. M = La(III), Ca(II) or UO_2(II). The crown is represented in bold.*

Herein the equilibria and the kinetics of the Copper(II)/(S)-α-alaninehydroxamate 12-MC-4 formation and its interaction with La(III) to give a 15-MC-5 have been investigated and, for the first time, a reaction mechanism for each of these processes is here presented (Chapter 5).

1.1 Hydroxamic acids: general properties

Hydroxamic acids may be regarded as derivatives of both hydroxylamines and carboxylic acids. They can be classified by distinguishing between primary (I) and secondary hydroxamic acids (II), that differ for the substitution of the N-hydrogen by a R' group (Scheme 1.5) (Ghosh, 1997).

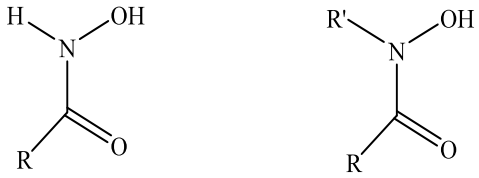

(I) (II)

Scheme 1.5 *Hydroxamic acids classification (I) primary acid (II) secondary acid.*

NMR studies (Brown et al., 1996) highlighted that these organic ligands present two stereo-isomers, *Z* and *E*, here represented in Scheme 1.5.

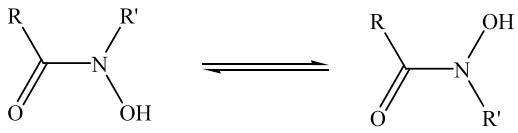

Z E

Scheme 1.6 *Z ⇆ E isomerization for hydroxamic acids.*

Transformation from Z to E conformation in N-metilacetohydroxamic acid has a rate constant of 3 s^{-1} (Birus et al., 2002); such a value, much lower than that expected for rotation around a single bond, is explained considering a partial double bond character for the hydroxamic C-N bond. In support of this hypothesis hydroxamic acids have been proved to exist in either of two tautomeric forms (Scheme 1.7).

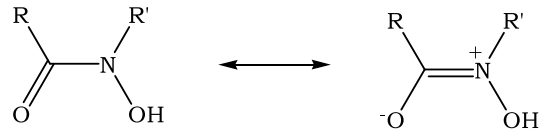

(A) (B)

Scheme 1.7 *Resonance structures for hydroxamic acids.*

Form (A) of Scheme 1.6 has been shown to be the predominant form (Exner and Kakac, 1963). It is worth to note the importance of the solvent role in promoting the E to Z conformational change. Indeed, protic solvents stabilize the Z conformation by forming intermolecular H-bonds (Scheme 1.8 A). Z conformation can also be stabilized by intramolecular H-bonds that do not involve the solvent (Scheme 1.8 B) (Brown et al., 1996).

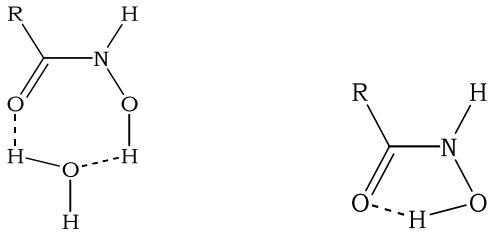

(A) (B)

Scheme 1.8 *(A) Intermolecular and (B) intramolecular H-bonds for a generic hydroxamic acid in its Z conformation.*

The questions about which of the *Z* or *E* conformation is prevailing and as whether hydroxamic acids undergo N or O deprotonation have generated wide debates and numerous papers have been published on these subjects (García et al., 2007). Whatever the preferred structure and the deprotonation process would be, it is out of question that, in order to form a mononuclear complex, hydroxamic acids should adopt the Z-conformation and the chelation process should involve O-deprotonation (Monzyk and Crumbliss, 1979).

1.1.1 Ionization of hydroxamic acids

Primary hydroxamic acids bear two potentially acidic protons respectively bound to the nitrogen and to the oxygen atom of the hydroxamate group (Scheme 1.5). Nevertheless, they behave as monoprotic acids and, as such, can dissociate to form an anionic species. Hydroxamic acids double deprotonation has never been observed even at the highest concentration of OH^- ions investigated (Exner et al., 1993). Possible structures for a hydroxamic acid anion are reported in Scheme 1.9.

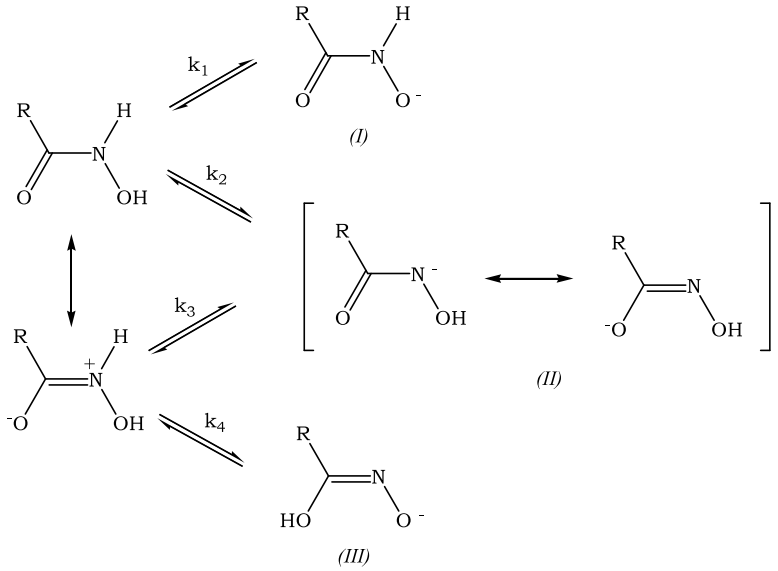

Scheme 1.9 *Possible ionization paths for hydroxamic acids.*

Exner and Kakac (Exner and Kakac, 1963) argue from spectroscopic evidence that the proton bound to the nitrogen atom is the acidic proton, and ionization gives rise to the N-anions shown in Scheme 1.9 (II). However, solvent contribution must be taken in account when determining the most stable anionic form. Recent studies have demonstrated a N-acidity in DMSO and in gas phase, and an OH^- acidity in aqueous solution. It has also been demonstrated that in the presence of mineral acids (at least 1 M) hydroxamic acids are able to bind a proton, assuming a base character (García et al., 2001). Possible proton binding sites of these molecules are shown in Scheme 1.10.

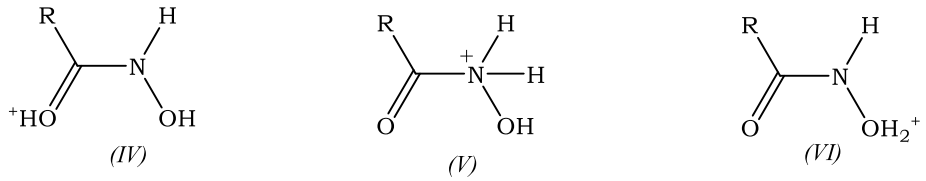

Scheme 1.10 *Possible protonation derivatives of primary hydroxamic acids.*

Experimental results show that both in solution and in the gas phase the carbonylic site is the favorite protonation centre, even if theoretical calculations have demonstrated that carbonyl oxygen and nitrogen are equally feasible to protonation (García et al., 2001).

1.1.2 Metal complexation of hydroxamic acids

Hydroxamic acid complexation reactions have been studied both in solution and in the solid state, initially with Fe(III) because of its particular relevance in the biological field, then with other metal ions as Co(II), Ni(II), Zn(II), and Cu(II). According to previous studies on metal complexation of hydroxamic acids, these ligands seemed to be able to bind just one metal ion. The great majority of the investigated systems displayed a coordination of the metal ion to the carbonylic oxygen and to the NH-OH group (Lindner and Goettlicher, 1969). {O,O} coordination, confirmed by X-ray crystallography (Brown et al., 1996) occurs via the OH group deprotonation and the consequent metal chelation by the carbonyl oxygen atom (Scheme 1.11).

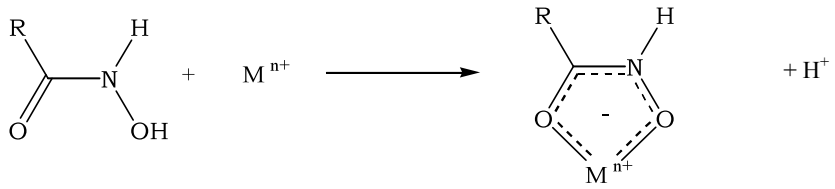

Scheme 1.11 *Metal ion (M^{n+}) {O,O} coordination by a generic hydroxamic acid.*

On the other hand, for aminohydroxamic acids ((NRR')CONHOH), a {N,O} coordination that involves the NH group deprotonation has been observed (Dobosz et al., 1999; Farkas et al., 2000) (Scheme 1.12).

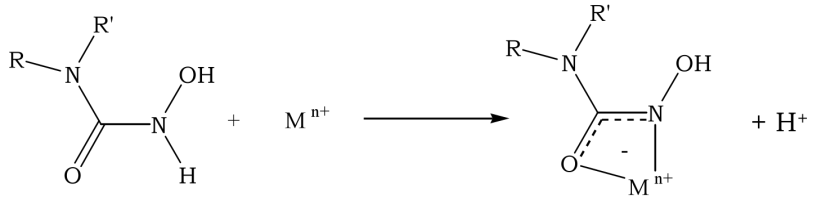

Scheme 1.12 *Metal ion (M^{n+}) {N,O} coordination by a generic aminohydroxamic acid.*

1.2 Complexation mechanism

It seems to be useful to summarize in this introduction the main aspects of the mechanism of metal ion complexation because of their relevance with respect to the investigated systems.

The general features of the mechanism of metal complexes formation in solution have been known since the 1960s, when Eigen and Tamm realized that aqueous solutions of

magnesium sulphate absorb ultrasound in an anomalous manner (Eigen and Tamm, 1962). They found out that such behavior is due to the formation of a complex between Mg^{2+} and SO_4^{2-}. Moreover the two bands of the ultrasound absorption spectrum indicate that the interaction between magnesium and sulphate ions is a two-step process (Figure 1.1).

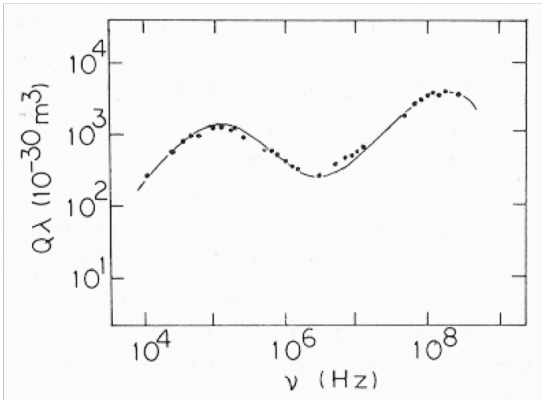

Figure 1.1 *Ultrasound spectrum of $MgSO_4$ in aqueous solution; $[MgSO_4] = 10^{-1} \div 10^{-2}$ M.*

Subsequent studies on the first series transition metal sulphates (Bechtler et al., 1970) showed that the peak at highest frequency (5×10^8 Hertz) is metal ion independent, while the peak at lowest frequency changes with metal ions going from 10^4 Hertz for Ni^{2+} to 7.5×10^6 Hertz for Mn^{2+} (Figure 1.2).

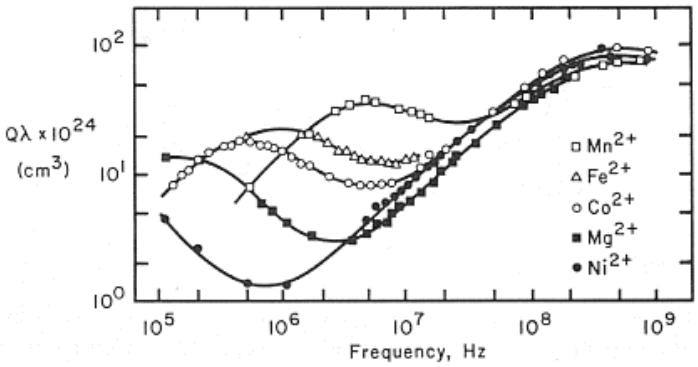

Figure 1.2 *Ultrasound spectrum of some divalent metal sulphates (0.5 M) in aqueous solution.*

These results supported the mechanism proposed by Eigen and Tamm (1962) which considers a first step, diffusion controlled, with the formation of an electrostatic ion pair

(outer sphere complex) between the metal and the ligand and a subsequent step where a water molecule leaves the coordination sphere and is replaced by a ligand one (Scheme 1.13). This second step is slower, its rate depending on the energy of the metal-ligand bond.

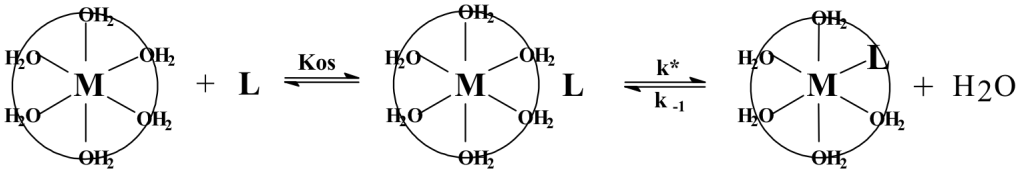

Scheme 1.13 *Eigen and Tamm mechanism.*

The complexation reaction between a metal ion and a bidentate ligand involves a three-step mechanism. Indeed, after the formation of the outer and inner-sphere complexes (first and second step), the final step is the loss of a second water molecule coupled with ring closure to give a bidentate complex (Scheme 1.14). This mechanism is generally referred to as the Eigen–Wilkins mechanism (Eigen and Wilkins, 1965). The rate-determining step is the loss of the first water molecule with the formation of the monodentate complex, while ring closure is most commonly rapid (Wilkins, 1964).

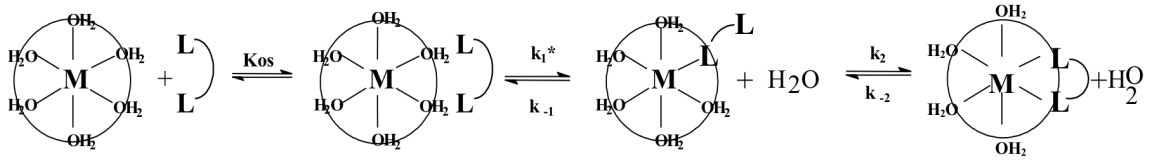

Scheme 1.14 *Eigen-Wilkins mechanism.*

1.2.1 The "ion pair"

The ion pair concept has been introduced by Bjerrum (1926) to overcome the deficiency of Debye-Huckel theory in explaining the thermodynamic behaviour of high charged ions in solution. An ion pair indicates a pair of oppositely charged ions held together by Coulomb attraction without formation of a covalent bond, which experimentally behaves as one unit. It can be identified as a couple of ions near enough to be able to differentiate their physical-chemical properties from those of independent solvated ions. The ion pair concentration is related to the free ions concentrations by the equilibrium constant K_{OS} (Scheme 1.13), which can be adequately described by the Fuoss equation (Connick and

Fiat, 1963; Fuoss, 1974)

$$K_{OS} = N\frac{4\pi}{3000}a^3 e^{-\frac{U(a)}{kT}} e^{\frac{U(a)\chi\cdot a}{1+\chi\cdot a}} \qquad (1.1)$$

where $U(a) = Z_M Z_L e_0^2 / aD$ is the electrostatic energy between M (of charge Z_M) and L (of charge Z_L) and the other parameters of equation (1.1) are defined as:

$\chi = \left(\frac{8\pi N e_0^2}{1000DkT}\right)^{1/2} (I)^{1/2}$ = reciprocal of the thickness of the ionic cloud defined on the basis of Debye-Hückel theory

e_0 = electron charge

a = distance of closest approach between ions in the ion pair (around 5 Å)

D = dielectric constant of the solvent

k = Boltzmann constant

T = temperature (e_0^2/DkT=7.15×10^{-8}cm at 25°C)

N = Avogadro number

I = ionic strength of the solution

The value of parameter "*a* " is unknown. However, comparison between the K_{OS} values of alkaline earth metals sulphates obtained from ultrasound spectrum and the values calculated with equation (1.1), let "*a* " be estimated as 5×10^{-8} cm.

1.2.2 The "solvent exchange"

The second step of Scheme 1.13 clarifies the fundamental role played by the solvent. Indeed, in this slow step the breaking of the M-OH_2 bond occurs and, therefore, this stage must have many characteristics in common with the solvent exchange process in the metal coordination sphere. Scheme 1.15 represents the substitution of a certain coordinated water molecule, H_2O*, with a non-coordinated one. The kinetic constant of this process, k_{H2O}, can be determined by a nuclear magnetic resonance technique (Connick and Fiat, 1963) and its value, strongly dependent on the nature of the cation, indicates its lability.

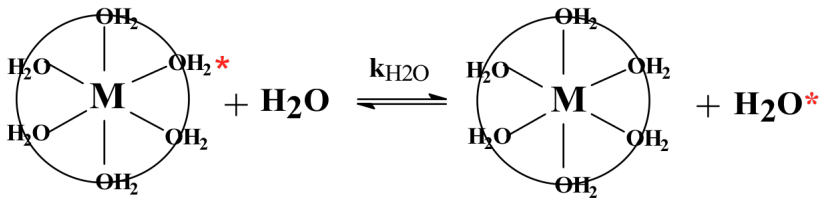

Scheme 1.15 *The solvent exchange process in the metal ion coordination sphere.*

Figure 1.3 shows the variation of the logarithm of k_{H2O} with the number of d electrons in different metal ions (Helm and Merbach, 1999). It can be clearly seen that Cr^{3+} and Co^{3+} ions are the most inert, while ions Cr^{2+} and Cu^{2+} are the most reactive.

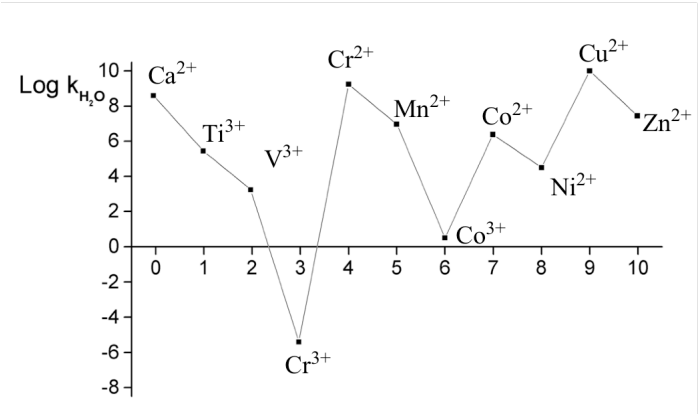

Figure 1.3 *Dependence of the rate constant of the H_2O exchange process on the number of d electrons in different cations (Helm and Merbach, 1999).*

It has been experimentally observed that, especially in the complexation of bivalent metal ions the k* value associated to the process in Scheme 1.13 coincides, within reasonable limits, with the k_{H2O} value associated with the reaction in Scheme 1.15.

1.2.3 Activation mechanisms

The pioneer kinetic studies on complexation reactions were carried out with the previously mentioned method based on ultrasound absorption, the use of which is, however, limited by high cost and difficulty of performance. Afterwards the most widely used techniques in the study of complexation reactions became stopped-flow, T-jump and P-jump (Bernasconi, 1976). Their response time is not short enough to allow the measurement of the first of the two stages in Scheme 1.13. Therefore the kinetics of the complex formation

between a metal ion and a monodentated ligand will be highlighted by a single signal, generally exponential, whose time constant, $1/\tau$, will depend on the reagent concentrations through the relation

$$\frac{1}{\tau} = \frac{K_{OS} k^{*} C_M}{1 + K_{OS} C_M} + k_{-1} \qquad (1.2)$$

which is valid in pseudo first order conditions, i.e. in excess of metal compared to the ligand ($C_M >> C_L$). If it is not possible with the above-mentioned techniques to evaluate the rate constants of the formation stage of the outer sphere complex formation, it is however possible to estimate its equilibrium constant K_{OS} through equation (1.2). By plotting $1/\tau$ against the metal concentrations, C_M, a curve that asymptotically tends to the value (k^*+k_{-1}) is obtained. The intercept on the Y axis provides k_{-1}, while the slope of the initial line is equal to k^*K_{OS}.

For conditions in which $K_{OS}C_M << 1$, equation (1.2) can be reduced to the simpler form:

$$\frac{1}{\tau} = K_{OS} k^{*} C_M + k_{-1} \qquad (1.3)$$

In this case the diagrams of $1/\tau$ in function of C_M are linear with an intercept of k_{-1} and a slope of $K_{OS}k^*$, which will be indicated as k. Therefore, for systems in which the following relation is valid

$$k = K_{OS} k^{*} \qquad (1.4)$$

it is not possible to experimentally determine k^* separately from K_{OS}. However K_{OS} can still be calculated through equation (1.1) and the value of this constant can be used to determine k^* using equation (1.4). The k^* value, determined as explained above, for complexation reactions of a given cation with different ligands is of great help in assigning the complexation mechanism of that cation. Scheme 1.13 indicates that the formation of the outer-sphere ionic pair is a general phenomenon which always occurs whenever two particles of opposite charge are found close enough, and is, therefore, independent of both the nature of the particles and the mechanism of the next step of interconversion of the outer-sphere complex into the correspondent inner-sphere complex. The activation

mechanisms of this second stage can be classified into dissociative or associative. The occurrence of one or the other activation types depends essentially on the metal. It can however happen that the same metal can shift from a dissociative to an associative activation mechanism by changing the ligand dimensions, but this possibility seldom occurs (Burgess, 1979).

A more careful examination of the kinetic behaviour of metal ions towards complexation reveals that a series of intermediate cases exist between a purely dissociative and a purely associative mechanism, exemplified in Scheme 1.16. This shows the transition from the pure dissociative mechanism (D), where the coordination sphere of the metal in the transition state contains only five solvent molecules, to the pure associative mechanism (A), in which the transition state coordination sphere holds as much as seven molecules. If the k* value is nearly the same, independently from the employed ligand, and also coincides with the rate constant of the solvent exchange process (equation (1.5))

$$k^* = k_{H2O} \qquad (1.5)$$

then it can be deduced that the energy of the second step in Scheme 1.13 is essentially held in the process of weakening of the M-OH_2 bond, which takes one of the coordinated H_2O groups far from the coordination sphere of the ionic pair before the ligand begins to enter. An empty site thus forms in the coordination sphere, which is then occupied by the ligand through a dissociative complexation mechanism.

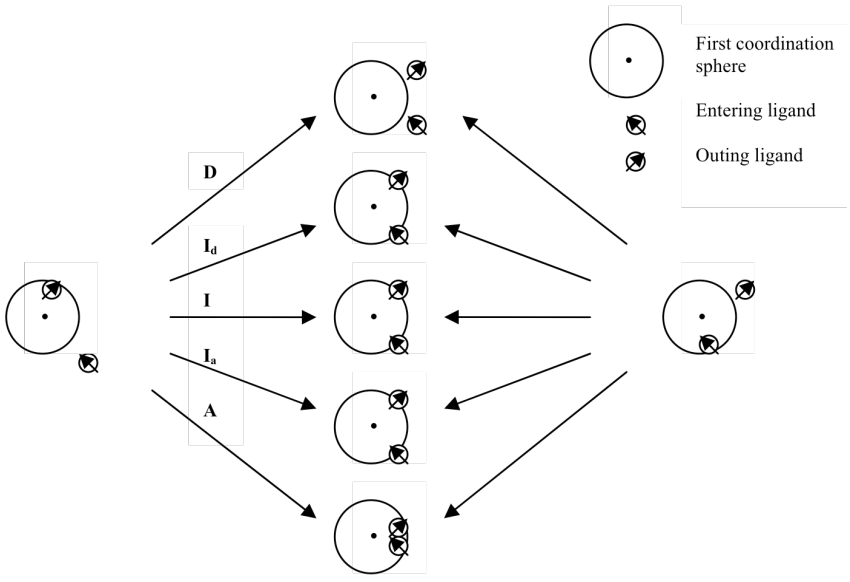

Scheme 1.16 *Possible formation mechanisms of a metal complex.*

In some rare cases this mechanism bears a completely dissociative character (D). If the H_2O molecule has not entirely left the metallic centre as the ligand starts entering the coordination sphere, the activation mode still shows a dissociative character, although at a lesser degree than the D mechanism. This activation mode, much more frequently, is indicated by the initials I_d (dissociative interchange) and the relation (1.5) can be applied to it as well. The activation mode I_a (associative interchange), is characterized by a transition state, more complex than the ionic pair state, in which the ligand is already quite into the metal coordination sphere, while the water has slightly moved out. Finally, the pure associative state A shows a transition state with six water and one ligand molecule completely inside the metal coordination sphere, but this is pretty rare as well. The concerted mechanism, I, is very interesting, its characteristics being intermediate between those of the I_d and I_a activation modes. Complex formation at In(III) displays these peculiarities (Ricciu et al., 2000). Scheme 1.16 clearly shows that the volume of the transition state decreases while going from dissociative to associative mechanisms, therefore the measurement of the activation volumes provides an important criterion, in addition to the one stated by the relation (1.5), to correctly assign the reaction mechanism.

CHAPTER 2

Materials and methods

2.1 Chemicals

All chemicals were analytical grade (Sigma Aldrich), exception made for (S)-α-alaninehydroxamic acid (Alaha), that was obtained within a collaboration with the University of Parma where it has been synthesized as reported by Smissman and Warner (Smissman and Warner, 1972).

Hydroxamic acids (SHA, BHA and Alaha) solutions were prepared by weighing the appropriate amounts of solid reagents (purity 99%) and dissolving them in doubly distilled water. These solutions were used within 3–4 days.

Iron perchlorate, $Fe(ClO_4)_3 \cdot 6H_2O$, was dissolved in perchloric acid to prevent the Fe(III) hydroxide precipitation. The Fe(III) concentration was measured by titrations with EDTA, pH between 2 and 3 for HCl, using KSCN as indicator. Concentration of the $HClO_4$ present in the solution was determined using a cationic exchange resin, titrating the eluate with NaOH (indicator phenophtaleine). Titrated H^+ moles corresponds to $HClO_4$ moles togheter with three times the Fe(III) moles.

Nickel perchlorate, $Ni(ClO_4)_2 \cdot 6H_2O$, was dissolved in perchloric acid too. Ni(II) concentration was measured by titration with EDTA at pH = 10 using murexide as an indicator.

Stock solutions of $CuCl_2 \cdot H_2O$ and $LaCl_3$ were prepared dissolving the analytical grade salts in pure water. Cu(II) and La(III) concentrations were measured by titration with EDTA.

Acetic buffer solution (pH = 4.75, 0.1 M) was prepared by weighing the appropriate amount of sodium acetate ($CH_3COONa \cdot 3H_2O$, 99.5%) and dissolving it in acetic acid (CH_3COOH, 99.5%).

Sodium Cacodylate [$(CH_3)2AsOONa$] buffer solution was prepared by weighing the solid reagent, of analytical grade, and dissolving it in pure water.

The anionic surfactant sodium-dodecyl sulphate (SDS), obtained from Sigma Aldrich (>99% pure), was employed without further purification. The c.m.c. of this surfactant is evaluated to be 8×10^{-3} M (Nakahara et al., 2005).

Perchloric acid (ca. 2 M) and sodium perchlorate or hydrocloric acid (ca. 0.1 M) and potassium chloride were used to attain the desired medium acidity and ionic strength.

2.2 Methods

2.2.1 UV-VIS Spectrophotometry

A Perkin-Elmer Lambda 35 spectrophotometer was used to record absorption spectra, to perform spectrophotometric titration and to follow slow reactions kinetics. The apparatus is equipped with jacketed cell holders, with temperature control within ±0.1°C (). Titrations were carried out at fixed wavelenght, by addition of increasing amounts of metal to the spectrophotometric cell conteining the ligand solution. When the metal was absorbing at the wavelenght chosen for the titration, the latter was carried out in the difference mode, i.e. adding the same amounts of the metal ion solution to both reference and measuring cells.

Kinetics of slow reactions were performed measuring the sample absorbance changes with time at fixed wavelenght. Temperature dependence of 12-MC-4 stability was analyzed recording absorption spectra from 20°C to 90°C, with a temperature increase rate of 0.5°C/min and an hold time of 2 min.

2.2.2 FTIR Spectrophotometry

Complexes obtained from reactions of Fe(III) with BHA and SHA were analyzed by attenuated total reflectance FTIR (FTIR-ATR) in solution using a Nexus 470 FTIR spectrophotometer from Nicolet Instrument Corporation. FTIR-ATR exploits the attenuation of light reflected internally in a germanium non-absorbing prism, due to energy absorption of an analyte in contact with the reflecting surface. To further enhance the attenuation, and consequently the absorption spectra, the prism has an oblong and trapezoidal shape to allow multiple internal reflections (Figure 2.1). The penetration depth of the absorption is in the magnitude of a few micrometers and is a function of the wavelength, the angle of the incident beam and the refractive index of both the ATR prism and sample. IR spectra of the two free ligands and of mixtures metal-ligand in different stoichiometric ratios were recorded. Contributes of water, reagents and background were subtracted from the raw spectra.

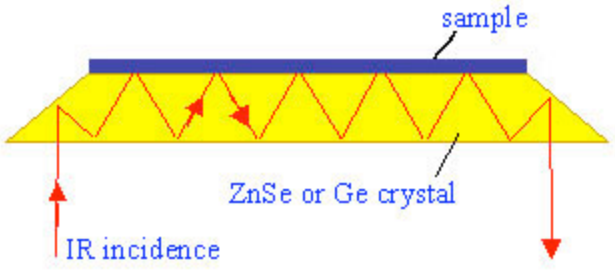

Figure 2.1 *IR radiation path into a cristal and a sample during a FTIR-ATR experiment.*

2.2.3 FAB-Mass Spectrometry

Fast Atom Bombardment (FAB)-Mass spectrometry measurements of 12-MC-4 and 15-MC-5 were recorded on a VG AutoSpec apparatus, using an ionization liquid secondary ion mass spectrometer ($LSMIS^+$), Cs^+ as bombarding ions and thioglycerol as the matrix. Although fragmentation is possible as a result of FAB-MS experimental conditions, it is less common and yields fragment ions peaks of lower intensity than Electron Ionization. Thus the obtained ion peaks are typically adducts of the species present in the initial solution formed with cations (i.e. H^+ or Na^+).

2.2.4 Stopped-Flow

The kinetic experiments for the three analyzed systems were performed on a stopped flow apparatus, by monitoring absorbance changes with time, after the fast mixing of the reactants. Small volumes of solutions are rapidly driven from syringes into a high efficiency mixer to initiate a fast reaction. The resultant reaction volume then displaces the contents of an observation cell thus filling it with freshly mixed reagents. The solution entering the flow cell is only a few milliseconds old. The age of this reaction mixture is also known as the dead time of the stopped-flow system. As the solution fills the stopping syringe, the plunger hits a block, causing the flow to be stopped instantaneously. Figure 2.2 shows a schematic representation of the instrument. The absorbance of the product of the reaction is measured in the time. As result a voltage variation, proportional to the absorbance at one chosen wavelenght, is obtained. The apparatus uses a HI-TECH KinetAsyst SF-61SX2 mixing unit, connected to the spectrophotometric line by two optical guides. Ultraviolet radiation, produced by a Hamamatsu L248102 Xenon 'quiet' lamp, or visible radiation produced by a green laser (λ_{em} = 648 nm) is passed through a

Baush and Lomb 338875 high intensity monochromator and then split into two beams. The reference beam is directly sent to a 1P28 photomultiplier, whereas the measuring beam is sent to the observation chamber through an optical quartz guide, to a second 1P28 photomultiplier. The outputs of the two photomultipliers are balanced before each shot. The resulting reaction transient is stored in a Tektronix digital oscilloscope. The kinetic curves were evaluated with the fitting package by Jandell (AISN software). Each shot was repeated at least 10 times and the resulting kinetic curves were averaged via an accumulation procedure. The given amplitudes, rate constants and initial rate are average values.

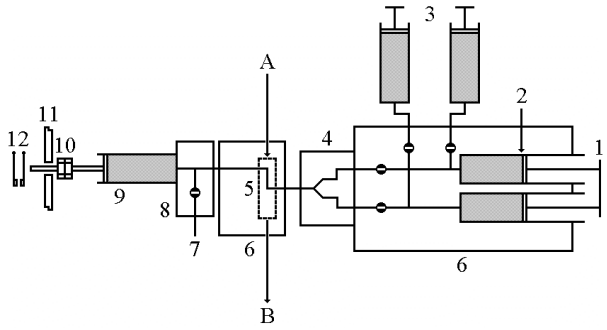

Figure 2.2 *Internal scheme of a stopped flow apparatus. A)Light input from monochromator and mirror box B)Light output to photomultiplier tube. 1)plunger 2)syringes 3)reservoir syringes 4)mixing chamber 5)cell 6)thermostating block 7)drain tube 8)drain valve block 9)stop syringe 10)adjustable stop nuts 11)mechanical stop 12)leaf-type trigger switch.*

2.2.5 Calorimetry

Cu(II)/(S)-α-Alaha system and complexes obtained from their reaction were analyzed by mean of Differential Scanning Calorimetry (DSC) and Isothermal Titrating Calorimetry (ITC). The reference and sample solutions have been carefully degassed under vacuum for 15 min while stirring prior to use.

All differential scanning calorimetry measurements have been performed with a TA Instruments nano DSC. A 0.30 mL sample containing both metal and ligand ($[CuCl_2]= 1\times10^{-2}$ M, metal to ligand ratio = 1.25, pH = 4.5, I = 0.1 M (KCl)) was placed in the sample capillary cell and the solvent, in the same conditions, was placed in the reference capillary cell. Calorimetric measurements have been performed at P = 1.5 atm and scan rate 1°C/min, in in the pH range between 3 and 8, where not only the 12-MC-4 is present in solution (Careri et al., 2003). In this way it has been possible to assign to each peak the

correspondent transition.

Isothermal titrating calorimetry experiments were performed using a TA Instruments nano ITC device at 25 °C. The instrument consists of two identical cells, one for the sample and the other for the reference. In a typical titration, with stirring at 300 rpm, 1 μL 170 mmol aqueous solution of (S)-α-Alaha taken in the syringe was injected in equal intervals of 300 s to the $CuCl_2$ aqueous solution (33 mmol) which was taken in the sample cell with 1.0 mL capacity. During the whole titration 50 μL of (S)-α-Alaha solution were added to $CuCl_2$ solution. The reference cell of the microcalorimeter was filled with ultrapure water and both the cells were maintained at the same temperature. When (S)-α-Alaha solution was injected to $CuCl_2$, the difference in heat needed to keep both the sample cell and reference cell at the same temperature was monitored. To calibrate the heat effects of dilution and mixing, the control experiments were performed by injecting the (S)-α-Alaha solution into a solvent solution under the same conditions and subtracted from the experimental data. The heat released by the dilution of $CuCl_2$ was considered negligible.

All thermodynamic analyses were evaluated with the fitting package Nano Analyze (Nano DSC program group).

2.2.6 Ultrafiltration

For the Ni(II)/SHA system in the presence of SDS the amounts of ligand in the aqueous and micellar phases were evaluated by means of ultrafiltration technique.

The ultrafiltration experiments were carried out in a batch stirred cell (Amicon, model 8050) with a capacity of 50 ml and an effective membrane area of 13.4 cm^2. (Figure 2.3) Ultrafiltration was performed as follows: 10 ml of solution containing the ligand and surfactant micelles was passed through the ultrafiltration cell under a 2 bar nitrogen pressure. The ligand adsorbed on the micelles is retained in the retentate (2 ml), while the aqueous phase containing uncomplexed ions passes through the membrane in the permeate (8 ml). Shortly after the conclusion of the procedure the ultrafiltration membranes were flushed with deionized water and if necessary they were regenerated according to the method recommended by Millipore (Amicon).

The amount of ligand recovered by ultrafiltration was assessed through UV-VIS spectroscopy.

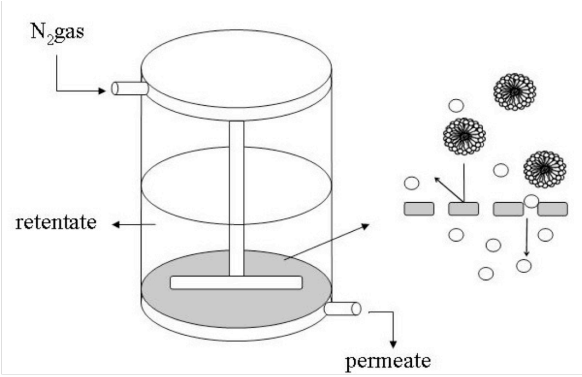

Figure 2.3 *Schematic view of an ultrafiltration cell.*

2.2.7 pH measurements

The hydrogen ion concentrations of the aqueous solutions were determined by pH measurements performed by a Metrohm 713 instrument. A combined glass electrode was used, after the usual KCl bridge was replaced by 3 M NaCl, to avoid precipitation of $KClO_4$. The electrode was calibrated by using $HClO_4$ or HCl solutions of known concentrations. This procedure enables conversion of the pH-meter output into $-\log[H^+]$ values.

CHAPTER 3

Ni(II) complexation by salicylhydroxamic acid in SDS.

Hydroxamic acids are often involved in metal ions transport through cell membranes (Neilands, 1976), due to their ability to form strong metal complexes and their partial hydrophobicity that allows them to pass through lipophilic mediums. In order to build up artificial systems able to mime hydrophobic membranes, micelle/water systems prove to be considerably useful. Actually, surfactants micelles form a hydrophobic pseudophase in water solution, which can have an effect on reactions overall rate and equilibrium constants. It was already demonstrated that hydrolysis processes of amphiphilic hydroxamate ions are influenced by the presence of surfactants in water (Ghosh, 1997; Ghosh and Tiwary, 2003; Ferrit et al., 2007). On the other hand, their complexation reactions in micellar solutions have never been investigated. The studyof metal binding in micelle media is interesting from the mechanistic standpoint (Monteleone et al., 2004) and in order to explore the conditions for the application of complex formation reactions in metal extraction and recovery processs (Gosh, 2004). There are some significant advantages in using a micellar solution over an organic solvent as hydrophobic bulk able to extract chemical species: micelles are distributed uniformly through the medium as nano-sized aggregates and no stirring of the medium is necessary, since the system is a single homogeneous macrophase. Secondly, in the presence of a negatively charged surface, such as is provided by the OSO_3– head groups of sodium dodecylsulfate (SDS), the metal ion will be strongly electrostatically attracted to the micelle surface. In addition, micelles are able to solubilize ligands with hydrophobic residues that can react with metal ions present on the surface where the reaction will be facilitated as the result of a local concentration effect on both reactants. Moreover, a metal complex with a hydrophobic ligand, once diffused toward a micelle, will be retained on it by hydrophobic forces.

This chapter reports on kinetics and equilibria of the binding of Ni(II) to salicylhydroxamic acid (SHA) in aqueous solution containing micelles of sodium dodecyl sulphate (SDS). Such a study is aimed to enlighten the complexation mechanism and the thermodynamic and kinetic parameters of this reaction and to evaluate the possibility of using SHA as an extraction agent.

3.1 Surfactants

A surfactant is a substance that reduces the surface tension of the medium in which it is dissolved. By lowering the interfacial tension between two media or interfaces the surfactant plays a key role in the removal and suspension of dirt. A surfactant molecule has a hydrophilic head and a long hydrophobic tail and for this reason it is often regarded as an amphiphilic molecule (Figure 3.1). Many of the physicochemical properties of these molecules in solution stem from this ambivalency. However, small changes in the architecture of the surfactants, which alter the balance between hydrophobic and hydrophilic properties, can result in dramatic changes in their behaviour in solution.

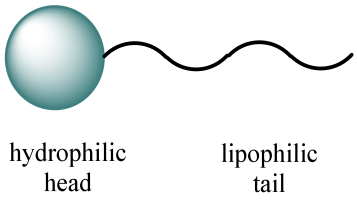

Figure 3.1 *Structure of a generic surfactant*

Surfactants can be categorized, according to the charge present in the hydrophilic portion of the molecule after dissociation in aqueous solution, in four main types: anionic, cationic, non-ionic, amphoteric/zwitterionic.

The main properties of surfactants concern adsorption and self-assembly processes. Surfactant molecules usually locate themselves at the interface between an oil and an aqueous phase or an aqueous and an air phase. This molecular property leads to the macroscopic properties of wetting, foaming, detergency and emulsion formation. Moreover, surfactant molecules tend to organise themselves into extended structures in water, giving rise to micelles, large aggregates, which, depending on the specific surfactant and solution conditions, can adopt a variety of shapes.

3.2 Micelles

A spherical micelle is the simplest surfactant aggregate formed in aqueous solution. Micelles are small aggregates with a size of few nanometers. They are formed in such a way that their hydrophilic head groups are exposed to the water medium and their hydrophobic tails form a water free core. The headgroups of the micelle are extensively hydrated. For ionic micelles, a large fraction of the counterions are located in the vicinity

of the headgroups. These counterions normally retain their first hydration shell. The part of the surfactant that contains the headgroups and a variable fraction of the counterions is called the Stern region. This region has an important role in solubilisation.

Micelle solutions can solubilise insoluble organic material by incorporating it either at the surface or in the inner core. This properties gives micellar solutions an important role in chemistry in terms of solubilising material, catalysing reactions and extractant (Engberts, 1992; Jones, 1999; Stalikas, 2002). Micelles are often depicted as static structures of orientated surfactant molecules, however they are very dynamic aggregates. Actually, they breakdown and reform rather rapidly (Lang et al., 1975; Aniansson et al., 1976; Tondre and Zana, 1978). Due to this dynamic character, the size and shape of micelles are subject to appreciable structural fluctuations. The number of surfactant monomers in a micelle is defined "aggregation number", *n*. Average micelles aggregation numbers are typically in the range of 40 - 100.

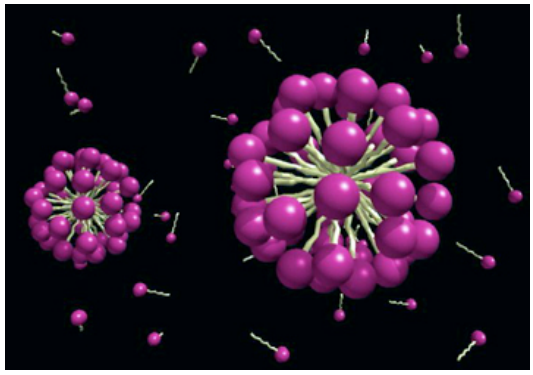

Figure 3.2 *Structure of a spherical micelle.*

3.2.1 Critical micelle concentration

The concentration of surfactant at which micelles first appear in solution is called the critical micelle concentration or CMC. Above the CMC, the concentration of free surfactant is essentially constant, while the micelle concentration increases approximately linearly with total surfactant concentration. The concentration at which micelles first become detectable depends on the sensitivity of the experiments used to determine the CMC. At this concentration, brusque changes in several physical properties take place. Actually, the CMC can be experimentally determined from the discontinuity or inflection point in the plot of a physical property of the solution as a function of surfactant concentration (Patist et al., 2001) as shown in Figure 3.3. A wide variety of techniques involving the measurement of physical properties have been used to determine CMC

values such as surface tension, electrical conductivity, light scattering, refractive index and viscosity.

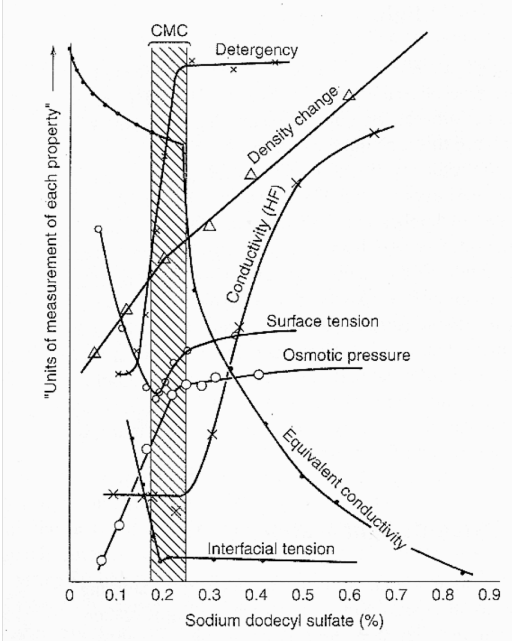

Figure 3.3 *Changes in some physical properties for an aqueous solution of sodium dodecyl sulphate (SDS) close to the CMC.*

Many factors are known to affect the CMC value in aqueous media. Among these are the surfactant structure, the presence of electrolytes or organic additives in solution, temperature, pressure and pH values.

3.2.2 Solubilization

One of the most important characteristics of micelles is their ability to take up all kinds of substances. Actually a number of solutes, which would normally be insoluble or slightly soluble in water, dissolve extensively in surfactant solution above the CMC. Binding of these compounds to micelles is generally driven by hydrophobic and electrostatic interactions.

Solubilisation is usually treated in terms of the pseudophase model, in which the bulk aqueous phase is regarded as one phase and the micellar pseudophase as another. This allows the affinity of the solubilisate for the micelle to be quantified by a partition coefficient, R, usually expressed as a ratio of concentrations. Solubilization is believed to occur at a number of different sites in the micelle (Rosen, 1989) and the nature of the solubilisate largely determines its position in the aggregate. Saturated hydrocarbons show a preference for the core of the micelle (Jobe et al., 1982). In contrast, solubilisates that

contain hydrophilic substituents, such as alcohols or amines, prefer to stay at the surface, where the hydrophilic groups can remain largely hydrated (Porter, 1994). The Stern region is particularly flexible in binding molecules as it contains both the highly hydrophilic surfactant head groups and hydrophobic domains due to backfolding of the surfactant tails as well as water molecules (Gruen, 1985). However, since microenvironments available for solubilization change continuously, due to the dynamic nature of micelles, any attempt to situate the solubilized molecule in specific sites of the micelle could be difficult.

3.2.3 Micellar Catalysis

Concerning reactive process, it has been recognized for long time, that the reaction medium plays an important role in controlling the mechanism and rates of chemical reactions. The chemical reactivity exhibited by molecules and ions organized around these assemblies, is often very different from their reactivity in pure water. Actually, chemical reactions can be influenced in three main ways: by an increase or decrease of rate reaction, by an alteration in the reaction pathway and by an alteration in the reaction stereochemistry. In the presence of ionic surfactants some reaction rates are dramatically enhanced over a narrow concentration range near the CMC to fall off more gradually with increasing surfactant concentration (Figure 3.4, curve (a)). In other reactions, the observed rates rose more gently to plateaus in enzyme-like fashion (Figure 3.4, curve (b)). A further series of reactions displayed the opposite behaviour beyond the CMC, considering that the reaction rates decreased (Figure 3.4, curve (c)).

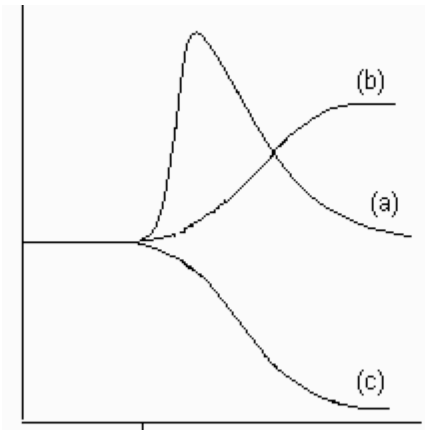

Figure 3.4 *Effect of surfactants on reaction rates. Curves (a) and (b) represent micellar catalysis while curve (c) is a typical example of micellar inhibition.*

The phenomenon of the rate enhancement is known as "micellar catalysis". The fact that the surfactant is not consumed in the reaction and that the surfactant concentration required to obtain such effects is usually very low, justifies the use of the term "micellar catalysis". The efficiency of micellar catalysis relies on two principal factors. First, there is the effect of the micellar environment on the rate-controlling step in the reaction mechanism. The relative free energies of the reactants and the transition state can be altered when the reaction takes place in the micellar phase instead of the bulk water (Romsted, 1976). A more important consideration is the localization of the reacting species in the relatively small volume of the micelles compared to the bulk solution. This leads to a large increase in the effective concentration and the observed rate increases accordingly. Thus rate enhancements of bimolecular and higher order reactions are a consequence of the localized concentration of reactants at the micelle-solution interface. The kinetic data analysis of chemical reactions in micelles generally involves the use of the well-known pseudophase model (Shinoda and Hutchinson, 1962; Menger and Portnoy, 1967), which assumes the micellar solution as consisting of two separate phases. The reaction may take place in both the aqueous and micellar pseudophases and the overall reaction rate is the sum of the rates in each pseudophase (Shinoda and Hutchinson, 1962). A rate promotion occurs when both reactants are preferentially located in the micelles, while a rate decrease follows if only one of the reactants has been incorporated into the micelles, since in the latter case the two reaction partners are separated.

3.3 Micellar Extraction

Micellar systems have attracted considerable attention in the last few years as potential extracting media and continue to have a broad appeal for extraction applications (Cöklen and Hatton, 1985; Stalikas, 2002; Juang et al., 2003). Solutes that bind to micelles in solution are extracted to different extents, depending on the micelle-solute binding interactions. Hydrophobic compounds, are favourably partitioned in the non-polar microenvironment, while metal ions can bind electrostatically to the polar head of the surfactant, or can be extracted by complexation with a ligand soluble into the micellar pseudo-phase, thus being preferentially in form of metallic chelates. For effective metal recovery, the separation of the micellar pseudo-phase from the aqueous phase has to be achieved. It can be carried out by means of ultrafiltration (Micellar Enhanced Ultrafiltration or Ligand Modified-Micellar Enhanced UltraFiltration) (Klepac et al., 1991; Fillipi et al., 1998).

3.3.1 Micellar-Enhanced Ultrafiltration

A large number of studies have demonstrated that the separation of the micellar pseudo-phase from the aqueous phase can be achieved by ultrafiltration using membranes with pore diameter smaller than the size of the micelle (Scamehorn et al., 1989). Ultrafiltration is a membrane separation process aimed at dissolved or dispersed particles, which have size ranging from 1-100 nm. As a consequence, the pore size is too large to reject small molecules (below 10^3 Da). Micellar Enhanced Ultrafiltration (MEUF) is a surfactant-based separation process in which surfactants are added to a waste stream to promote the removal of small molecules. MEUF has been widely used to remove metal ions (Scamehorn et al., 1994; Juang et al., 2003; Li et al., 2006) and organic contaminants (Kim et al., 1998; Doulia and Xiarchos, 2007; Zaghbani et al., 2007) from dilute aqueous solution. Metal ions or organic molecules as hydroxamic acids, in which we are mainly interested, can be recovered through MEUF, once they are attracted on the micelle surface. The micellar solution is subsequently passed through an ultrafiltration membrane with pore sizes small enough to retain the micelles and the associated reactants.

3.4 Determination of the acid dissociation constant of SHA in the presence of SDS.

The hydrogen ion concentration in water generally differs from the value on the micelle surface. For instance, in the presence of SDS micelles, the negatively charged surface will attract protons resulting in an increase in the proton concentration at the surface with a consequent decrease in the pH. Hartley and Roe (Hartley and Roe, 1940) showed that the surface pH_S is related to the bulk pH_W, at 25 °C, by the following equation:

$$pH_S - pH_W = -\Psi / 59.2 \qquad (3.1)$$

where Ψ is the surface potential of the micelle in mV. The high surface potential of the SDS micelle (~ 120 mV) leads to a decrease in the local pH at the surface that, according to equation (3.1) is equivalent to about two units. This result shows that $[H+]_S/[H+]_W \approx 100$, i.e. the proton concentration on the micelle surface is one hundred times higher than in water. The pK_A of a ligand that is located on the micelle surface is also shifted. Actually, the major influence on the pK_A shift is attributed to the increased proton concentration close to the micelle surface, rather than an effect on the intrinsic pK_A of the ligand, arising from the change in environment (James and Robinson, 1978). Again following Hartley and

Roe (Hartley and Roe, 1940) at 25°C the surface pK_A, $(pK_A)_S$, is related to the bulk pK_A, $(pK_A)_W$, by equation (3.2):

$$(pK_A)_S - (pK_A)_W = \Psi / 59.2 \qquad (3.2)$$

According to the above considerations any evaluation of data obtained for micellar systems requires the knowledge of the surface pK_A, $(pK_A)_S$. Hence, the $(pK_A)_S$ value of the ligand used in the present study (SHA) has been measured in the presence of SDS.
Salicylhydroxamic acid, here employed to complex Ni(II), is a weak acid with three protonation sites: the carbonyl oxygen, the aminic nitrogen and the phenolic group . The hydrogen ion equilibria of SHA can be represented as follows:

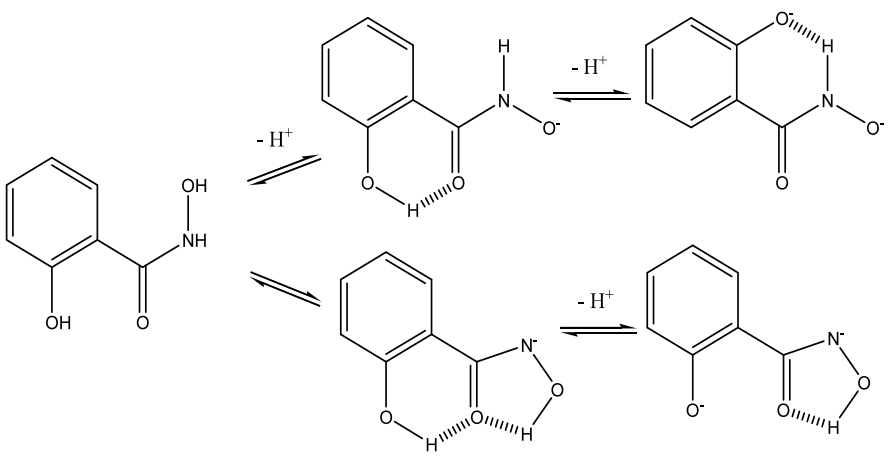

Figure 3.5 *Dissociation equilibria of SHA.*

The first acid dissociation constant of SHA in the presence of SDS has been measured in this thesis for the first time. The same value of pK_{A1} has been measured in pure water solution, $(pK_{A1})_W$ in order to determine the term $\Psi / 59.2$ which should be employed to evaluate the hydrogen ion concentration on the micellar surface according to equation (3.1). The pK_{A1} of SHA have been evaluated in water and in SDS solutions by means of spectrophotometric titrations. In particular, it has been indirectly measured by exploiting the protonic exchange reaction between SHA and dihydrogen phosphate (reaction (3.3)).

$$HL^- + H_2PO_4^- \rightleftarrows HPO_4^{2-} + H_2L \qquad (3.3)$$

Spectrophotometric titrations were carried out by adding known amounts of HCl in the spectrophotometric cell containing a known amount of SHA and an excess of Na_2HPO_4. The absorbance values at 238 nm were analyzed according to equation (3.4) (see Appendix I).

$$\frac{C_{HL}}{\Delta A} = \frac{1}{\Delta\varepsilon} + \frac{1}{K\Delta\varepsilon}\frac{[HPO_4^{2-}]}{[H_2PO_4^-]} \qquad (3.4)$$

where C_{HL} is the total ligand concentration, $\Delta A = A - \varepsilon_{HL}C_{HL}$, $\Delta\varepsilon = \varepsilon_{H2L} - \varepsilon_{HL}$ and K represents the equilibrium constant of reaction (3.3). This constant is defined as $K = K_{HA}/K_{A1}$, where K_{HA} refers to the acid dissociation of $H_2PO_4^-$. The analysis of a typical titration according to equation (3.4) is shown in Figure 3.6.

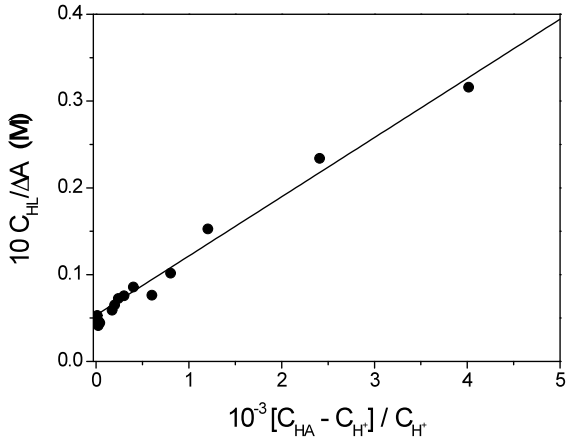

Figure 3.6 *Analysis of a spectrophotometric titration for the determination of pK_{A1} of SHA in SDS 3.5×10^{-2} M. $C_{HL} = 1\times10^{-4}$ M; $C_{HA} = 1\times10^{-2}$ M; λ = 238 nm; T = 298 K.*

Using the pK_{HA} value of NaH_2PO_4 in SDS 2×10^{-2} M, that is an average value of the investigated SDS concentrations ($pK_{HA} = 6.95 \pm 0.02$) (Ghezzi, 2008) the pK_{A1} values of SHA at each SDS concentration, reported in Table 3.1, have been obtained from plots as that shown in Figure 3.6. The value of pK_{A1} in water is in agreement with the literature data ($pK_{A1} = 7.56$) (García et al., 2007).

Comparison of the pK_{A1} values in water and SDS solution yields $(pK_{A1})_S - (pK_{A1})_W = 1.7$ as an average value of the data of Table 3.1. According to the relationship $\Delta pK = \Delta pH$ (Hartley and Roe, 1940; James and Robinson, 1978) one can conclude that the hydrogen ion concentration on the SDS micelles is higher by a factor of about 50 compared to water.

Table 3.1 *Dependence of SHA pK_{A1} on SDS concentration.*

10^2 [SDS] (M)	pK_{A1} (SHA)	ΔpK_{A1} (SHA)
0	7.6	0.0
0.4	9.4	1.8
0.7	9.3	1.7
1.5	9.3	1.7
2.4	9.2	1.6
3.5	9.1	1.5
6.0	9.1	1.5

3.5 Extraction of SHA and Ni(II)/SHA complex by MEUF.

Micellar enhanced ultrafiltration (MEUF) has been used to evaluate the extent of the adsorbtion of salicylhydroxamic acid and its complex with Ni(II) on the surfactant. Solution of water and different amounts of SDS, containing 10^{-3} M SHA was subject to an ultrafiltration procedure. After the micellar phase (retentate) was separated (extracted) from the liquid matrix (permeate), a spectrum of the permeate was recorded and compared with that of the initial solution. The extraction procedure was applied also to measure the extent of extraction of the of the free metal (M) and the Ni(II)/SHA complex (ML). The yield of the extraction process for each species is expressed by the retention coefficient, R_i (equation (3.5)).

$$R_i = \frac{C_i^W}{C_i^S} \tag{3.5}$$

where C_i^w and C_i^{SDS} are the molar concentrations of the i-th reactant in water and in SDS respectively. Ultrafiltration experiments have been performed for samples containing different amounts of SDS, but it has been observed that the retention coefficients do not change their values varying the surfactant concentration. It turns out that $R_L = 0.87$, $R_M = 0.25$ and $R_{ML} = 0.32$ at each investigated SDS concentration. Note that salicylhydroxamic acid displays a fair distribution between the aqueous and the micellar phase, while its complex with Ni(II) tends to stay more on the micelle surface, as it is sensitive not only to the hydrophobic effect, but also to the electrostatic attraction of its positive charge by the negatively charged SDS micelles.

3.6 Complex Formation Equilibria.

The interactions of Ni(II) with SHA in SDS micellar solution is revealed by the spectral changes occurring in the UV region (Figure 3.7). All titrations have been performed under conditions of metal excess ($C_M \geq 10\ C_L$), where only 1:1 complexes are formed.

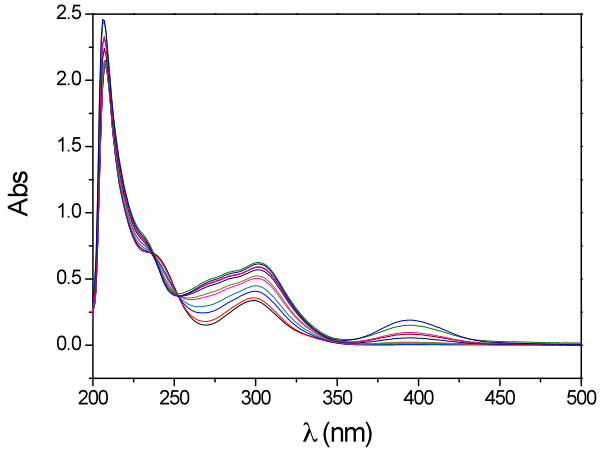

Figure 3.7 *Spectral changes recorded during a spectrophotometric titration of SHA with Ni(II). pH=5.41, [SDS]= 3.5×10^{-2} M, I=0.2 M, T=25°C.*

Spectrophotometric titrations of SHA with $Ni(ClO_4)_2$ were performed at 304 nm, where the spectral change is the largest, with the aim of evaluating the equilibrium constant, K_{app}, of the binding reaction (3.6)

$$M_f + L_f \leftrightarrows ML_T \qquad (3.6)$$

where M_f and L_f are the total concentrations of uncomplexed metal and ligand, whereas ML_T is the total complex concentration.

In the presence of surfactant the expression for K_{app} is:

$$K_{app} = \frac{[ML_T]^W + [ML_T]^S}{([M_f]^W + [M_f]^S)([L_f]^W + [L_f]^S)} \qquad (3.7)$$

The superscripts *W* and *S* denote the concentrations of the reactants in the aqueous and micelle pseudophase respectively.

Experiments were performed in the pH range between 4.2 and 5.9 for different SDS concentrations. Figure 3.8 shows a typical titration curve at pH = 5.2 and *I* = 0.2 M ($NaClO_4$).

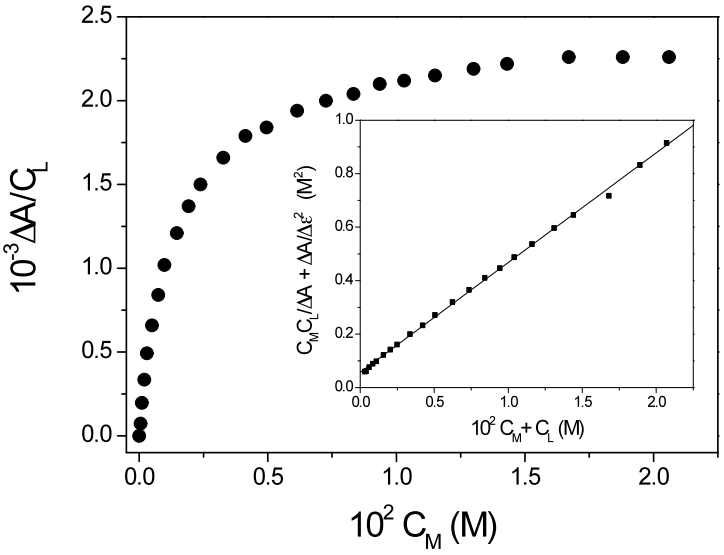

Figure 3.8 *Binding isotherm deriving from a spectrophotometric titration of SHA with Ni(II). [SDS] = 3.5×10^{-2} M, pH = 5.41, I = 0.2 M, λ = 304 nm, T = 298 K. Inset: analysis of the titration by means of equation (3.8).*

Titrations were analyzed according to equation (3.8) (derivated in Appendix II) that gives a straight line whose intercept and slope provide the equilibrium constant, K_{app}, together with the change in extinction coefficient, Δε (inset of Figure 3.8).

$$\frac{C_M C_L}{\Delta A} + \frac{\Delta A}{\Delta \varepsilon^2} = \frac{1}{K_{app}\Delta\varepsilon} + \frac{C_M + C_L}{\Delta\varepsilon} \qquad (3.8)$$

It should be noticed that application of equation (3.8) requires an iterative procedure since Δε is not known "a priori". Hence the term $\Delta A/\Delta\varepsilon^2$ is disregarded on a first approximation and is then calculated from the slope of the straight line obtained by plotting $C_MC_L/\Delta A$ vs. (C_M+C_L). This Δε value will be used to re-evaluate the $(C_MC_L/\Delta A + \Delta A/\Delta\varepsilon^2)$ term and so on, until convergence is reached.

The analysis of the equilibria and kinetics (described below) has been based on a general reaction pattern, which includes possible interaction between the metal and the two different ligand forms (Scheme 3.1).

As displayed by MEUF extraction results, SHA is present just partially on the micelles surface, while a considerable amount of it remains in the aqueous phase, therefore the

measured K_{app} in the presence of the surfactant includes the contributions of the apparent reaction that takes place in both the phases of the solution. By inserting equation (3.5) in the expression of K_{app}, is possible to separate the contributions to the equilibrium of the aqueous and micellar phase and evaluate the extent of the complexation reaction in the micelle phase only, in terms of K_{app}^{S} (equation (3.9)).

$$K_{app}^{S} = \left(K_{app} - \frac{K_{app}^{W}}{a} \right) \times b \tag{3.9}$$

where *a* and *b* are two numerical coefficients that depend on the fractions of metal and ligand in the aqueous and micellar phase, evaluated as reported in equations (3.10) and (3.11).

$$a = \left(1 + \frac{1}{R_M} \right) \times \left(1 + \frac{1}{R_L} \right) \tag{3.10}$$

$$b = \left(1 + R_M \right) \times \left(1 + R_L \right) \tag{3.11}$$

The trend of the apparent binding constant with $[H^+]$ does not change on going from aqueous solution (García et al., 2007) to micellar solution, hence Scheme 3.1, that was worked out for the reaction in water, was assumed as suitable to represent the overall binding process in SDS micellar medium too.

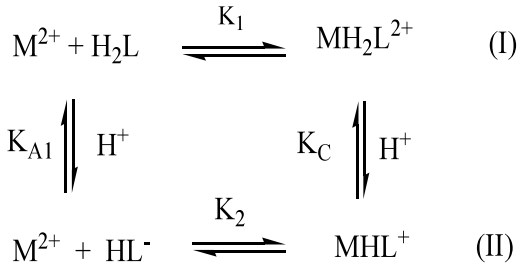

Scheme 3.1 *Reactive scheme for the Ni(II)/SHA system in SDS micellar solution.*

The acidity dependence of K_{app}^{S} is given by equation (3.12)

$$\frac{K_{app}^{S}}{\alpha\beta} = K_1 + K_2 \frac{K_{A1}}{[H^+]} \qquad (3.12)$$

where K_1 and K_2 are the equilibrium constants of the individual steps (I) and (II) respectively, whereas K_{A1} is the dissociation constant of ligand. The molar fraction of the ligand, α, is defined as $[H^+]/(K_{A1}+[H^+])$, while β represents the molar fraction of the free form of metal, Ni^{2+}, and is equal to $[H^+]/(K_H+[H^+])$, where $K_H = 1.38\times10^{-10}$ M is the first dissociation constant of the $[Ni(H_2O)_6]^{2+}$ ion in water (Baes and Mesmer, 1976) and it is even smaller in SDS, so that $\beta = 1$. Figure 3.9 collects all the apparent constants found by spectrophotometer analysis and shows how the reaction is improved at higher pH values and for SDS concentrations near to the CMC.

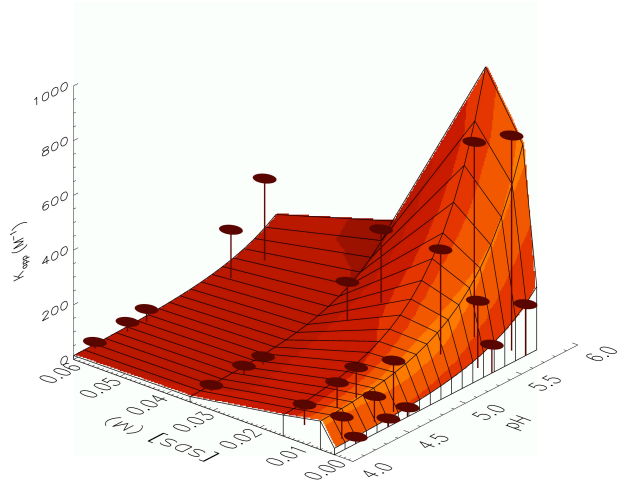

Figure 3.9 *K_{app}^{SDS} dependence on $[H^+]$ and [SDS] for the Ni(II)/SHA system. I = 0.2 M; T = 298 K.*

According to Scheme 3.1 is possible to deduce the dependence of K_C on the other individual equilibrium constants, being $K_C = K_2K_{A1}/K_1$.

The values of the obtained individual constants, at each analyzed SDS concentration, are collected in Table 3.2.

Table 3.2 *Dependence of the equilibrium constants on [SDS] for the Ni(II)/SHA system at 298 K and I = 0.2 M ($NaClO_4$).*

10^2 [SDS] (M)	K_1^S (M^{-1})	10^{-5} K_2^S (M^{-1})	10^{10} K_{A1}^S (M)	10^5 K_C^S (M)
0	115	0.05	250	0.1
0.4	20.1-21.6[a]	8.6-8.6[a]	3.89	1.7-1.5[a]
0.7	94.3-101.3[a]	21.1-38.0[a]	4.79	1.1-1.8[a]
1.5	62.2-54.3[a]	20.7-19.1[a]	6.92	2.3-2.4[a]
3.5	15.7-12.2[a]	5.0-4.3[a]	8.32	2.7-2.9[a]
6.0	12.3-11.4[a]	2.5-3.6[a]	8.51	1.7-2.7[a]

[a]*Values obtained from kinetic experiments as $K_1 = k_1/k_{-1}$, $K_2 = k_2/k_{-2}$, $K_C = (K_{A1}\, k_2\, k_{-1})/(k_{-2}\, k_1)$.*

3.7 Complex Formation Kinetics

The kinetics of Ni(II) binding to SHA have been investigated under pseudo first-order conditions ($C_M >> 10\ C_L$) using the stopped-flow method.

The obtained kinetic curves are monoexponential in the range of pH between 4.2 and 5.7 and at I = 0.2 M (Figure 3.10A), and the kinetic effect is ascribed to formation of a mononuclear complex between Ni(III) and SHA. The behavior becomes more complex at the higher analyzed pH value (pH = 5.9), where the system displays two kinetic effects (Figure 5B). The analysis of the recorded traces provided the amplitude and time constants, $1/\tau_{fast}$ and $1/\tau_{slow}$, of the two corresponding kinetic effects. Experiments carried out keeping constant the pH, ligand and perchlorate concentration and varying the metal concentration show a good linearity of $1/\tau_{fast}$ versus C_M (Inset of Figure 3.10A), according to equation (3.13).

$$1/\tau_{fast} = k_{f,fast}C_M + k_{d,fast} \qquad (3.13)$$

Thus, a linear interpolation of the experimental data would provide the values of the apparent complex formation ($k_{f,fast}$) and dissociation ($k_{d,fast}$) rate constants of reaction (3.6), i.e. the apparent reaction for formation of ML_T.

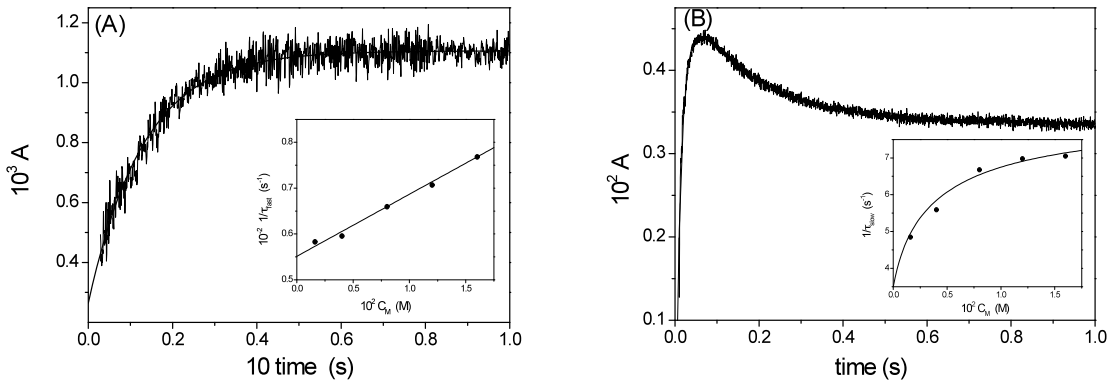

Figure 3.10 *Kinetic relaxation curves for the complexation reaction of Ni(II)/SHA system in [SDS] = 6×10^{-2} M; I = 0.2 M; λ = 304 nm; T = 298 K. (A) Fast effect: pH = 4.2; C_M = 1.6×10^{-2} M; Inset: time constant values dependence on Ni(II) concentration for the fast effect; (B) Fast and slow effects: pH = 5.9; C_M = 4×10^{-3} M; Inset: time constant values dependence on Ni(II) concentration for the slow effect.*

As done for the static experiments, the balanced partition of the ligand between the two phases in solution was taken into account also for the evaluation of the kinetic parameters. The direct and reverse apparent kinetic constants were thus splitted into two contributions, concerning the aqueous and the micellar phase. In such a way it was possible to consider the complexation kinetics just in the micellar phase. For this purpose a kinetic equation that involves two separate contributions has been derived in Appendix IV (equation (3.14)).

$$\frac{1}{\tau_{fast}} = \left(k^W_{f,fast} \frac{R_M R_L}{(1+R_M)(1+R_L)} + k^S_{f,fast} \frac{1}{(1+R_M)(1+R_L)} \right) C_M + \left(k^W_{d,fast} R_L + k^S_{d,fast} \right) \frac{1}{1+R_L} \quad (3.14)$$

where the forward and reverse kinetic constants in water are indicated as $k^W_{f,fast}$ and $k^W_{d,fast}$, while in the micellar phase they are pointed out as $k^S_{f,fast}$ and $k^S_{d,fast}$. Equation (3.14) represents a straight line, whose slope and intercept correspond respectively to the forward ($k_{f,fast}$) and reverse ($k_{d,fast}$) constants of the reaction in the overall solution (reaction (3.6) and equation (3.13)). As $k^W_{f,fast}$ and $k^W_{d,fast}$ were already known from literature (García et al., 2007), and the global constants $k_{f,fast}$ and $k_{d,fast}$ have been evaluated from the dependence of $1/\tau_{fast}$ on C_M, $k^S_{f,fast}$ and $k^S_{d,fast}$ were determined by comparing equations (3.13) and (3.14) for each SDS concentration. Both $k^S_{f,fast}$ and $k^S_{d,fast}$ were found to depend on the medium

acidity. According to Scheme 3.1, the dependencies of $k^S_{f,fast}$ and $k^S_{d,fast}$ on [H$^+$] should be given by equations (3.15) and (3.16), respectively

$$\frac{k^S_{f,fast}}{\alpha\,\beta} = \left(k_1 + \frac{k_2 K_{A1}}{[H^+]} \right) \tag{3.15}$$

$$\frac{k^S_{d,fast}}{\gamma} = \left(k_{-2} + \frac{k_{-1}[H^+]}{K_C} \right) \tag{3.16}$$

where α and β have been already defined above and $\gamma = K_C/([H^+] + K_C)$, with $K_C = [MHL^+][H^+]/[MH_2L^{2+}]$. Thus, for each SDS concentration a value of γ has been determined, using the corresponding value of K_C (Table 3.2) and the acid concentration evaluated according to equation (3.1). The plot of $k^S_{f,fast}/\alpha\beta$ versus 1/[H$^+$] displays a linear trend at each SDS concentration as shown in Figure 3.11A, where the results of [SDS] = 3.5×10^{-2} M are represented. The data fit according to equation (3.14) yields the reaction parameters k_1 and k_2 reported in Table 3.3.

Table 3.3 *Reaction parameters for the Ni(II)/SHA system at different SDS concentrations. I = 0.2 M; T = 298 K.*

10^2 [SDS] (M)	$10^{-3}\,k_1^S$ ($M^{-1}s^{-1}$)	$10^{-2}\,k_{-1}^S$ (s^{-1})	$10^{-6}\,k_2^S$ ($M^{-1}s^{-1}$)	k_{-2}^S (s^{-1})
0	2.6	1.3	0.032	6.3
0.3	4.4	2.0	4.6	5.4
0.7	22.8	2.3	16.8	4.4
1.5	9.7	1.8	10.5	5.5
3.5	2.5	2.1	2.2	5.0
6.0	2.3	2.0	1.7	4.8

The value of $k^S_{d,fast}/\gamma$ was found to depend linearly on [H$^+$] (Figure 3.11B) hence, according to equation (3.15) the reverse kinetic constants, k_{-1} and k_{-2} have been determined. The values of the obtained individual rate constants are reported in Table 3.4. The apparent equilibrium constant in micelle (K^S_{app}) has been evaluated from the kinetic constants ratio, $k^S_{f,fast}/k^S_{d,fast}$, in the pH range where only the fast kinetic effect is observable. The values so obtained are in good agreement with those provided by the static experiments (Figure

3.11C). The accordance of k_1/k_{-1} and k_2/k_{-2} values with K_1 and K_2 obtained from the thermodynamic analysis (Table 3.2) strongly supports the effectiveness of the proposed reaction mechanism.

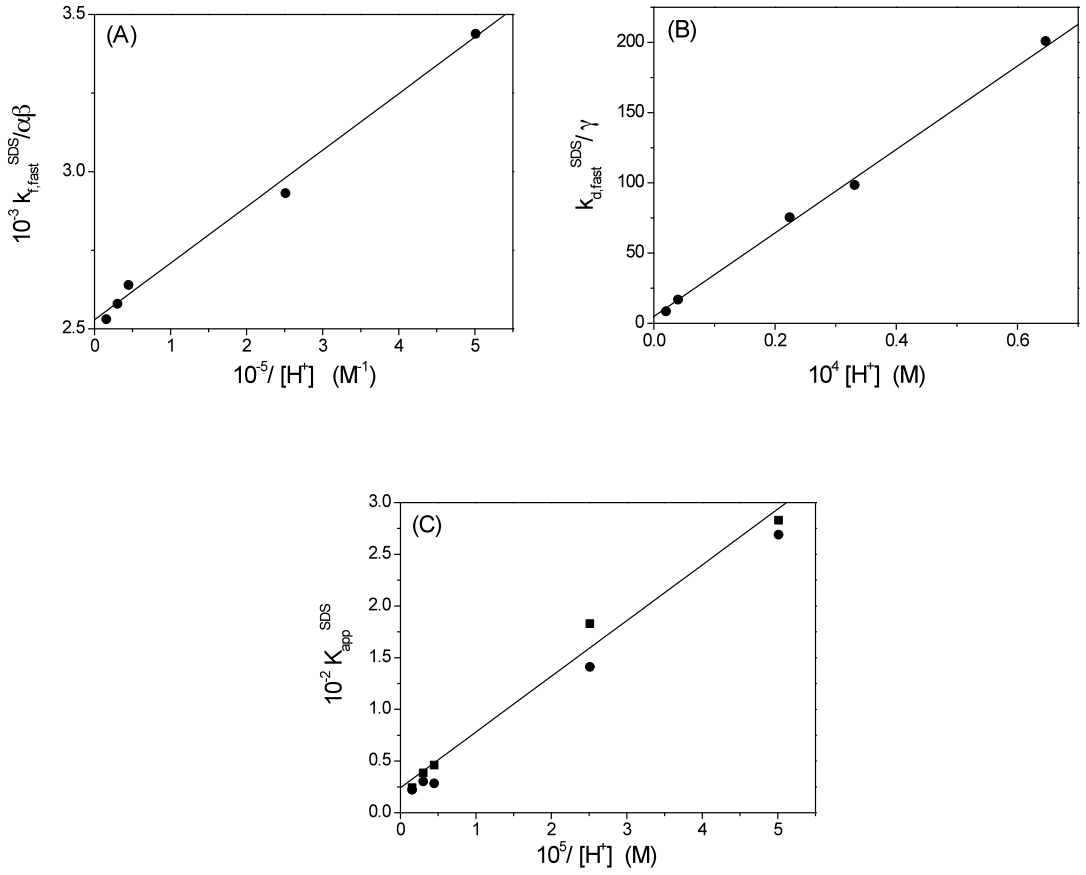

Figure 3.11 *Kinetic behavior for the fast effect of the Ni(II)/SHA reaction in SDS 3.5×10^{-2} M, I = 0.2 M, T = 298 K. (A) Dependence of the forward rate constant, $k_{f,fast}^{S}$, on hydrogen ion concentration. (B) Dependence of the reverse rate constant, $k_{d,fast}^{S}$, on hydrogen ion concentration. (C) Dependence of K_{app}^{S} on hydrogen concentration, evaluated from kinetic experiments, as $k_{f,fast}^{S}/k_{d,fast}^{S}$ (■) and from spectrophotometric titrations (●).*

Concerning the slow kinetic effect, it is worth to note that this is observed just at the higher analyzed pH value, pH = 5.9 (Figure 3.10B). Contributions to kinetic parameters values in the two phases have been separated for the slow effect too; therefore we are able to report the results in the pure micellar phase. The binding process, in this case, can be described by the two-step sequence (3.17).

$$M_f + L_f \rightleftarrows ML_{T,I} \rightleftarrows ML_{T,II} \tag{3.17}$$

The apparent equilibrium constant, K_{app}^{S}, should be a function of the rate constants of the two processes observed in the kinetic experiments, as shown in equation (3.18).

$$K_{app} = \frac{k_{f,fast}}{k_{d,fast}}\left(1 + \frac{k_{f,slow}}{k_{d,slow}}\right) \tag{3.18}$$

As commented before, the observed dependence of the rate constants on $[H^+]$ suggests that several forms of both the ligand and the complex, differently protonated, should be involved in the binding process. Sequence (3.17) can thus be depicted in a more detailed form, as shown in Scheme 3.2.

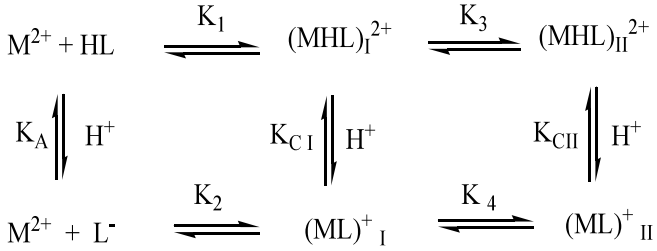

Scheme 3.2 *Reactive scheme for the Ni(II)/SHA system, involving the slow effect, in SDS micellar solution.*

The overall rate constants of the slow effect, $k_{f,slow}$ and $k_{d,slow}$ is expressed by equation (3.19) which requires that values of $1/\tau_{slow}$ tend to level off at the highest values of C_M. This requirement is verified by the experimental trend displayed by the data pairs plotted in the inset of Figure 3.10B.

$$\frac{1}{\tau_{slow}} = \frac{K_{app,fast}k_{f,slow}C_M}{1 + K_{app,fast}C_M} + k_{d,slow} \tag{3.19}$$

Separation of the contributions to $1/\tau_{slow}$ of the reaction in the two phases has been done, resulting in equation (3.20), which is derived in Appendix IV.

$$\frac{1}{\tau_{slow}} = \left[\frac{K^{W}_{app,fast} k^{W}_{f,slow} R_M R_{ML}}{1 + R_M + K^{W}_{app,fast} R_M C_M} + \frac{K^{S}_{app,fast} k^{S}_{f,slow}}{1 + R_M + K^{S}_{app,fast} C_M} \right] \frac{C_M}{1 + R_{ML}} + \left[k^{W}_{d,slow} R_{ML} + k^{S}_{d,slow} \right] \frac{1}{1 + R_{ML}} \qquad (3.20)$$

By using the literature values (García et al., 2007) for the reaction parameters in water solution and the $K^{S}_{app,fast}$ value obtained from the thermodynamic experiments, the values of the forward and reverse constants for the slow kinetic effect have been derived. Values of $k^{S}_{f,slow}$ and $k^{S}_{d,slow}$ are collected in Table 3.4.

Table 3.4 *Time constants of the slow kinetic effect at different SDS concentrations for the Ni(II)/SHA system. I = 0.2 M; T = 298 K.*

10^2 [SDS] (M)	$k^{S}_{f,slow}$ (s^{-1})	$k^{S}_{d,slow}$ (s^{-1})
0	3.8	4.2
0.3	3.9	4.2
0.7	3.6	4.3
1.5	4.3	4.0
3.5	3.7	3.9
6.0	3.9	4.2

3.8 Micellar Catalysis

In the presence of SDS, Ni^{2+} ion will be attracted electrostatically by the negatively charged micelle surface, whereas SHA will be retained on the micelle by hydrophobic forces. Under these circumstances, the reaction on the micelle surface is favored as the result of a local concentration increase of both reactants (James and Robinson, 1978). Spectrophotometric titrations were performed at different SDS concentrations, for each pH value, in order to evaluate the extent of the micellar catalysis on Ni(II) reaction with SHA. Introduction of the correct value of K_{A1} for each SDS concentration in equation (3.11) enabled us to estimate K_1 and K_2 of the complexation reaction, whose values are reported in Table 3.2 together with K_{A1} and K_C.

It is found that K_1 and K_2 depend on SDS concentration in a similar way (for pH = 4.2÷5.9), both constants exhibiting a maximum at a surfactant concentration close to the CMC. Also the rate constants of the binding process display all the same trend for each analyzed pH value. Figure 3.12A shows the effect of SDS on the rate constants of complex formation. The values of k_f^S show the maximum rate enhancement for a surfactant

concentration slightly lower than the CMC, corresponding to 7×10^{-3} M. The same dependence on SDS concentration is observed for the reverse constant of the fast kinetic effect, k_d^S, (Figure 3.12B) and the apparent constant K_{app}, obtained as $k_{f,fast}^S / k_{d,fast}^S$ (Figure 3.12C). This behavior is characteristic of the catalysis effect of SDS micelles on the Ni(II)/SHA complexation, being the observed trend typical of a general bimolecular reaction rate in the presence of surfactant catalysis.

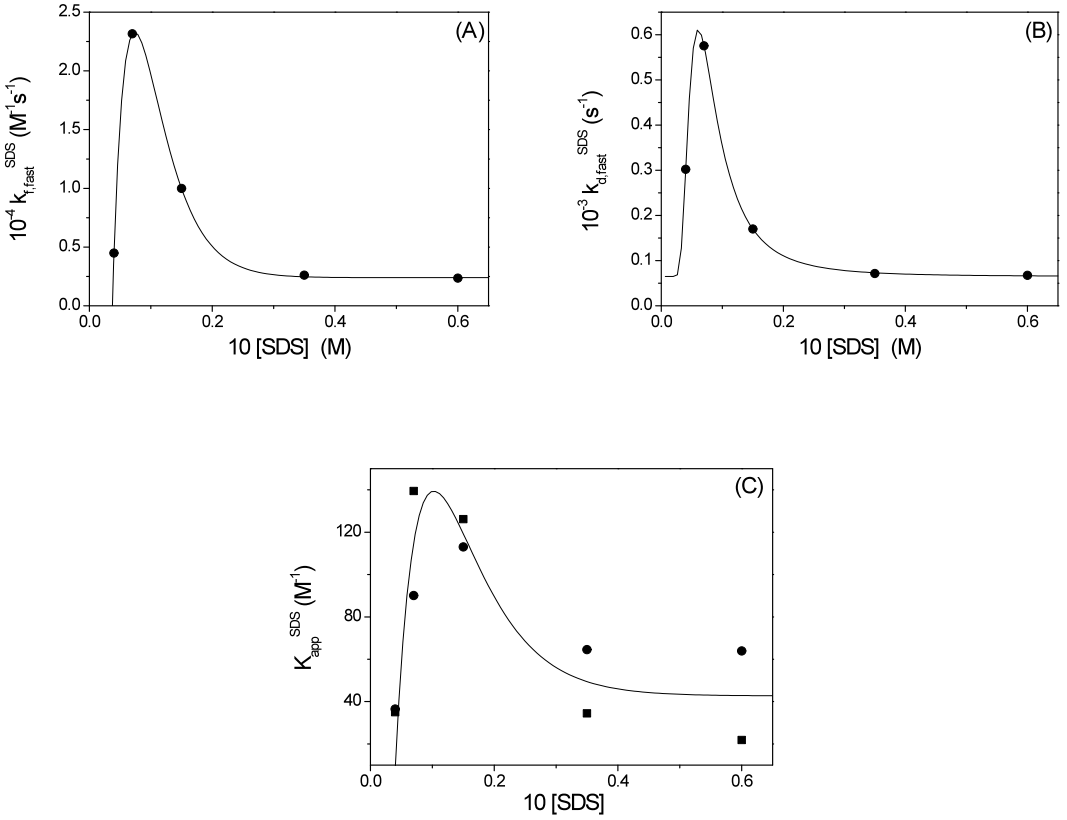

Figure 3.12 *Micellar catalysis for the system Ni(II)/SHA at pH = 4.65, I = 0.2 M, T = 298 K. (A) Dependence of the forward rate constant,* $k_{f,fast}^S$*, on the SDS concentration. (B) Dependence of the back rate constant,* $k_{d,fast}^S$*, on the SDS concentration. (C) Dependence of the equilibrium constant obtained from spectrophotometric titrations (■) and expressed as* $k_{f,fast}^S / k_{d,fast}^S$ *(●) on the SDS concentration.*

3.9 Discussion

Table 3.1 shows that the pK_{A1} values of SHA do increase on going from water to SDS solution, but less than observed in the case of ligands completely adsorbed on the micelle surface (Ghezzi et al., 2007; Biver et al., 2009). For these ligands the ΔpK_A value is about 2, in agreement with the relationship $\Delta pK_A = \Psi/59.2$, where Ψ is the surface potential (120mV for SDS) (Hartley and Roe, 1940). The lower value of ΔpK_{A1} observed for SHA could be ascribed to the fact that this ligand is adsorbed only partially on SDS and, by consequence, the obtained acid dissociation constant value is intermediate between the value in water and the value in SDS. For both the complex formation equilibria and kinetics, separation of reaction contributions in the aqueous and micellar phase has proven to be essential to analyze the system. The separation procedure worked out in this thesis is of a completely general character and is suitable for any system that is partitioned between two different phases. Actually, we have applied the same treatment to an investigation on the system Ni(II)/PBHA (Phenylbenzohydroxamic acid) in SDS, previously performed in our laboratory that was not yet analyzed. As PBHA is equally distributed between water and micellar phase, separation of the two contributions, according to the method here described, resulted to be a successful approach also in this case.

Concerning the complex formation equilibria, Table 3.2 shows that the values of K_1 are rather insensitive to the presence of SDS, whereas the values of K_2 display a dramatic increase on addition of surfactant. Also, differently from K_{A1}, the acid dissociation constant of the protonated complex does not display important change in the presence of micelles. This behaviour is in apparent contrast with that of the Ni(II)/PADA system (Monteleone et al., 2004) where MHL is strongly stabilized by SDS, as shown by the large decrease of K_C and the large increase of K_1 which becomes close to K_2. However, the contrast can be removed if one considers that concerning PADA the proton of MHL is bound to the amino group and, therefore, stays far from the reaction site. In this case, the increased proton concentration on the SDS surface inhibits the proton loss from the complex. On the other hand, in the case of SHA, the proton, being bound to the hydroxamate group, is part of the reaction site and should necessarily be removed in order the metal-oxygen bond to be formed. The high tendence to form the chelate (with proton expulsion) overcomes the proton mass action acting in the opposite direction, resulting in a value of K_2 much higher than that of K_1.

Concerning the complex formation kinetics of the Ni(II)/SHA system, Table 3.2 shows that SDS exherts a catalytic effect on the steps of formation of both MHL (k_1) and ML (k_2). This effect is expected since both steps are bimolecular and reaches its maximum at [SDS] = 0.07 M, corresponding to the surfactant CMC. Looking at the reverse steps, Table 3.2 shows that $k_{-1} >> k_{-2}$, in agreement with the fact that k_{-2} includes the work needed to overcome the energy barrier necessary to break the chelate bond. Both k_{-1} and k_{-2} are independent of the SDS concentration, as expected since the complex dissociation steps are monomolecular. The reaction of complex formation of $Ni(H_2O)_6^{2+}$ are known to follow the I_d mechanism for which it turms out that $k = K_{OS}k^*$, where K_{OS} is the stability constant of an outer-sphere complex, while k* is the rate of water replacement by the ligand in the inner solvation shell of the metal. The Eigen's criterion states that, in the case of the I_d mode of activation, $k^* = k_{H2O}$, being k_{H2O} the rate constant for the process of water exchange at $Ni(H_2O)_6^{2+}$ ion. Since k_{H2O} refers to a monomolecular process it is unlikely that its value depends on the presence of the surfactant. On the other hand, owing to the reaction restricted geometry provided by surfactant surface, the value of K_{OS} does increase on transferring the reactants from the water to SDS, thus explaining the dependence of k_1 and k_2 on [SDS].

The slow kinetic effect, which was observed also in aqueous solution (García et al., 2007) was explained considering that the formation of the Ni-SHA chelate induces the rotation of the phenol group around the C-C bond. Therefore, the formed complex will pass from the *cis* to the *trans* conformation. Note that this *cis* ⇆ *trans* rotation is a mononuclear process in both directions, so its reaction rate is expected to be independent on [SDS], as experimentally found (Table 3.4).

The *trans* conformation is in principle suitable to allocate a second metal ion, thus providing the basic unti necessary for metallacrowns formation (Pecoraro et al, 1996).

Such a dinuclear complex was neither observed in the previous The slow kinetic effect, which was observed also in aqueous solution (García et al., 2007) nor in the present investigation. However in this thesis work it has been isolated in water solution of Fe(III), as reported in next chapter.

CHAPTER 4

A route to metallacrowns: Fe(III) and its complexation by salicylhydroxamic and benzohydroxamic acid

Iron is an essential element in all organisms but its supply is restricted by its extreme insolubility under physiological conditions. For this reason, microorganisms produce low molecular weight chelating agents, called siderophores, that can solubilize iron from the environment by complexing and transporting it into the cells (Neilands, 1976). An important structural feature of many siderophores is the incorporation of hydroxamate groups, which are capable of selectively binding Fe(III) in the presence of other biologically important metal ions. Actually, both natural and sintetic hydroxamic acids are able to coordinate Fe(III) with very high affinity (Albrecht-Gary and Crumbliss, 1998; Santos et al., 1998), giving rise to simple complexes or also to self-assembled macromolecules, as metallacrowns.

Salicylhydroxamic acid (SHA), in conjunction with highly charged metal ions as Fe(III), is well suited to the synthesis of metallacrowns, because of its ability to act as a ditopic ligand. SHA can, in principle, bind two Fe(III) ions, giving rise to a dinuclear, fully deprotonated complex which will constitute the basic unit of a SHA based metallacrown (Pecoraro et al., 1996). The structure of such a precursor complex was hypothesized by Pecoraro et al. (Pecoraro et al., 1996; Mezei et al., 2007), but never isolated. Actually, the experimental evidence so far available on M^{2+}/SHA systems denies full deprotonation and formation of 2:1 complexes of SHA. As shown in the previous chapter, it has been observed that the divalent Ni(II) forms with SHA only mononuclear complexes where the N-H proton remains bound to the nitrogen atom, irrespective of the strong polarization effect induced by the divalent metal ion bound at the hydroxamate O,O site.

In this chapter a kinetic, thermodynamic and infrared spectroscopic investigation of the binding of Fe(III) to SHA is presented. For control purposes, the same study has been carried out also for the system Fe(III)/benzohydroxamic acid, BHA (Scheme 1.1 of Chapter 1). The obtained results show that the final product of the reaction corresponds to a complex as that depicted in Scheme 4.1; the thermodynamic and kinetic features of the process leading to formation of this complex have been worked out.

Prior to the study of the binding of Fe(III) to the above mentioned hydroxamic acids, the thermodynamic and kinetic behaviors of solutions of $Fe(ClO_4)_3$ have been investigated at different $HClO_4$ concentrations in order to better understand the mechanism of the metal-ligand binding reaction, which is coupled to metal hydrolysis and self-aggregation processes.

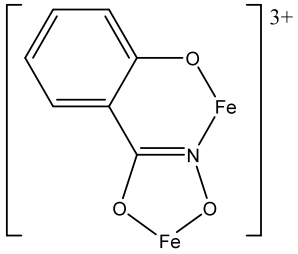

Scheme 4.1 *The structure assumed for the dinuclear complex of SHA that can represent the repetitive unit of a SHA based metallacrown.*

4.1 Fe(III) hydrolysis and self-aggregation equilibria

The processes of Fe(III) hydrolysis and self-aggregation in aqueous solution have been investigated by UV/VIS spectrophotometry, at I = 1 M ($NaClO_4$) and at $[H^+]$ values between 0.01 M and 1 M ($HClO_4$). Lower acid concentrations have not been used, in order to avoid precipitation of $Fe(OH)_3$. The spectrum of $Fe(ClO_4)_3$ in 1 M $HClO_4$ displays a band centred at 240 nm whose intensity becomes negligible at values of λ higher than 300nm (Figure 4.1A). The maximum intensity does not display any horizontal shift on changing the $Fe(ClO_4)_3$ concentration and a plot of the absorbance at 240 nm *vs* Fe(III) concentration (Figure 4.1B) yields a straight line; both observations indicate that the only species present at $[H^+]$ = 1 M is $Fe(H_2O)_6^{3+}$.

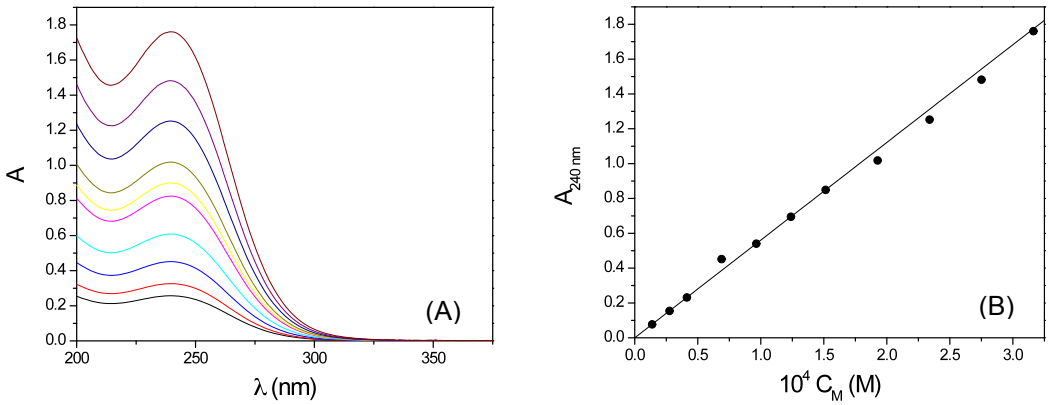

Figure 4.1 *(A) UV-visible spectra of $Fe(ClO_4)_3$; (B) Absorbance dependence on C_M at λ = 240 nm. $[H^+]$ = 1 M, $[Fe(ClO_4)_3]$ = 1.4×10^{-5} to 2.7×10^{-3} M; I = 1 M ($HClO_4$), T = 298 K.*

Figure 4.2A shows the spectrum of $Fe(ClO_4)_3$ at different concentrations, recorded at $[H^+]$ = 0.01 M. In this case, the absorption band moves towards higher wavelengths (a shoulder between 450 and 500 nm can be observed) and the Beer-Lambert law is not longer obeyed (Figure 4.2B), revealing the presence of more than a single species in solution and related equilibrium processes.

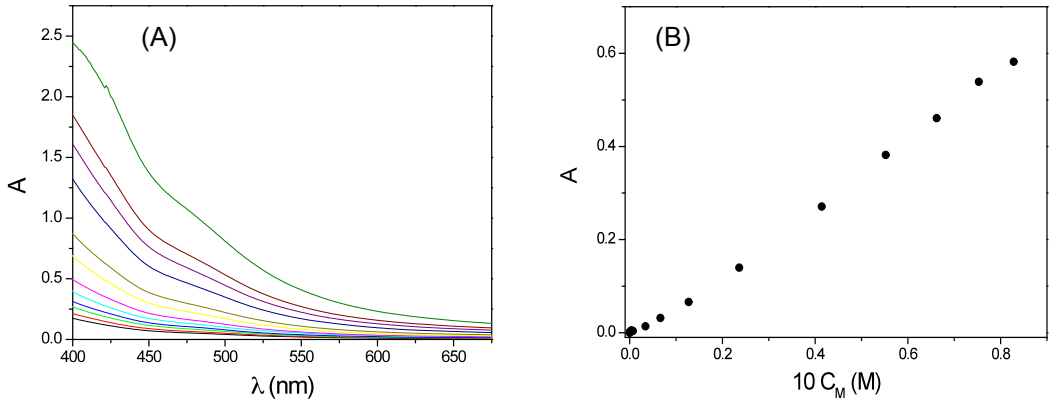

Figure 4.2 *(A) UV-visible spectra of $Fe(ClO_4)_3$; (B) Absorbance dependence on C_M at λ = 240 nm. $[H^+]$ = 1.2×10^{-2} M, $[Fe(ClO_4)_3]$ = 1.4×10^{-5} to 4.4×10^{-3} M; I = 1 M ($NaClO_4$), T = 298 K.*

The equilibria between the species are originated by hydrolysis and self-aggregation processes, which have been analyzed on the basis of the reaction Scheme 4.2. Reactions (4.1)-(4.3) are suggested by the results of the kinetic experiments described below.

$$Fe^{3+} + H_2O \underset{}{\overset{K_H}{\rightleftharpoons}} FeOH^{2+} + H^+ \qquad (4.1)$$

$$2FeOH^{2+} \underset{k_{-D}}{\overset{k_D}{\rightleftharpoons}} Fe_2(OH)_2^{4+} \qquad (4.2)$$

$$Fe_2(OH)_2^{4+} + FeOH^{2+} + H_2O \underset{k_{-T}}{\overset{k_T}{\rightleftharpoons}} Fe_3(OH)_4^{5+} + H^+ \qquad (4.3)$$

Scheme 4.2 *Reactions involved in Fe(III) hydrolysis and aggregation processes.*

Concerning the analysis of the static measurements of the equilibria (4.1)-(4.3), the absorbance of solutions of $Fe(ClO_4)_3$ was measured at different metal and acid concentrations and the data have been analysed using a multivariate non-linear least square treatment, as described in Appendix V. The values of K_H, $K_D = k_D/k_{-D}$, and $K_T = k_T/k_{-T}$ obtained by such an analysis are reported in Table 4..

Table 4.1 *Reaction parameters for hydrolysis and self-aggregation reactions of Fe(III); I = 1 M ($HClO_4/NaClO_4$), T = 298 K.*

10^3K_H (M)	$10^{-3}K_D$ (M^{-1})	$10^{-1}K_T$ (M^{-1})	$10^{-3}k_D$ ($M^{-1}s^{-1}$)	k_{-D} (s^{-1})	$10^{-1}k_T$ ($M^{-1}s^{-1}$)	k_{-T} (s^{-1})	k_D' [a] ($M^{-1}s^{-1}$)	k_{-D}' [a] (s^{-1})
1.9	2.3	4.9	[b]1.5 [c]1.3	[b] 0.56	[c]4.3	[c]1.1	65	0.030

[a] *rate parameters for reaction (4.5).*

[b] *from kinetics at $[H^+] = 0.1$ M.*

[c] *from kinetics at $[H^+] = 0.01$ M.*

4.2 Fe(III) hydrolysis and self-aggregation kinetics

Kinetics of the system (4.1)–(4.3) have been investigated using the stopped-flow technique. The experiments have been performed in the concentration-jump mode by mixing a given volume of a $Fe(ClO_4)_3$ solution, brought at the desired pH and ionic strength value, with an equal volume of water brought to the same pH and ionic strength value. Reaction (4.1) of Scheme 4.2 involves the proton loss/acquisition from a water molecule coordinated to Fe(III); this process is very fast and its rate cannot be measured by the stopped-flow technique; the kinetic effects measured should be thus related to the self-aggregation steps (4.2) and (4.3) of Scheme 4.2. Experiments at $[H^+] = 1$ M do not show any kinetic effect. Actually, according to the equilibrium data of Table 4.1 it can be deduced that, at $[H^+] = 1$ M, the species by far prevailing is the Fe^{3+} ion. On the other hand, stopped-flow experiments performed at $[H^+] = 0.1$ M give rise to monoexponential kinetic curves (Figure 4.3A), revealing the occurrence of a single kinetic effect.

The dependence of the time constant $1/\tau$ on $[Fe(ClO_4)_3]$, at this acidity value, is linear. The dynamic behavior of the system can be rationalized taking into account steps (4.1) and (4.2) of the reaction Scheme 4.2. At this level of the analysis step (4.3) can be neglected, as the equilibrium data of Table 4.1 show that, at $[H^+] = 0.1$ M, the trimer concentration is very small. Reaction (4.1) can be always considered equilibrated, as it is much faster than reaction (4.2). Under these circumstances the concentration dependence of the reciprocal relaxation time can be described by equation (4.4)

$$1/\tau_f = 4\, K_H\, k_D\, [FeOH^{2+}]/([H^+] + K_H) \;+\; k_{-D} \qquad (4.4)$$

where $[FeOH^{2+}]$ has been evaluated from C_M, the analytical Fe(III) concentration, using the relationship $[FeOH^{2+}] = \alpha_{FeOH} C_M$. The molar fraction of FeOH, α_{FeOH}, is evaluated as described in Appendix V. The plot of $1/\tau_f$ *vs* $[FeOH^{2+}]/([H^+]+K_H)$ is linear (insert of Figure 4.3A) and allows to obtain the values of k_D and k_{-D} as the slope and the intercept of the obtained straight line, respectively (Table 4.1).

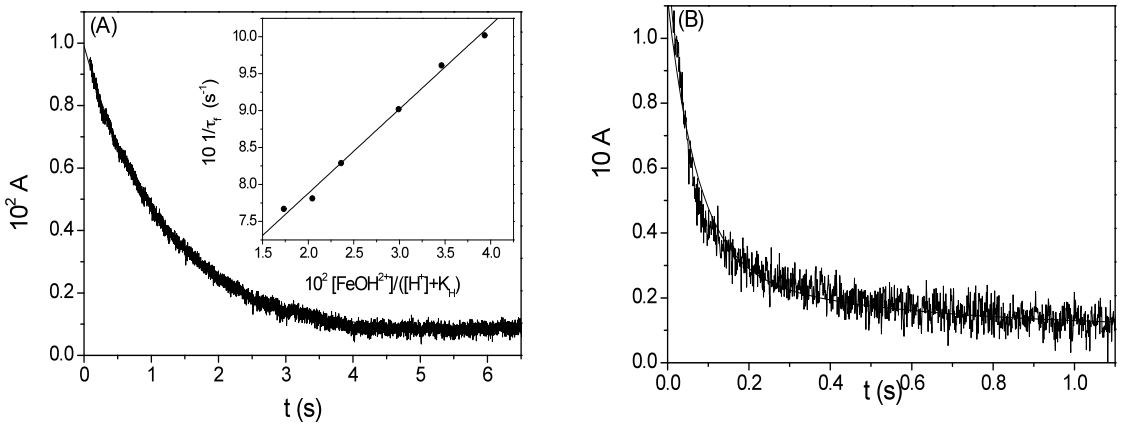

Figure 4.3 *Stopped-flow experiments showing the kinetic behavior of $Fe(ClO_4)_3$ solutions upon dilution jumps at I = 1 M ($HClO_4$/$NaClO_4$) and T = 298 K: (A) C_M = 0.11 M, $[H^+]$ = 0.1 M; (B) C_M = 0.036 M, $[H^+]$ = 0.01 M. Note that while curve (A) is perfectly monoexponential, curve (B) deviates from the monoexponential behavior shown by the continuous line. Inset: plot of the kinetic data according to equation (4.4).*

Table 4.2 shows that the values of $1/\tau_f$ decrease on rising the proton level up to $[H^+]$ = 0.1 M and then exhibit a small but well defined increase for 0.1 M ≤ $[H^+]$ ≤ 0.2 M. This behavior reveals that a further reaction step (step (4.5)), competes with step (4.2) for the formation of the dimer.

$$FeOH^{2+} + Fe^{3+} \underset{k'_{-D}}{\overset{k'_{D}}{\rightleftarrows}} Fe_2(OH)_2^{4+} + H^+ \qquad (4.5)$$

This process becomes more important at the highest investigated acidities, where the ratio $[Fe^{3+}]/[FeOH^{2+}]$ becomes high and where H_3O^+ can actively compete with H_2O to attack the dimer, thus favoring its decomposition into monomers.

Table 4.2. *Dependence of the relaxation times, $1/\tau_f$ and $1/\tau_s$ for the self-aggregation reaction of Fe(III) on the hydrogen ion concentration; $C_M = 0.1M$, $I = 1M$ ($HClO_4/NaClO_4$), $T = 298\ K$.*

$[H^+]$ (M)	$1/\tau_f$ (s^{-1})	$1/\tau_s$ (s^{-1})
0.01	13	2.2
0.02	4.3	1.7
0.03	2.3	1.5
0.04	1.4	-
0.05	1.3	-
0.06	1.1	-
0.08	0.83	-
0.10	0.77	-
0.13	0.78	-
0.16	0.85	-
0.20	1.1	-

Taking into account also reaction (4.5), the fast effect time constant dependence on $[H^+]$ turns into equation (4.6)

$$1/\tau_f = 4(k_D + k'_D[H^+]/K_H)(K_H/([H^+] + K_H))[FeOH^{2+}] + (k_{-D} + k'_{-D}[H^+]) \qquad (4.6)$$

An estimation of k'_D and k'_{-D} (Table 4.1) has been done by applying a statistical treatment to equation (4.6) imposing to K_H, k_D and k_{-D} the values previously obtained.

Experiments performed at $[H^+] = 0.01$ M give, instead, biexponential kinetic curves (Figure 4.3B). The change of behavior should be ascribed to the involvement of step (4.3) that, at this lower acidity level gives a considerable contribution to the observed kinetics. In this case the fast relaxation step could not be analyzed as a fast equilibrium not affected by the slow effect, because the two effects (steps (4.2) and (4.3)) are poorly separated in the time scale and influence each other. Therefore a full kinetic analysis of coupled reactions was applied to the Scheme 4.2. The Castellan's method (Castellan, 1963) was employed, which makes use of the exchange rates to obtain the concentration dependencies of fast ($1/\tau_f$) and slow ($1/\tau_s$) relaxation times (see Appendix VI). The rate constant of steps (4.2) and (4.3) have been evaluated by combining them as shown in equations (4.7) and (4.8), according to a procedure developed in our laboratory (D'Amico et al., 2002) which has been adapted to the present system (see Appendix VI).

$$1/\tau_f + 1/\tau_s = (4\chi_D + \chi_T)\, C_M + (\chi_{-D} + \chi_{-T}) \qquad (4.7)$$

$$1/\tau_f \times 1/\tau_s = 6\chi_D\chi_T C_M^2 + 4\chi_D\chi_{-T} C_M + \chi_{-D}\chi_{-T} \quad (4.8)$$

where χ_D, χ_T, χ_{-D} and χ_{-T} are apparent rate parameters linked to the individual rate constants of steps (4.2) and (4.3) as shown below. A plot according to equation (4.7) is shown in Figure 4.4A. The slope and intercept of the straight line interpolating the data points provide $4\chi_D + \chi_T = (139 \pm 2)\ M^{-1}s^{-1}$ and $\chi_{-D} + \chi_{-T} = (1.7 \pm 0.2)\ s^{-1}$ respectively. On the other hand, the parabolic function represented in Figure 4.4B, which corresponds to equation (4.8), enables us to obtain the parameters $6\chi_D\chi_T = (1.4 \pm 0.1)\times10^3\ M^{-2}s^{-2}$, $4\chi_D\chi_{-T} = (1.4 \pm 2)\times10^2\ M^{-1}s^{-2}$ and $\chi_{-D}\chi_{-T} = (1 \pm 0.7)\ s^{-2}$. Combination of these parameters yields the apparent rate constants, which are linked to the individual rate constant of Scheme 4.2 by the relationships $k_D = \chi_D K_H^2/(K_H + [H^+])^2$, $k_T = \chi_T K_H/(K_H + [H^+])$, $k_{-D} = \chi_{-D}$ and $k_{-T} = \chi_{-T}/[H^+]$. The rate constants evaluated at $[H^+] = 0.01$ M are reported in Table 4.1.

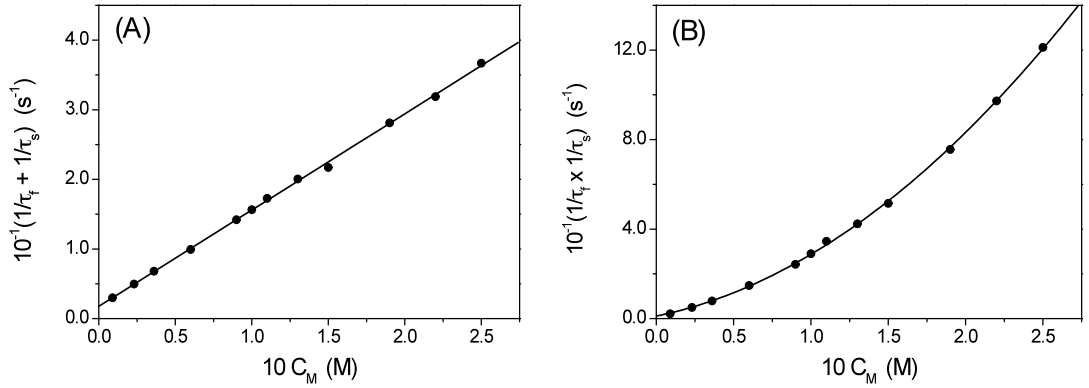

Figure 4.4 *Dependence $1/\tau_f + 1/\tau_s$ (A) and $1/\tau_f \times 1/\tau_s$ (B) on C_M at $[H^+] = 0.01$ M, I = 1 M ($HClO_4/NaClO_4$), T = 298 K.*

Special attention has been paid to the characteristic of the reverse reaction of step (4.3) since in literature two different formulas, $Fe_3(OH)_4^{5+}$ and $Fe_3(OH)_3^{6+}$, have been proposed for the trimer (Sommer and Margerum, 1970).

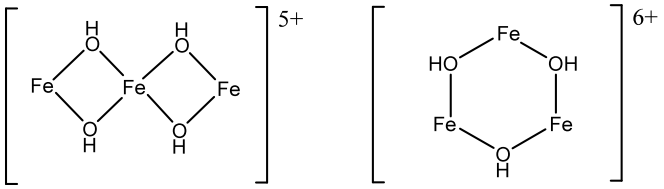

$Fe_3(OH)_4^{5+}$ $Fe_3(OH)_3^{6+}$

Scheme 4.3 *Proposed molecular structures for the Fe(III) trimer.*

If the trimer structure had corresponded to the formula $Fe_3(OH)_3^{6+}$, its formation from dimer and $FeOH^{2+}$ would not involve any loss of protons, thus the reverse step would be independent of the hydrogen ion concentration. On the contrary, formation of $Fe_3(OH)_4^{5+}$ should involve the loss of a proton with a consequent dependence of the reverse step on $[H^+]$. In order to clarify this point a series of experiments was devised where a solution containing the preformed trimer was mixed with given amounts of $HClO_4$ and the time constant of the trimer decomposition, $1/\tau_{diss}$, has been measured for each $[H^+]$ value. The rate constant $1/\tau_{diss}$ resulted to be directly proportional to $[H^+]$ (Figure 4.5), thus indicating that the main trimer formed is $Fe_3(OH)_4^{5+}$.

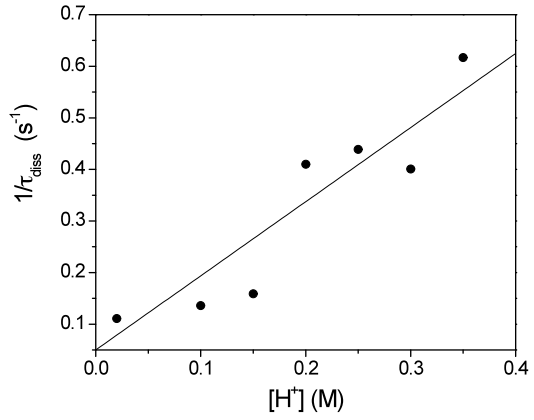

Figure 4.5 *Dependence of the rate constant of trimer decomposition on the hydrogen ion concentration; I = 1 M ($HClO_4$/$NaClO_4$), T = 298 K.*

Beside the above-described kinetic processes, a very slow reaction was detected in the time scale of hours (Figure 4.6). This reaction, whose time path was monitored by classical spectrophotometry, is ascribed to formation of more complex Fe(III) aggregates, and was not further investigated.

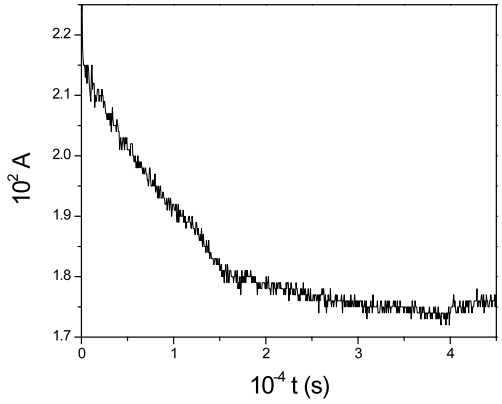

Figure 4.6 *Kinetic trace recorded by spectrophotometric measurements for Fe(III).* C_M = 2×10^{-4} *M,* λ = *532 nm,* $[H^+]$ = *0.1 M, I = 1 M* ($HClO_4/NaClO_4$) *and T = 298 K.*

4.3 Formation equilibria of the Fe(III)/BHA and Fe(III)/SHA complexes

The equilibria of the interaction of Fe(III) with BHA and SHA have been investigated by spectrophotometric titrations at I = 1 M ($NaClO_4$) in the acidity range 0.01 M ≤ [$HClO_4$] ≤ 1 M. All titrations were performed under conditions of metal excess in order to exclude formation of complexes as ML_2 or ML_3.

4.3.1 The Fe(III)/BHA system

Titrations of BHA with Fe(III) provide monophasic binding isotherms (Figure 4.7), which represent the formation of a 1:1 complex (ML_T), according to the apparent reaction (4.9)

$$M_f + L_f \overset{K_{1app}}{\rightleftarrows} ML_T \qquad (4.9)$$

where M_f and L_f represent free metal and free ligand, respectively.

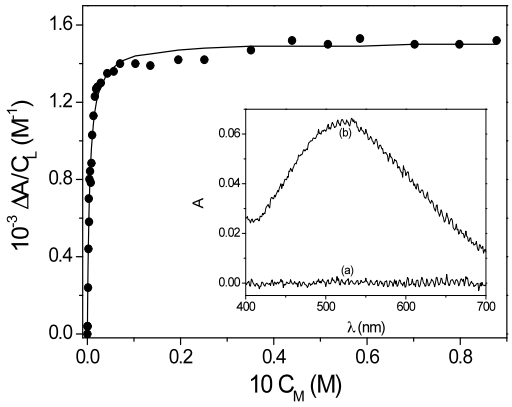

Figure 4.7 *Binding isotherm for the interaction of Fe(III) with BHA at I = 1 M ($HClO_4/NaClO_4$) and T = 298 K. Inset shows the spectral change induced by complex formation; [BHA] = 2.5×10^{-4} M, [H^+] = 0.1 M, inset: (a) C_M = 0 M, (b) C_M = 1.7×10^{-1} M.*

The binding isotherms have been analyzed according to equation (4.10)

$$\Delta A/C_L = \Delta\varepsilon\, K_{1app}\, C_M/(1 + K_{1app}\, C_M) \qquad (4.10)$$

where $\Delta A = (A - A_0)$, $\Delta\varepsilon = (\varepsilon_{ML} - \varepsilon_L - \varepsilon_M)$ and K_{1app} is the equilibrium constant of the apparent reaction (4.9). The dependence of K_{1app} on [H^+] displays the rather unusual behavior shown in Figure 4.8.

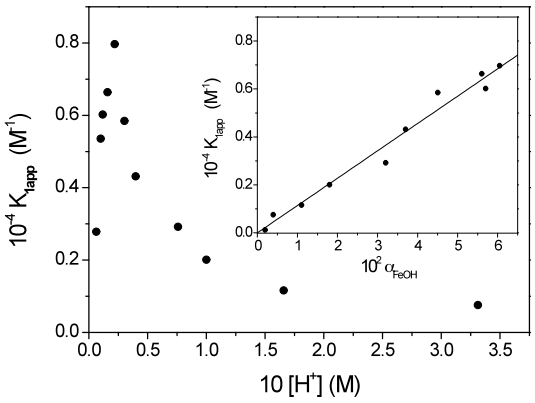

Figure 4.8 *Dependence of the apparent binding constant, K_{1app}, for the Fe(III)/BHA system on [H^+] at I = 1 M ($HClO_4/NaClO_4$) and T = 298 K. Inset: dependence of K_{1app} on α_{FeOH}, the molar fraction of $FeOH^{2+}$ ion.*

Such a dependence can be rationalized taking into account a mechanism involving coupling between the processes of complex formation and the processes of hydrolysis and aggregation of Fe(III). At $[H^+]$ values lower than 0.025 M dimer and trimer formation subtract metal to complexation, so K_{1app} decreases as $[H^+]$ tends to zero. At the highest $[H^+]$ values complex formation is also hindered because the concentration of the reactive species of the metal, $FeOH^{2+}$, is reduced. Moreover, for $[H^+] \geq 1M$, BHA tends to form the species $BHAH^+$ (Garcia et al., 2001), which is reluctant to bind the metal. As a result, the dependence of K_{1app} on $[H^+]$ exhibits a maximum. On the basis of the reaction Scheme 4.2 the $[H^+]$ dependence of K_{1app} is given by equation (4.11)

$$K_{1app} = \alpha_{FeOH} K_{ML} \qquad (4.11)$$

where K_{ML} is the equilibrium constant of reaction (4.12).

$$FeOH^{2+} + H_2L \overset{K_{ML}}{\rightleftarrows} FeHL^{2+} + H_2O \qquad (4.12)$$

A plot of K_{1app} *vs* α_{FeOH} according to equation (4.11) yields a straight line (insert of Figure 4.8) whose slope provides the value of K_{ML} reported in Table 4.3.

Table 4.3 *Reaction parameters for complex formation reactions of Fe(III) with BHA and SHA; I = 1 M ($HClO_4/NaClO_4$), T = 298 K.*

	$10^{-5} K_{ML}$ (M^{-1})	$10^{-2} K_{M2L}$ (M^{-1})	$10^{-4} k_1$ ($M^{-1}s^{-1}$)	$10k_{-1}$ (s^{-1})	$10^{-7} K_D k_2$ (s^{-1})	$K_D K_2 k_3/K_{ML}$ (s^{-1})	$k_{-3}K_{CH}$ ($M^{-1}s^{-1}$)
BHA	1.1	-	1.8	1.2	-	-	-
SHA	1.3	4.6	[a]1.4	[a]0.04	-	-	-
			[b]1.6	-	1.1	95	1.6

[a] *from data at $[H^+] = 1$ M,* [b] *from data at $[H^+] = 0.1$ M*

4.3.2 The Fe(III)/SHA system

The thermodynamic study of the Fe(III)/SHA system reveals two different behaviors depending on the medium acidity. For high [H^+] values the binding isotherms are monophasic as those obtained for the Fe(III)/BHA system while for lower [H^+] values they become biphasic (Figure 4.9), indicating that, under these circumstances, a further binding step becomes operative.

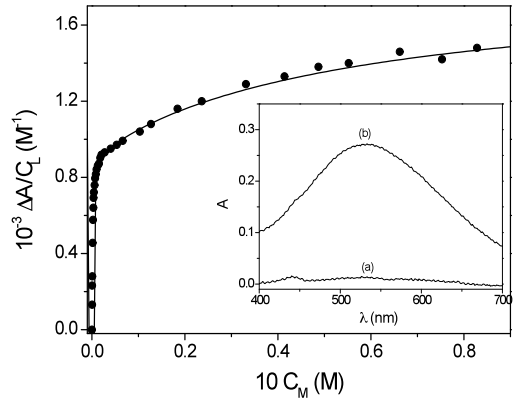

Figure 4.9 *Binding isotherms for the interaction of Fe(III) with SHA* at *I=1 M ($HClO_4$/$NaClO_4$) and T = 298 K. Inset shows the spectral change induced by complex formation; [SHA] = 2.5×10^{-4} M, [H^+] = 0.022 M, inset: (a) C_M = 0 M, (b) C_M = 1.7×10^{-1} M.*

Therefore, formation of a dinuclear complex has been supposed, according to equation (4.13).

$$FeH_2L^{2+} + FeOH^{2+} \overset{K_{M2L}}{\rightleftarrows} Fe_2L^{3+} + H_3O^+ \qquad (4.13)$$

Titration curves have been analyzed using equation (4.14) (Rossotti and Rossotti, 1961).

$$\Delta A/C_L = (\Delta\varepsilon_1 K_{1app} C_M + \Delta\varepsilon_2 K_{1app} K_{2app} C_M^2)/(1+K_{1app} C_M + K_{1app} K_{2app} C_M^2) \qquad (4.14)$$

where $\Delta\varepsilon_1 = (\varepsilon_{MLT} - \varepsilon_{Lf} - \varepsilon_{Mf})$, $\Delta\varepsilon_2 = (\varepsilon_{M2LT} - \varepsilon_{Lf} - \varepsilon_{Mf})$, and K_{2app} is the equilibrium constant for formation of M_2L_T from reaction of ML_T with M_f. Note that, in the case of monophasic behavior, equation (4.14) is reduced to equation (4.10).

The values of both K_{1app} and K_{2app} depend on [H^+] as shown in Figure 4.10A and 4.10B, respectively.

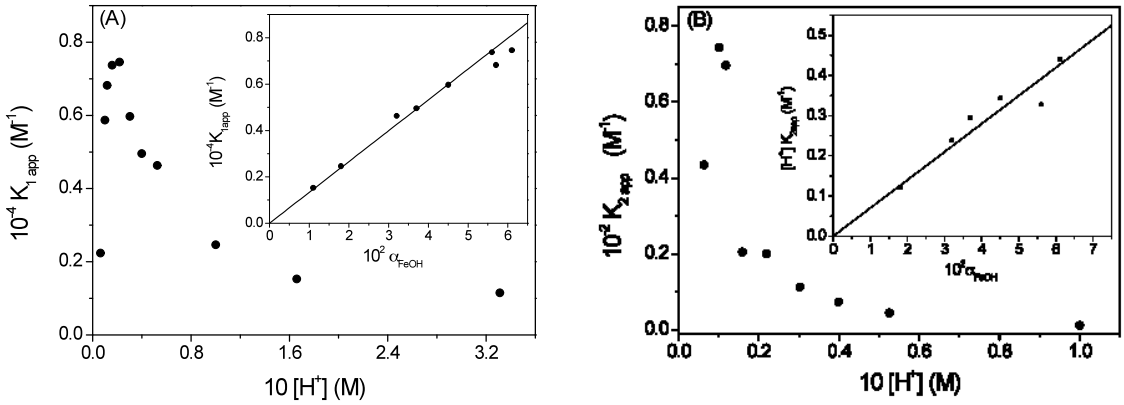

Figure 4.10 *Dependence of the apparent binding constants, K_{1app} and K_{2app}, for the Fe(III)/SHA system on $[H^+]$ at I = 1 M ($HClO_4/NaClO_4$) and T = 298 K; (A) plot of K_{1app} vs $[H^+]$, inset: dependence of K_{1app} on α_{FeOH}. (B) plot of K_{2app} vs $[H^+]$, inset: dependence of $[H^+]\times K_{2app}$ on α_{FeOH}.*

The trend of K_{1app} is similar to that observed for the Fe(III)/BHA system and has been analyzed using equation (4.11), being now $K_{ML} = [FeH_2L^{2+}]/[FeOH^{2+}][H_3L]$, while the trend of K_{2app} has been analyzed using the equation (4.15)

$$K_{2app} = K_{M2L}\,\alpha_{FeOH}/[H^+] \qquad (4.15)$$

A plot of $[H^+]\times K_{2app}$ *vs* α_{FeOH} yields the value of K_{M2L}, the equilibrium constant of reaction (4.13). The values of K_{ML} and K_{M2L} are reported in Table 4.4.

4.4 Fe(III)/BHA and Fe(III)/SHA complexes formation kinetics

The kinetics of Fe(III) binding to BHA and SHA have been investigated under pseudo-first order conditions ($C_M/C_L \geq 10$) using the stopped-flow method. For both systems coupling of complex formation with Fe(III) hydrolysis and self-aggregation processes has been taken into account.

4.4.1 The Fe(III)/BHA system

The kinetic traces obtained for the binding of Fe(III) to BHA are monoexponential (Figure 4.11) and the dependence of $1/\tau$ on C_M is linear (Figure 4.12) in the range of $[H^+]$ concentration between 0.1 M and 1 M.

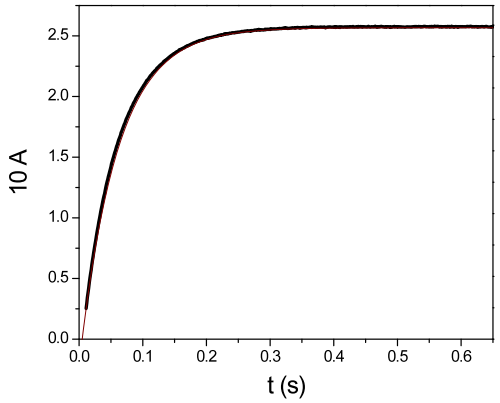

Figure 4.11 *Stopped-flow traces recorded at λ = 520 nm upon mixing BHA 2.5×10^{-4} M and $Fe(ClO_4)_3$ 9.0×10^{-3} M at I = 1 M ($HClO_4/NaClO_4$) and T = 298 K.*

The rate of reaction largely increases on reducing $[H^+]$ from 1 M to 0.1 M, in parallel with the increase of $[FeOH^{2+}]$ induced by the $[H^+]$ reduction. This observation indicates that $FeOH^{2+}$ is the reactive species, while the hexa-aquoion Fe^{3+}, although present in large excess at both acidity levels, reacts with BHA to a negligible extent. It can be assumed, therefore, that, in the case of BHA, the prevailing binding step is represented by reaction (4.12).

Taking into account that reaction (4.12) is coupled to the hydrolysis and self-aggregation steps through the common species $FeOH^{2+}$ and that $[M_f] \approx C_M$, the concentration dependence of the relaxation time of the complex formation reaction is given by the relationship (4.16) where $\alpha_{FeOH}C_M = [FeOH^{2+}]$.

$$1/\tau = k_1 \alpha_{FeOH} C_M + k_{-1} \qquad (4.16)$$

Equation (4.16) also explains the kinetic behavior of the system at $[H^+]$ = 0.01M. Here, a descending deviation from linearity can be observed in the plot of $1/\tau$ *vs* C_M (Figure 4.12).

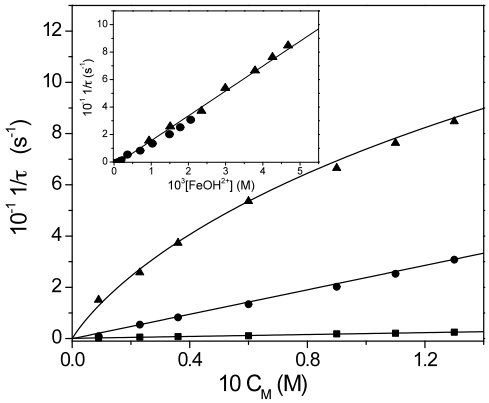

Figure 4.12 *Dependence of $1/\tau$ on C_M at different $[H^+]$ values for the Fe(III)/BHA system at I = 1 M ($HClO_4/NaClO_4$) and T = 298 K; [BHA] = 2.5×10^{-4} M, $[H^+]$ =1 M ■, 0.1 M ●, 0.01 M ▲. The inset represents the dependence of $1/\tau$ on $[FeOH^{2+}]$, calculated at all acidities by the relationship $[FeOH^{2+}] = a_{FeOH} C_M$.*

Such a deviation depends on the behavior of α_{FeOH} that, at $[H^+]$ = 0.01M, decreases as the metal ion content is raised, owing to the self-aggregation steps, which become more important and subtract the reactive species $FeOH^{2+}$ to the binding process. When considering, instead, a plot of $1/\tau$ *vs* $[FeOH^{2+}] = \alpha_{FeOH} C_M$ (insert of Figure 4.12), all data points lie on a single straight line according to equation (4.16), which provides the values of k_1 and k_{-1} collected in Table 4.4.

4.4.2 The Fe(III)/SHA system

For this system kinetics are still monoexponential at $[H^+]$ = 1.0 M, provided that $C_M \leq$ 0.04 M (Figure 4.13A).

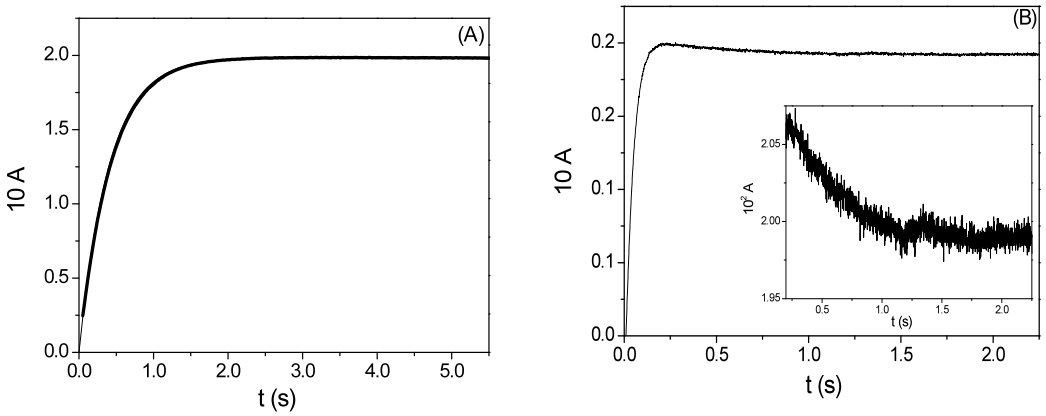

Figure 4.13 *Stopped-flow traces recorded at λ = 532 nm upon mixing SHA 2.5×10^{-4} M and $Fe(ClO_4)_3$ 9.0×10^{-3} M at I = 1 M ($HClO_4/NaClO_4$) and T = 298 K; (A) $[H^+]$ = 1.0 M (monoexponential trace), (B) $[H^+]$ = 0.01 M (biexponential trace). The inset shows the slowest of the two effects on a magnified scale.*

In these conditions the metal concentration dependence of the relaxation time is linear (Figure 4.14A), as for the system Fe(III)/BHA. Hence, the observed kinetic effect is ascribed, also in this case, to formation of a mononuclear complex between Fe(III) and SHA.

The behavior becomes more complex at $[H^+]$ = 0.1 M and even more at $[H^+]$ = 0.01 M (Figure 4.13B). Actually, the system displays now two kinetic effects, in contrast with the behavior of the Fe/BHA system where, under similar conditions, simple kinetics have been observed. The metal concentration dependence of the faster effect is parabolic (Figure 4.14B), revealing a second-order dependence of the corresponding binding step with respect to the metal ion. On the other hand, the rate constant of the slow kinetic effect displays a linear dependence on $[FeOH^{2+}]$ (Figure 4.14C).

The kinetic features of the Fe(III)/SHA system can be rationalized on the basis of the reaction Scheme 4.4 where H_3L denotes the uncharged triprotonated SHA molecule.

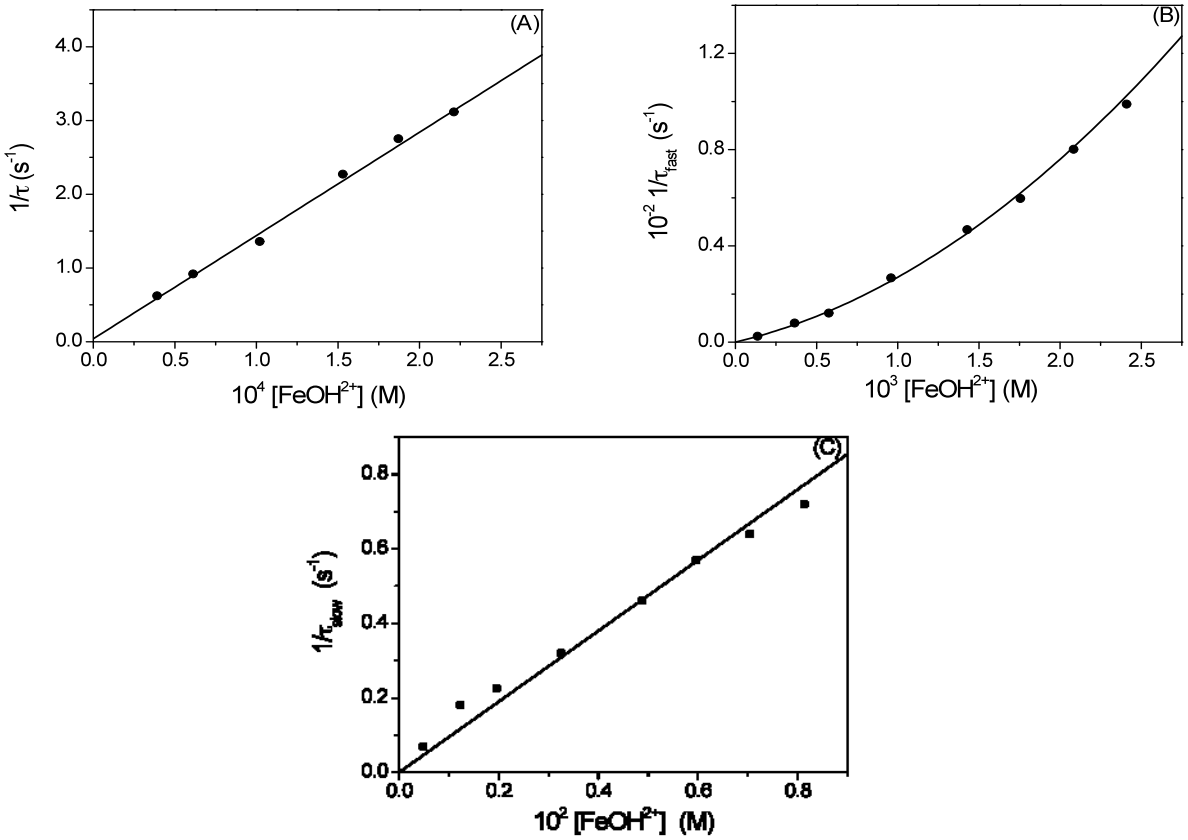

Figure 4.14 *Dependence of the relaxation time on [$FeOH^{2+}$] for the Fe(III)/SHA system under different acidity conditions at I = 1 M ($HClO_4$/$NaClO_4$) and T = 298 K; (A) [H^+] = 1.0 M; (B) [H^+] = 0.1 M (fast effect); (C) [H^+] = 0.1 M (slow effect).*

Fast effect:

$$FeOH^{2+} + H_3L \underset{k_{-1}}{\overset{k_1}{\rightleftharpoons}} FeH_2L^{2+} + H_2O \qquad (4.17)$$

$K_D \Big\| \; FeOH^{2+} \qquad\qquad K_C \Big\| \; FeOH^{2+}$

$$Fe_2(OH)_2^{4+} + H_3L \underset{k_{-2}}{\overset{k_2}{\rightleftharpoons}} Fe_2OHH_2L^{4+} + H_2O \qquad (4.18)$$

Slow effect:

$$Fe_2OHH_2L^{4+} \underset{k_{-3}}{\overset{k_3}{\rightleftharpoons}} Fe_2HL^{4+} + H_2O \overset{1/K_{CH}}{\rightleftharpoons} Fe_2L^{3+} + H_3O^+ \qquad (4.19)$$

Scheme 4.4 *Reaction scheme for Fe(III) complexation with SHA.*

Since the two kinetic effects are widely separated in the time scale, the fast step has been analyzed separately from the slow one, while, in the analysis of the slow effect, reactions (4.17) and (4.18) are taken into account as pre-equilibrium steps. The expressions of the relaxation times for the two kinetic effects (equation (4.20) and (4.21)) have been derived as described in Appendix VII. The values of the parameters obtained by this analysis are reported in Table 4.4.

$$1/\tau_{fast} = k_1[FeOH^{2+}] + K_D k_2[FeOH^{2+}]^2 + (k_{-1} + K_C k_{-2}[FeOH^{2+}])/(1 + K_C[FeOH^{2+}]) \quad (4.20)$$

where $K_C = [Fe_2OHH_2L^{4+}]/[FeH_2L^{2+}][FeOH^{2+}]$;

$$1/\tau_{slow} = K_D K_2 k_3[FeOH^{2+}]^2/(1+K_1[FeOH^{2+}] + K_2 K_D[FeOH^{2+}]^2) + k_{-3}K_{CH}[H^+]/(1+K_{CH}[H^+]) \quad (4.21)$$

where $K_{CH} = [Fe_2\ HL^{4+}]/[Fe_2L^{3+}][H^+]$.

The fast effect has been analyzed according to equation (20). Since the intercept of the parabolic function expressing $1/\tau_{fast}$ *vs* $[FeOH^{2+}]$ is close to zero (Figure 4.14B), the third term of equation (4.20) has been neglected. Concerning the slow effect, the linear dependence of $1/\tau_{slow}$ on $[FeOH^{2+}]$ (Figure 4.14C) indicates that in the denominator of the second term of equation (4.21) the inequality $K_1[FeOH^{2+}] >> 1 + K_2K_D[FeOH^{2+}]^2$ holds. The intercept value obtained from the plot of Figure 4.14C is very small, hence the contribution of the reverse step of reaction (4.19) cannot be evaluated using equation (4.21). For this reason, the slow reaction has been investigated in the reverse direction by mixing in the stopped flow apparatus the preformed 2:1 complex with known amounts of $HClO_4$. Dependence of the time constant on the acid concentration is linear (Figure 4.15), in agreement with reaction (4.19), where just one proton is involved. Therefore, in equation (4.21) it must be $K_{CH}[H^+] << 1$ and so the slope of the straight line of Figure 4.15 directly yields $k_{-3}K_{CH}$.

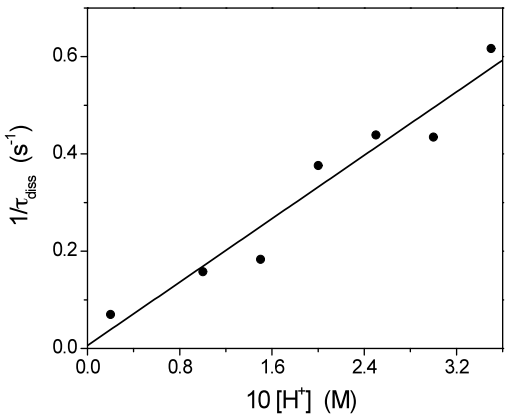

Figure 4.15 *Dependence of the rate dissociation, $1/\tau_{diss}$, on the hydrogen ion concentration for the Fe(III)/SHA system at I = 1M ($HClO_4/NaClO_4$), T = 298 K.*

4.5 FTIR Experiments

Infrared spectra of aqueous solutions of BHA and SHA have been recorded at pH = 1.66 ($[H^+]$ = 0.022 M) and *I* = 1 M. Moreover, the spectra of Fe(III)/ligand mixtures in the stoichiometric ratio C_M/C_L = 1 and 2 have been recorded also at pH = 1.66, where the extent of complex formation is maximum. Concerning the Fe(III)/BHA system, Figure 4.16A shows that the peaks corresponding to the vibrational frequency of N-H (3300 cm^{-1}) (Artemenko et al., 1980; Kaczor et al., 2005) do not display a remarkable change on going from free BHA solution to mixtures of BHA and $Fe(ClO_4)_4$. Therefore, comparison of the spectra shows clearly that Fe(III) is chelated by BHA through the O,O oxygen atoms, and that only the 1:1 complex is formed.

Concerning the Fe(III)/SHA system, comparison of the spectrum of free SHA with those of the C_M/C_L = 1 and C_M/C_L = 2 mixtures (Figure 4.16B) shows that, as in the case of the Fe(III)/BHA system, Fe(III) binds to SHA through the O,O oxygen atoms. Moreover, comparison of the spectral behavior of the C_M/C_L = 1 and C_M/C_L = 2 mixtures reveals that the bands corresponding to the phenol O_P-H (3463 cm^{-1}) and N-H stretching (3300 cm^{-1}) (Artemenko et al., 1980; Kaczor et al., 2005) which, in the C_M/C_L = 1 mixture, are well evident (although overlapped) between 3000 and 3400 cm^{-1}, are reduced to a large extent in the C_M/C_L = 2 mixture. This result indicates that in the binuclear complex the second Fe(III) ion is bound to SHA through the O_P,N site.

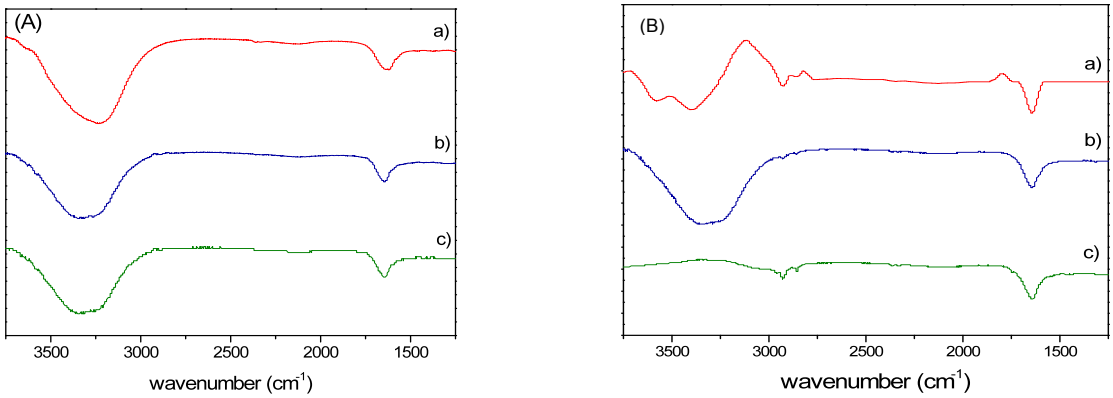

Figure 4.16 *FTIR spectra of the investigated systems; [H⁺] = 0.022 M, I = 1M ($HClO_4/NaClO_4$), T = 298 K. [BHA] or [SHA] = 5×10^{-3} M. (A) The Fe(III)/BHA system: a) BHA, b) Fe(III):BHA = 1:1, c) Fe(III):BHA = 2:1. (B) The Fe(III)/SHA system: a) SHA, b) Fe(III):SHA = 1:1, c) Fe(III):SHA = 2:1.*

4.6 Discussion

4.6.1 Fe(III) hydrolysis and self-aggregation

Fe(III) aggregation processes have been widely investigated since long time (Wendt, 1969; Sommer and Margerum, 1970; Baes and Mesmer, 1976), even though some controversies still remained, expecially concerning the trimer structure (Sommer and Margerum, 1970). Some results obtained in this thesis are in good agreement with those already present in literature; other ones represent a novelty feature, which better clarifies the aggregation reaction mechanism.

The value of the equilibrium constant for dimer formation obtained in this work from kinetics, as $k_D/k_{-D} = 2.7\times10^3$ M, compare quite satisfactory with the value derived from the spectrophotometric titration (Table 4.1). Moreover, both values compare very well with the literature data (Baes and Mesmer, 1976). Actually, the equilibrium constant for dimerization, K_D, obtained in this thesis can be converted to the value quoted by Baes and Mesmer, K_D^{BM} (2.3×10^{-3} M at *I* = 1 M and 298 K), using the relationship $K_D^{BM} = [Fe_2O^{4+}][H^+]/[Fe^{3+}]^2 = K_D\times K_H^2$. On applying such an equation we obtain $K_D^{BM} = 2.7\times10^{-3}$ M.

The rate constant k_D (Table 4.1) obtained in this work (I = 1.0 M) has been compared with that published by Sommer and Margerum (6.4×10^2 M s^{-1}, *I* = 4.0 M, *T* = 298 K) (Sommer and Margerum, 1970). Their ratio, $k_{D,\ I=4.0M}/k_{D,\ I=1.0M}$ gives a value of 0.46, according to

Davies equation (Davies, 1962), where, for a bimolecular reaction having reactant charge product +4, the general rate constant ratio, $k_{I=4.0M}/k_{I=1.0M}$ has to be equal to 0.5.

On the other hand, the same procedure shows that our rate constant k_D is somewhat higher than the value of 8.1×10^2 M^{-1} s^{-1} derived by conversion at I = 1 M of the Wendt datum (4.5×10^2 M^{-1} s^{-1}, $I = 0.6$ M, $T = 298$ K (Wendt, 1969)) using the Güntelberg equation (Guntelberg, 1926).

Concerning the reverse step, our value of k_{-D} should be considered in agreement with the value of 0.42 s^{-1} reported by Po and Sutin (Po and Sutin, 1971) who investigated the dimer dissociation, but somewhat higher than that obtained by Sommer and Margerum (Sommer and Margerum, 1970).

Concerning the process of formation/dissociation of the trimer, Table 4.1 shows that the agreement between the value of K_T obtained from static experiments and that obtained from kinetics as k_T/k_{-T} is excellent. Two possible structures have been assumed for trimer (Sommer and Margerum, 1970) namely $Fe_3(OH)_4^{5+}$ and $Fe_3(OH)_3^{6+}$ (Scheme 4.3). $Fe_3(OH)_3^{6+}$ can form straightforward by addition of the $FeOH^{2+}$ ion to the dimer, whereas formation of $Fe_3(OH)_4^{5+}$ would require the improbable encounter of $Fe_2(OH)_2^{4+}$ with the doubly hydrolysed monomer $Fe(OH)_2^{+}$ present in extremely low amounts. Alternatively, $Fe_3(OH)_4^{5+}$ could be formed by the evolution of $Fe_3(OH)_3^{6+}$. If this were the case equation (4.3) should be rewritten in more detailed form, corresponding to equation (4.22).

$$Fe_2(OH)_2^{4+} + FeOH^{2+} + H_2O \rightleftarrows Fe_3(OH)_3^{6+} + H_2O \overset{K_B}{\rightleftarrows} Fe_3(OH)_4^{5+} + H^+ \qquad (4.22)$$

According to reaction (4.22), the rate constant for the process of trimer dissociation, $1/\tau_{diss}$, would be expressed by equation (4.23) where K_B is the acid dissociation constant of the $Fe_3(OH)_3^{6+}$ ion.

$$1/\tau_{diss} = k_T[H^+]/(K_B + [H^+]) \qquad (4.23)$$

The linear dependence of $1/\tau_{diss}$ on $[H^+]$ indicates that $K_B >> [H^+]$ and, therefore, that $[Fe_3(OH)_4^{5+}] >> [Fe_3(OH)_3^{6+}]$.

Finally, concerning the very slow step that has been observed, it has been ascribed to formation of more extended aggregates whose structure is difficult to predict. On the basis of this work results and previous literature data, it is only possible to guess that they could

form by addition of the $FeOH^{2+}$ ion to an already formed aggregate since the union of two identical aggregates is disfavored by the electrostatics of the system. For instance, the union of two dimers to give a tetramer (charge product = +16) experiences a repulsion effect larger than that corresponding to the union of a trimer with $FeOH^{2+}$ (charge product = +10). Actually, simple calculations based on the electrostatic theory of electrolytes (Prue, 1966) show that the increased repulsion results in a free energy penalty of 4.3 kcal mol^{-1} when the charge product rises from +10 to +16.

4.6.2 Complex formation of Fe(III) with BHA and SHA

It has been found that the value of K_{ML} reported in Table 4.3 for the Fe(III)/BHA 1:1 complex compares excellently with $K_{ML} = Q_f/K_H = 1.0\times10^5$ M^{-1} derived from Q_f = [FeHL][H]/[Fe][H_2L] = 1.7×10^2 measured by Monzyk and Crumbliss at 25°C and I = 1.1 M ($HClO_4$/$NaClO_4$) (Monzyk and Crumbliss, 1979). The kinetic study demonstrates that in the formation of the 1:1 complexes the reactive form of Fe(III) is $FeOH^{2+}$. Although a small contribution from $Fe(H_2O)_6^{3+}$ could be expected (Monzyk and Crumbliss, 1979) and experimentally found for instance in Fe(III)/Salicylate systems (Mentasti et al., 1982), this was found to be negligible in the explored range of concentrations of the present investigation. The value of k_1 for Fe/BHA reported in Table 4.3 compares fairly well with the value of 4.3×10^3 $M^{-1}s^{-1}$ by Monzyk and Crumbliss at I = 2 M (Monzyk and Crumbliss, 1979).

More important for the focus of the present work, are the results concerned with the binding of the second Fe(III) ion to SHA. According to the reaction Scheme 4.4 the species $[Fe_2OHH_2L]^{4+}$ can form by direct attack of H_3L to the dimer $Fe_2(OH)_2^{4+}$ or/and by reaction of the $FeOH^{2+}$ monomer with the FeH_2L monochelate. According to the Scheme 4.4 it turns out that $K_C = K_DK_2/K_1$ = 5.2 M^{-1}. This finding indicates that the formation of $Fe_2OHH_2L^{4+}$ from FeH_3L^{3+} and $FeOH^{2+}$ is largely disfavored with respect to the interaction of the dimer with H_3L. It should be mentioned that direct attacks of $Fe_2(OH)_2^{4+}$ to ligands were observed in the case of Tiron (Chatlas and Jordan, 1994), tropolone (Secco et al., 1999), and 5-nitro tropolone (Secco and Venturini, 1999). However, the dimeric complexes observed in these systems, behave as unstable species (Chatlas and Jordan, 1994; Lente and Fabian, 2002), which loose a Fe^{3+} or $FeOH^{2+}$ ion leaving the 1:1 complex as the final product of the complex formation reaction. On the contrary, in the case of the Fe(III)/SHA system, here investigated, the dinuclear complex is a stable species, as

indicated by the UV-vis, kinetic and IR experiments. The stabilization of the second iron atom within a single ligand molecule is undoubtedly provided by the O_P,N site of SHA, as in the case of BHA, which is lacking in the phenol group, none of the used techniques revealed the presence of a dinuclear complex.

The study of the ability of SHA to form a dinuclear complex with Fe(III) is interesting in the perspective of its ability to form metallacrowns. Moreover, the dinuclear complex observed in this work is stabilized by the high charge density of Fe^{3+} ion, which facilitates the expulsion of protons from the O_P,N site. The obtained results (the linear increase of the rate of decomposition of the dinuclear complex on rising $[H^+]$, the FTIR spectra, the ability of the proposed mechanism to explain the experimental data) all conduct to the deduction that both Fe(III) ions are chelated by the two reaction sites of SHA while the ligand is fully deprotonated, in agreement with the structure shown in Scheme 4.1. This structure displays the sequence Fe(A)–N–O–Fe(B) which constitutes the network linking the metals contained in the ring of metallacrowns such as the 12-MC-4 and 15-MC-5 (Pecoraro et al., 1996; Mezei et al., 2007).

The study described in this chapter has been published in Inorganic Chemistry (Beccia et al., 2011).

CHAPTER 5

Metallacrowns: mechanism of formation of Cu(II)/(S)-α-alaninehydroxamic acid 12-MC-4 and its interaction with La(III).

Aminohydroxamic acids are among the ligands most extensively employed for the synthesis of metallacrowns (MCs). They are characterized by the presence of an amino ($-NH_2$) and a hydroxamic acid functional group (-CO-NH-OH) separated by a spacer. In aliphatic aminohydroxamates, the spacer consists of a chain of one, two or three carbon atoms, leading to α-, β- and γ-aminohydroxamic acids, respectively (Scheme 5.1).

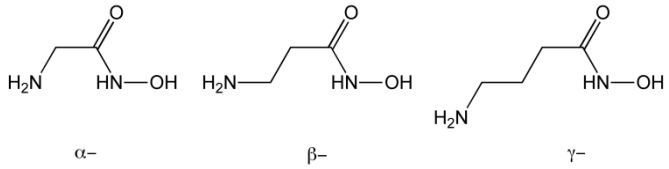

Scheme 5.1 *Representations of α-, β-, and γ-aminohydroxamic acids.*

Aminohydroxamic acids in their deprotonated form are able to bind metal ions, and the three most relevant coordination modes are depicted in Scheme 5.2 (Kurzak et al., 1991).While the coordination modes 3(A) and 3(B) give rise to mononuclear metal complexes, the third coordination mode 3(C) that is the same observed for the system Fe(III)/SHA, described in the previous chapter, is essentially associated to the formation of polynuclear species (Farkas and Buglyó, 1990; Kurzak et al., 1991; Kroczewska et al., 2006).

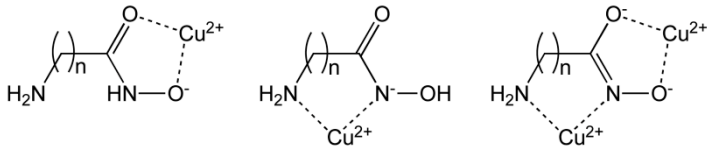

Scheme 5.2 *Coordination modes of aminohydroxamic acids (n = 1, 2 or 3 for α-, β-, and γ-aminohydroxamic acids, respectively.(A) (O,O-); (B) (N,N-); (C) (N,N)-(O-,O-).*

Actually by self-assembly of a proper number of such dinuclear complexes, a closed structure, denoted as metallacrown, can be obtained (Scheme 5.3).

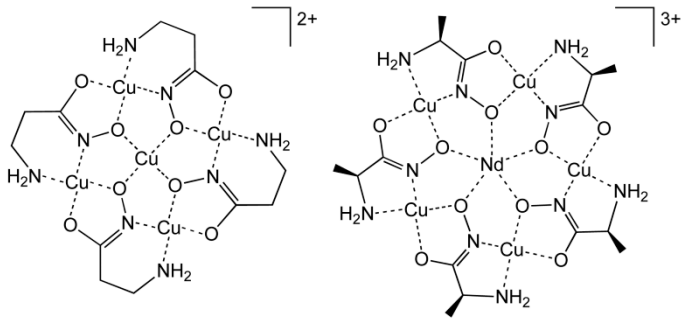

(A) (B)

Scheme 5.3 *Representation of (A) 12-MC-4 of Cu(II) and β-alaninehydroxamic acid (β-Alaha); (B) 15-MC-5 of Cu(II), Nd(III) and (S)-α-alaninehydroxamic acid (α-Alaha).*

Metallacrowns are able to encapsulate a *core metal ion* in the central oxygen cavity, while the other metal ions involved in the bridging coordination of the ligands are called *ring metals* (Tegoni and Remelli, 2012). This chapter focuses on processes involving MCs containing Cu^{2+} as the ring metal in the metallacrown scaffold.

As 12-MC-4 complexes are topologically related to squares (Scheme 5.3A), the most favorable arrangement is achieved by making use of β-aminohydroxamates as ligands. In fact, by bisecting the chelating rings formed by β-aminohydroxamates, an angle of 90° is obtained (Scheme 5.4(A)).

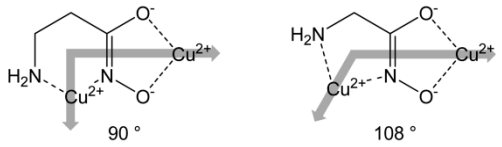

(A) (B)

Scheme 5.4 *Structures of the conceptual building blocks of metallacrowns: 12-MC-4 (A) and 15-MC-5 (B).*

A number of Copper(II) 12-MC-4 with different β-aminohydroxamates were isolated and extensively characterized in the solid state(Gibney et al., 1994). On the other hand, α-aminohydroxamates were employed in the synthesis of 15-MC-5 (Scheme 5.3B) containing Cu(II) as ring metal and lanthanides(III), calcium(II) or uranyl(VI) as core metal; in fact for these ligands the topological requirements are satisfied with the formation

of a pentagon-like metallamacrocycle(Stemmler et al., 1999). The wider angle (108°) in α-aminohydroxamates (Scheme 5.4b) leads to a planar arrangement of the structure with formation of a 15-membered metallamacrocycle. These geometric requirements constitute the basis of the "metallacrown structural paradigm"(Pecoraro et al., 1997),proposed by Lah and Pecoraro in the early 1990s. On the other hand, in 2001 it was demonstrated that also α-aminohydroxamates can form copper(II) 12-MC-4 complexes in solution (Tegoni et al., 2008), for which a non-planar and tensioned cup-like structure was proposed. This complex has been isolated in the solid state as a powder but not yet been structurally characterized (Seda et al., 2006),although its structure has been supported by DFT calculations (Tegoni et al., 2008).

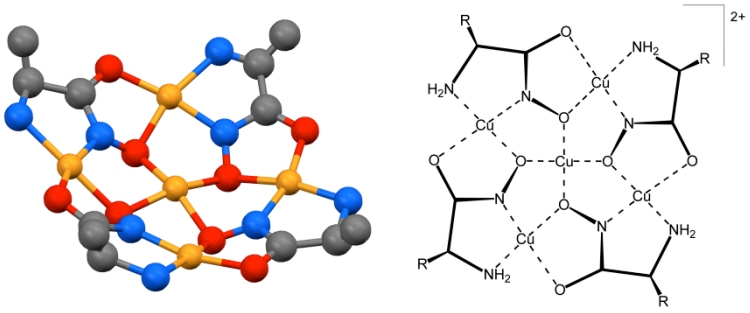

Figure 5.1 *Representation of the 12-MC-4 metallamacrocycle of Cu(II) and α-aminohydroxamic acids. The ball and stick representation on the left shows the cup-shaped arrangement of the scaffold.*

Both the 12-MC-4 and the 15-MC-5 complexes are self-assembled molecular architectures. In fact, when the proper conditions (for instance metal-to-ligand stoichiometric ratios and pH) are satisfied, metallacrowns assemble in solution with no need for the operator to address the assembly. However, no specific studies on the mechanism of these self-assemblies with the possible identification of transient species are reported so far in the literature.

5.1 12-MC-4 self-assembly equilibrium

An attempt to investigate the equilibria present in the Cu(II)/(S)-α-Alaha system has been made using UV spectrophotometry. Titration of (S)-α-Alaha with a Cu(II) solution has been carried out at pH=4.75 and I = 0.1 M. By analyzing the absorbance at 340 nm, where the spectral change is the largest, a binding isotherm has been obtained which reveals the formation of 12-MC-4 (Figure 5.2).

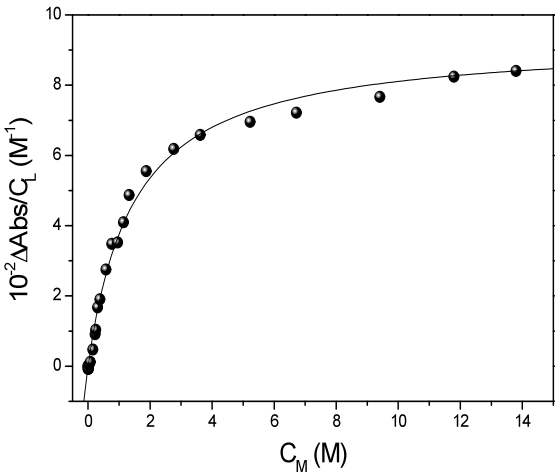

Figure 5.2 *Binding isotherm for the reaction between Cu(II) and (S)-α-Alaha. C_L=2.5×10^{-4} M. λ= 340 nm; I=0.1 M; pH=4.5; T=298 K.*

However, previous investigations on the equilibria of the Cu(II)/(S)-α-Alaha system, based on the evaluation of the number of protons emitted during complexation, proved that at pH = 4.5 the species $[CuL]^+$ exists too, as shown in Figure 5.3 (Careri et al., 2003). Therefore, titration curve of Figure 5.2 includes the contributions of the reaction of formation of both 12-MC-4 and $[CuL]^+$.

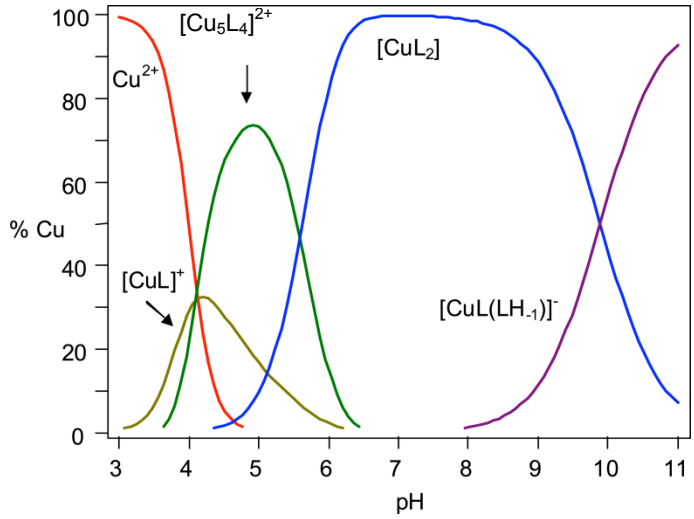

Figure 5.3 *Representative distribution diagram of the Cu(II)/(S)-α-Alaha system in aqueous solution.* $C_M = 1\times10^{-3}$ *M, Cu/L = 1:3; I = 0.1 M; T = 298 K.*

5.2 12-MC-4 self-assembly kinetics

Kinetics of Cu(II) interaction with (S)-α-Alaha have been investigated by the stopped-flow technique. Experiments have been performed at λ = 340 nm and *I* = 0.1 M (KCl). Formation reactions of simple Cu(II) complexes equilibrate very rapidly, as Cu(II) water exchange rate constant, that is indicative of its complexation rate, has a value of 10^9 s^{-1}(see Chapter 1). Therefore, their rates are too fast to be measured by the stopped-flow technique; the observed kinetic effects should be thus related to the formation of a more complex product, as 12-MC-4. Actually, reactions between metals and ligands that involve the building of several covalent bonds are slower compared to the typical complex formation reactions of a given metal ion. As a check, the complexation reaction of Cu(II) with BHA (benzohydroxamic acid), that doesn't form metallacrowns, has been analyzed by the stopped-flow technique and no kinetic curves could be observed. In order to form metallacrowns, reactants concentrations close to the stoichiometric ratio 1:1 have to be used. Therefore, the kinetic analysis had to be carried out at C_M/C_L values far from pseudo-first order conditions and an exponential fitting of the experimental data was not possible. Thus, kinetics of metallacrown formation were analyzed by the initial rates method.

5.2.1 Reaction order determination

In order to define the rate law for the 12-MC-4 self-assembly process, reaction orders with respect to the individual reactants have been determined by using the method of the initial rates. This approach requires measuring the rate of reaction, $v°$, at the beginning of the

reactive process, before any significant change in reactants concentrations could occur. The initial part of a kinetic curve can be assimilated to a straight line whose slope corresponds to the initial rate of the reaction ($v°$). The initial reaction rate depends on reactants concentrations as shown in equation (5.1).

$$\log v° = \log k + x \log C_M + y \log C_L \qquad (5.1)$$

For $C_L = C_M$, equation (5.1) turns into equation (5.2), which allows to determine the global reaction order (x+y).

$$\log v° = \log k + (x+y) \log C_L \qquad (5.2)$$

The experimental trend of log $v°$ *vs* log C_L for experiments where $C_M = C_L$ is reported in Figure 5.4. The obtained reaction order is (x+y)=2.7.

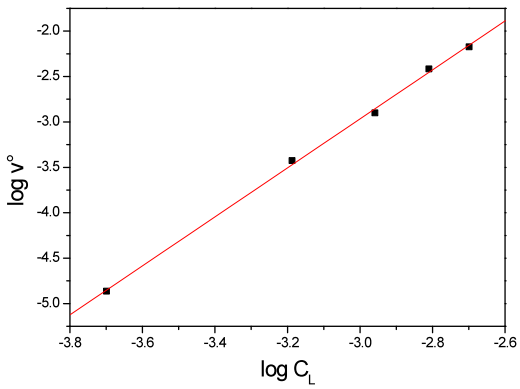

Figure 5.4 *Logarithmic dependence of the initial rate, v°, on ligand concentration, C_L, for the Cu(II)/HL system. C_M=C_L, I=0.1 M, pH=4.5, T=25°C.*

Initial rates analysis has also been applied to a series of kinetic curves obtained by using a constant metal excess ($C_M = 2\times10^{-2}$ M). In this case, C_M can be included in the constant term of equation (5.1), which turns into equation (5.3).

$$\log v° = \log k' + y \log C_L \qquad (5.3)$$

where $k' = kC_M^x$. By using equation (5.3) it has been possible to calculate the reaction order respect to the ligand (y). The reaction order respect to the metal (x) can be obtained using a constant ligand excess ($C_L = 2\times10^{-2}$ M). The relation between $v°$ and C_M is now given by equation(5.4).

$$\log v° = \log k'' + x \log C_M \qquad (5.4)$$

with $k'' = k\, C_L^y$. The obtained values for the reaction orders and the rate parameter k are reported in Table 5.1. The finding that reaction orders assume fractional values, in the range between 1 and 2, reveals that the metallacrown formation occurs in more than one reactive step. Actually, when the global reaction consists of various steps having different reaction orders respect to a reactant, the total reaction order value results to be fractional.

Table 5.1 *Reaction orders and rate constant for Cu(II)/(S)-α-Alaha 12-MC-4 self-assembly. pH = 4.75; T = 298 K.*

x	y	10^{-4} k
1.4±0.1[a]	1.3±0.1[a]	3.9±1.2[a]
1.4±0.1[b]		3.9±1.3[b]
1.5±0.1[c]		180±1.6[c]

[a]*average values from experiments performed with $C_M>>C_L$, $C_M<<C_L$ and $C_M = C_L$ (this section); I = 0.1 M;* [b]*results from plots of logv° vs logC_M (section 5.2.3); I = 0.1 M;* [c]*results from plots of logv° vs logC_M (section 5.2.3); I = 0.9 M.*

5.2.2 Rate and amplitude dependence on pH

(S)-α-alaninehydroxamic acid ((S)-α-Alaha) reaction with Cu(II), to form the 12-MC-4 ($[Cu_5L_4]^{2+}$) metallacrown, involves (O,O) and (N,N) coordinations with expulsion of twelve protons, according to reaction (5.5).

$$5\ Cu^{2+} + 4\ H_2L^+ \rightleftarrows [Cu_5L_4]^{2+} + 12\ H^+ \qquad (5.5)$$

The pH dependence of the formation of the $[Cu_5L_4]^{2+}$metallacrown, also denoted as 12-MC-4, has been, thus, investigated. Stopped-flow experiments have been performed at different pH values (2.5 < pH < 7), keeping constant ionic strength, metal and ligand

concentrations (with C_M:C_L = 5:4, according to 12-MC-4 stoichiometry). The recorded stopped-flow traces display two kinetic effects. The initial rates of the reaction have been evaluated for each pH value. As this estimation involves only the initial linear part of the kinetic curves, the determined rate values are concerned only with the fast kinetic effect. On the other hand, the amplitudes of both the fast and the slow kinetic effect were both accessible to evaluation. The obtained initial rates and the amplitudes of both the fast and the slow kinetic effect display a bell-shaped trend (Figures 5.5 and 5.6), with a maximum value at about pH = 5.This trend is perfectly comparable with that of the speciation curve of 12-MC-4 (Figure 5.3) (Careri et al., 2003), confirming that the observed reaction corresponds to the macrocycle formation.

At pH values lower than 3.4 and higher than 7 no kinetic effects have been observed. Actually, as reported in the speciation curves of Figure 5.3, in strong acidic medium the species $[CuL]^+$ is prevailing, while at low acidity values $[CuL_2H_{-1}]^-$ forms. Formation rates of both these simple complexes are too high to be measured with the stopped-flow technique.

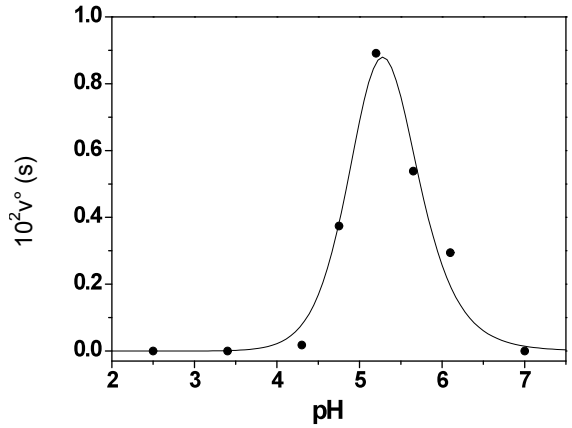

Figure 5.5 *pH dependence of the initial rate values for the Cu(II)/(S)-α-Alaha system;* $C_M = 6.25\times10^{-4}$ *M,* $C_L = 5.0\times10^{-4}$ *M, I = 0.1 M, λ = 340nm, T = 298 K.*

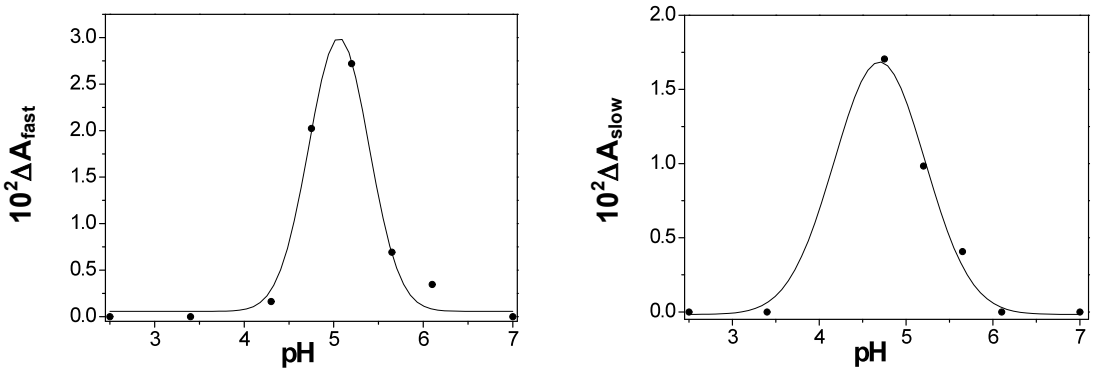

Figure 5.6 *pH dependence of the amplitude values for the Cu(II)/(S)-α-Alaha system;* $C_M = 6.25\times10^{-4}$ *M,* $C_L = 5.0\times10^{-4}$ *M, I = 0.1 M,* λ *= 340nm, T = 298 K.*

5.2.3 Rate dependence on Cu(II) concentration at different ionic strength values

The dependence of 12-MC-4 formation kinetics on Cu(II) concentration has been investigated too, in order to understand under which conditions formation of the transient species and the final product of the reaction are favored. Stopped-flow curves recorded at metal-to-ligand concentration ratios lower than 5:4 (that corresponds to metallacrown stoichiometry) display a monophasic behavior (Figure 5.7A), while a second kinetic effect is observed for metal to ligand ratios higher than 5:4 (Figure 5.7B). Experiments have been carried out at pH = 4.75 and at two different ionic strength values (*I* = 0.1 M and *I* = 0.9 M).

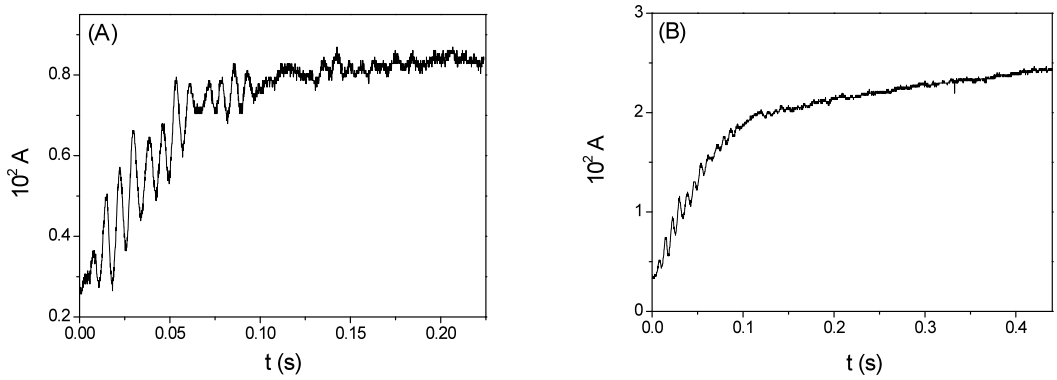

Figure 5.7 *Kinetic relaxation curves for the reaction of Cu(II))/(S)-α-Alaha system at* $C_L = 5.0\times10^{-4}$ *M, I = 0.1 M, pH = 4.75,* λ *= 340nm, T=298 K. (A)* $C_M/C_L = 0.3$*, the curve is monophasic; (B)* $C_M/C_L = 2$*, the curve is biphasic.*

The initial rate of the reaction is proportional to the reactants concentrations, according to equation (5.3) and the plot of log$v°$ vs logC_M gives a straight line (Figure 5.8), whose slope corresponds to the reaction order respect to the metal ion, *x*. The obtained values for *x* at *I* = 0.1 M and *I* = 0.9 M (Table 5.1) are in very good accordance with that resulting from experiments carried out with an excess of ligand (section 5.2.1).

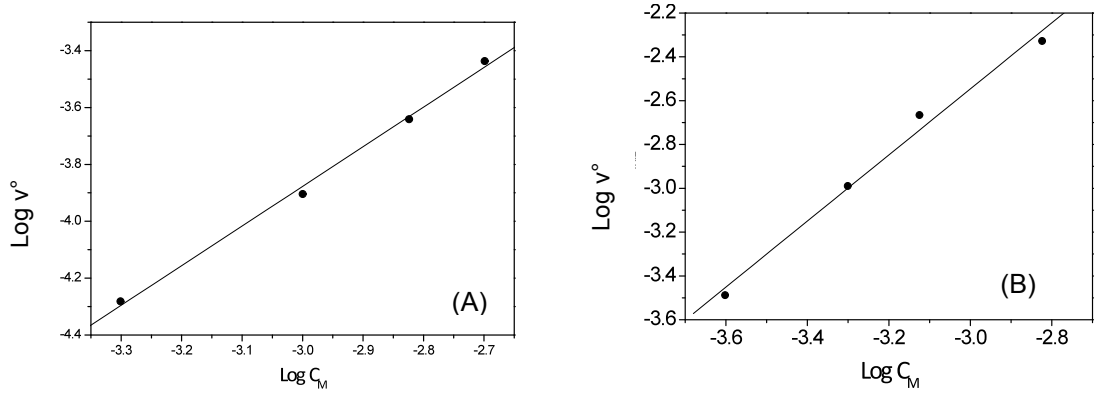

Figure 5.8 *Dependence of the initial rate on metal ion concentration for the Cu(II)/(S)-α-Alaha system.*$C_L = 5.0\times10^{-4}$ *M, pH=4.75,* λ *= 340nm, T = 298 K; (A) I = 0.1 M, (B) I = 0.9 M.*

By inserting the reaction orders values (x and y) in equation(5.3), the rate constant, k, has been evaluated at both the analyzed ionic strengths. As reported in Table 5.1, on going from I = 0.1 M to I = 0.9 M, the k value becomes higher by a factor of about 50, suggesting an interaction between molecules that have charges of the same sign and that consequently feel a reduction of the repulsion effect as the salt concentration increases.

5.2.4 Rate dependence on ionic strength

Kinetics of this system have been also analyzed at constant pH value (pH = 4.75), varying the level of added salt. The initial rate of the reaction depends linearly on ionic strength, as shown in Figure 5.9, confirming the rate enhancing effect at high salt concentrations.

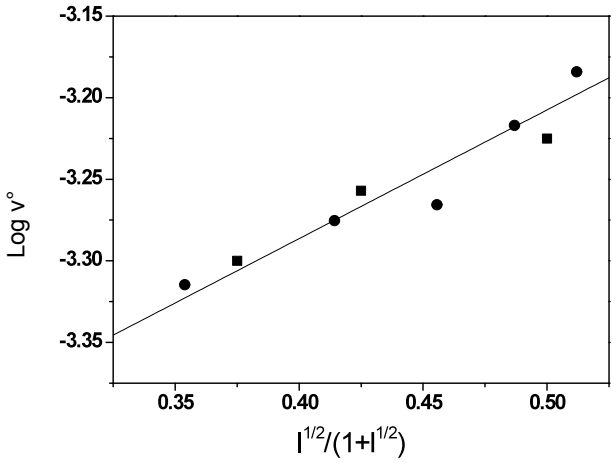

Figure 5.9 *Dependence of the logarithm of the initial rate on ionic strength, according to equation (5.8), for the Cu(II)/(S)-α-Alaha system.* C_M *= 6.25×10*$^{-4}$ *M* C_L *= 5.0×10*$^{-4}$ *M, pH=4.75,* λ *= 340nm,T = 298 K.•counterion =* Cl^-*; ■counterion =* ClO_4^-.

The slope of the obtained straight line gives, according to Güntelberg equation (5.6) (Guntelberg, 1926), the charge product of the reactive species for the rate determining step, Z_AZ_B, that for the analyzed system resulted to assume a value of 1± 0.07.

$$\log v^\circ = \log v^\circ_{I=0} + 1.01 Z_A Z_B \frac{I^{1/2}}{1+I^{1/2}} \qquad (5.6)$$

Parameter $v^\circ_{I=0}$represents the initial rate at $I = 0$.

Kinetics experiments at various ionic strength values, using perchlorate rather than chloride as counterion have been also performed, to ensure that the increase of the reaction rate with salt concentration was actually due to an ionic strength effect and not to an interaction with Cl^- ions. Indeed, the experimental values of logv° obtained in the presence of ClO_4^- stay on the same straight line as those obtained using chloride salts (Figure 5.8).

The obtained value of Z_AZ_B indicates that the Cu(II)/(S)-α-Alaha self-assembly mechanism to form 12-MC-4 involves a fast reaction step that takes place arising from two metal-ligand complexes having unit charge. According to this result, 12-MC-4 formation (reaction 5.5) can be drawn up in a first approximation as in reaction Scheme 5.5, where the observed fast kinetic effect corresponds to the interaction between two $[CuL]^+$ complexes, which have both Z = +1. These molecules arise from reaction of (S)-α-Alaha

with Cu(II) (step (5.7)), which is considered as a pre-equilibrium, being too fast to be kinetically observed.

$$Cu^{2+} + H_2L^+ \rightleftharpoons CuHL^+ + H^+ \qquad (5.7)$$

$$2\ CuHL^+ \rightleftharpoons Cu_2HL_2^{2+}{}_{(D2)} \text{ or } Cu_2HL_2^{2+}{}_{(D3)} \qquad (5.8)$$

$$2\ Cu_2HL_2^{2+}{}_{(D2)} + Cu^{2+} \rightleftharpoons Cu_5L_4^{2+} + 2\ H^+ \qquad (5.9)$$

Scheme 5.5 *Reaction mechanism for Cu(II)/(S)-α-Alaha self-assembly to form the12-MC-4 metallacrown.*

Reaction (5.8) gives rise to two dimeric isomers. These are formed in parallel with the same probability since Cu^{2+} ion reacts with ligands according to the SN_1IP mechanism and therefore exhibits the same reactivity towards oxygen and nitrogen sites of Alaha. The reaction depends on ionic strength and, actually, the product of the reactants charges for this step assumes a unitary value. Step (5.10), which is related to the slow kinetic effect, actually can be splitted in more than one process, as the hypothesis of more consecutive bimolecular processes is more reasonable than that of just one multimolecular collision, which directly gives the final product 12-MC-4.

5.2.5 Dimer formation process

Dimer formation has been investigated under conditions of ligand excess, for which just the fast kinetic effect is observed (Figure 5.6A), thus dimer formation should precede metallacrown self-assembly (slow effect) and the kinetic analysis becomes simpler. Experiments have been performed at pH = 4.75, I = 0.1 M and for C_M/C_L from 2×10^{-2} to 3×10^{-1}.

In this case, working under pseudo-first order conditions, it is possible to analyze the kinetic curves, as those of Figure 5.6A, using a monoexponential equation and to obtain the time constant, $1/\tau$.Experiments show a good linearity of $1/\tau$ versus C_M, according to equation (5.11) that has been derived as shown in Appendix IIIB.

$$\frac{1}{\tau} = 4k_{f,2}[CuL^+] + k_{d,2} \qquad (5.11)$$

Data fitting has been performed using an iterative method. In a first approximation the $[CuL^+]$ value has been estimated to be equal to C_M. Such an approximation is reasonable if we consider that reaction (5.7) is quantitative at pH = 4.75(Farkas et al., 1989). Once $k_{f,2}$and $k_{d,2}$determined, $K_{2app} = k_{f,2}/k_{d,2}$is estimated and to put its value in equation (5.12), in order to determine the equilibrium total dimer ($D_2 + D_3$) concentration.

$$[M_2L_2] = \frac{2C_M + K_{2,app}^{-1} - \sqrt{(2C_M + K_{2,app}^{-1})^2 - 4C_M^2}}{2} \qquad (5.12)$$

The equilibrium ML concentration is estimable from the mass conservation relationship:

$$[CuL^+] = C_M - 2\,M_2L_2 \qquad (5.13)$$

Thus the obtained $[CuL^+]$ value is reintroduced in equation (5.11) to reevaluate $k_{f,2}$ and $k_{d,2}$,until convergence is reached. The final values of $k_{f,2}$, $k_{d,2}$ and $K_{2,app}$ are achieved after few iterations and reported in Table 5.2. Note that k_{f2} and k_{d2} are overall rate constant including formation an dissociation of the two dimers respectively.

Table 5.2 *Kinetic and equilibrium constants for the Cu(II)/(S)-α-Alaha dimer formation. pH= 4.5; I = 0.1 M; T = 298 K.*

10^{-6} K_{1app} (M^{-1})	$10^{-4}k_{f,2}$ (M^{-1} s^{-1})	$k_{d,2}$(s^{-1})	$10^{-3}K_{2app}$(M^{-1})
1.7	3.6	19	1.8

5.2.6 Reverse reaction kinetics

Kinetics of the reverse reaction of step (5.9) have been investigated too, since it's not nearly evident that this process follows the same microscopic mechanism of the direct reaction. In order to clarify this point and confirm the proposed mechanism for 12-MC-4 formation, a series of experiments was devised where a solution containing the preformed 12-MC-4 was mixed with calibrated amounts of HCl and the time constant of the

metallacrown decomposition, $1/\tau_{diss}$, has been measured for each $[H^+]$ value. A typical kinetic curve of the dissociation process is shown in Figure 5.10, while dependencies of the amplitude, A_{diss}, and rate constant, $1/\tau_{diss}$, of the kinetic curves on $[H^+]$ are reported in Figure 5.11.

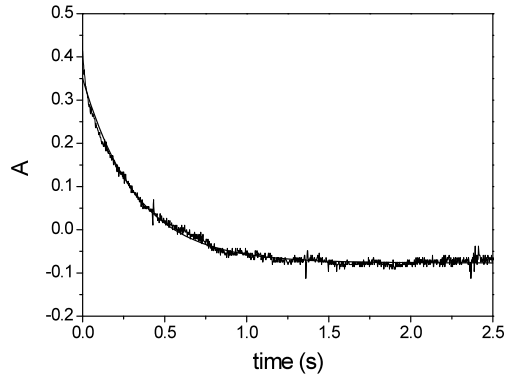

Figure 5.10 *Kinetic relaxation curve for the dissociation reaction of the Cu(II))/(S)-α-Alaha 12-MC-4 metallacrown.* $C_{12\text{-}MC\text{-}4} = 1.0 \times 10^{-4}$ *M, I = 0.1 M, pH = 3.5 (after mixing),* λ *= 340nm, T=298 K.*

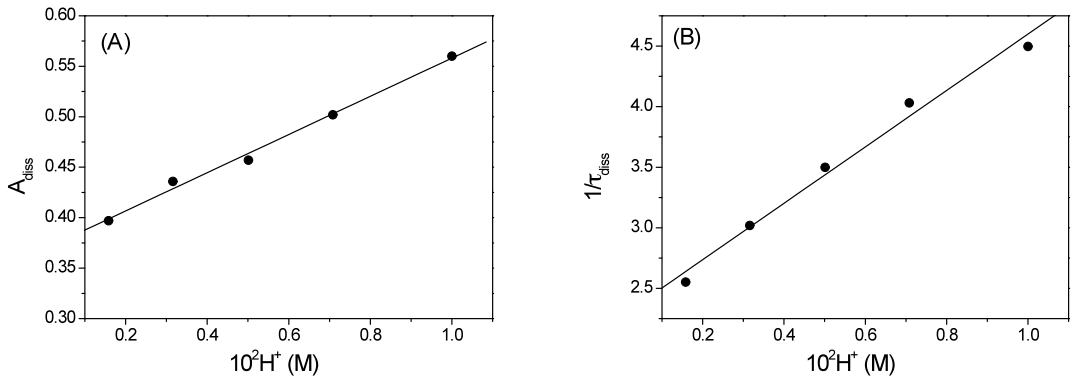

Figure 5.11 *(A) Amplitudes,* A_{diss}*, and (B) rate constants,* $1/\tau_{diss}$*, dependence on* $[H^+]$ *for the reverse reaction of Cu(II)/(S)-α-Alaha 12-MC-4 self assembly; I = 0.1 M,*λ *= 340 nm, T = 298 K.*

The increase of the amplitude values with the acid level shows that reaction (5.9) is not irreversible, but is an equilibrium process, whose position is displaced by the release of protons. Moreover, the fact that step (5.9) is reversible is confirmed by the positive value of the intercept of the plot in Figure 5.9B, which reveals that also the direct step of reaction

(5.9) is present. On the other hand, the first order dependence of $1/\tau_{diss}$ on acid concentration denotes the involvement of just one proton in the rate-determining step of the metallacrown decomposition. Thus, it is reasonable to suppose that a monoprotonated intermediate species of 12-MC-4 forms and then further decomposes to give the products of metallacrown decomposition.

5.3 FAB-MS for the system Cu(II)/(S)-α-Alaha

Mass Spectrometry experiments on Cu(II)/(S)-α-Alaha solutions have been performed in the pH range between 2 and 10. Fast Atomic Bombardment ionization has been used, which is relatively soft and so gives rise to a restricted fragmentation.
Three complexes were detected. Moreover, fragmentation of the pentanuclear species was obtained only at high voltage conditions, strongly supporting that 12-MC-4 is already present in solution, rather than formed in the gas phase (Table 5.3).

Table 5.3 *FAB-MS ions peaks for Cu(II) complexes with (S)-α-Alaha.*

ion	m/Z
Cu_2L	192
$[CuL_2H_{-1}]K_2^+$	345
$[Cu_4L_4H_{-4}]$	664
$[Cu_5L_4H_{-4}]\ Cl^+$	762

5.4 12-MC-4 thermal stability

Thermal stability of the Cu(II)/(S)-α-Alaha metallacrown has been investigated by means of Differential Scanning Calorimetry (DSC) and UV-vis experiments. Comparison of results obtained with these techniques allowed to define the processes that take place at temperature values higher than room temperature.

5.4.1 UV-vis analysis

UV-vis experiments have been performed at pH = 4.5, where the formation of 12-MC-4 is favored, and at I = 0.1 M. Spectra of a preformed 12-MC-4 solution recorded in the temperature range between 20° and 90°C, show an evident decrease of the absorbance values at T = 86°C and λ = 340 nm, that is the wavelength where 12-MC-4 displays its

typical maximum absorption (Figure 5.12). Such a process is consistent with the rupture of the metallacrown scaffold and it has been observed at the same temperature in the DSC experiments.

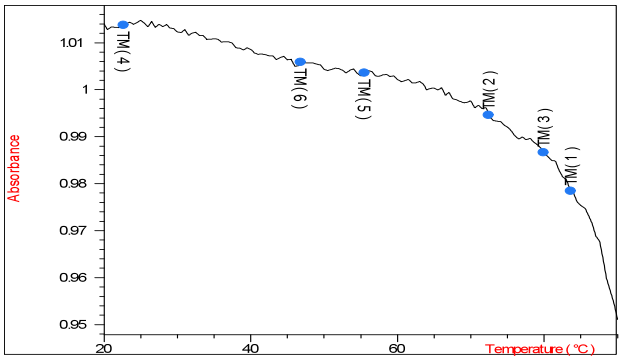

Figure 5.12 *Absorbance dependence on temperature for the Cu(II)/(S)-α-Alaha 12MC4. λ = 340 nm; pH = 4.75; I = 0.1 M.*

5.4.2 DSC analysis

DSC analysis of the 12-MC-4 has been carried out at two different pH values (pH = 3; 4.5), where the species $[CuL]^+$ and 12-MC-4 are present in solution. At pH = 3 a peak at 63°C has been observed (Figure 5.13A), ascribed to decomposition of $[CuL]^+$, which is the only species in solution at such a pH value(Careri et al., 2003).The total enthalpy change for this process (equation (5.17)) is given by the sum of ΔH of reactions (5.14) and (5.15), as reported in equation (5.18). The calculated value, ΔH_{CuL}, is not so far from that obtained from integration of the experimental curve. At pH = 4.5 the same transition is still observable, but a further and most evident peak appears at 90°C (Figure 5.13B), which corresponds to 12-MC-4 breakage, according to UV-Vis experiments.

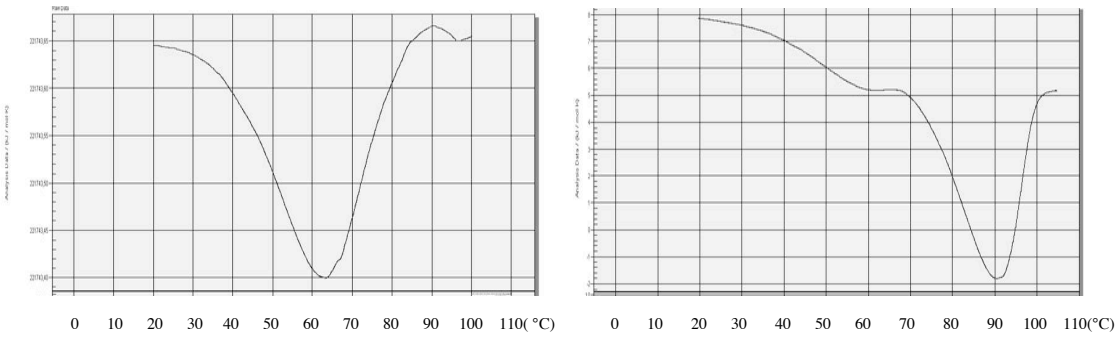

Figure 5.13 *DSC curves for the 12-MC-4. (A) pH = 3; (B) pH = 4.5; scan rate = 1°C/min; P = 1.5 atm.*

By combining equations (5.14) and (5.16) (charges omitted) it has been possible to evaluate the theoretical ΔH of the metallacrown rupture (equation (5.19)), as shown in equation (5.20). The evaluated value of ΔH_{12MC4}resulted to be close to the experimental one obtained in the same conditions. Calculated and experimental ΔH for both the species are reported in Table 5.4.

$H_2L \leftrightarrows 2H+L \qquad (\Delta H_1)$ (5.14)

$M+L \leftrightarrows ML \qquad (\Delta H_2)$ (5.15)

$5M+4L \leftrightarrows M_5L_4 \qquad (\Delta H_3)$ (5.16)

$ML + 2H \quad M + H_2L$ (5.17)

$\Delta H_{CuL} = -(\Delta H_1^0 + \Delta H_2^0)$ (5.18)

$M_5L_4 + 8H \quad 5M + 4\ H_2L$ (5.19)

$\Delta H_{12MC4} = -(4\Delta H_1^0 + \Delta H_3^0)$ (5.20)

Table 5.4 *Enthalpy variation for the Cu(II)/(S)-α-Alaha system decomposition at different pH values. ΔH_i in KJ mol^{-1}.*

pH	$-\Delta H_{CuL}$ (reaction 5.17)	$-\Delta H_{12MC4}$ (reaction 5.19)
3.0	17.6	-
	29.8[a]	-
4.5	-	160
	-	166[a]

[a]*Theoretical values obtained from equations (5.17)-(5.18) using literature values for ΔH_1, ΔH_2 and ΔH_3(Tegoni et al., 2008).*

A study on the reversibility of the reaction has been performed too. After the first scan, the sample has been cooled to the original temperature and rescanned. Since after the first scan the product of the reaction was completely and irreversibly changed, no thermotransition peaks could be observed either in the cooling or in the second heating scan.

5.4.3 ITC analysis

An isothermal calorimetric titration of Cu(II) with (S)-α-Alaha was performed. The titration curve shows two equivalent points respectively at copper-to-ligand ratio of 2 and 4/5, corresponding to formation of the complexes Cu_2L and $[Cu_5L_4]^{2+}$, i.e. the 12-MC-4 metallacrown (Figure5.14). Therefore, this result is an evidence of metallacrown formation but also enlights the presence of the dinuclear complex in metal excess conditions. Up to now such a complex, that provides the rationale for Cu(II) 12-MC-4 metallacrowns, was never observed as a stable species in solution. The only isolated dinuclear complex of a hydroxamic acid is that deriving from the complexation of Fe(III) by salicylhydroxamic acid, obtained in this thesis work and described in the previous chapter.

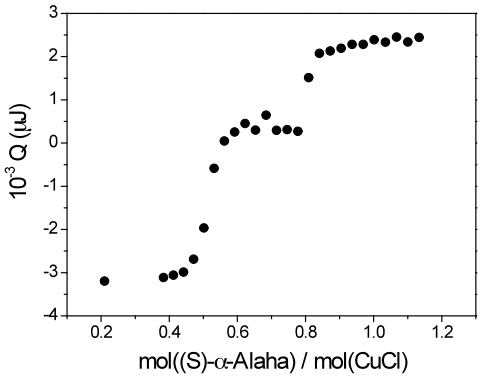

Figure 5.14 *ITC curve for the system Cu(II)/(S)-α-Alaha. pH = 4.5, I = 0.1 M, T = 298 K.*

As described above, the mechanism of 12-MC-4 formation/decomposition of 12-MC-4 has been worked out, by using a variety of analysis techniques. In next sections we report on 12-MC-4 interaction with La(III), showing that the final product of this reaction ($[LaCu_5L_5]^{3+}$, also denoted as 15-MC-5) is formed through the La(III)-induced reassembly of the 12-MC-4.

5.5 15-MC-5 self-assembly equilibrium

The interaction of La(III) with Cu(II)/(S)-α-Alaha 12-MC-4 has been revealed by spectral changes in the visible region. Spectrophotometric titrations of preformed 12-MC-4 with $LaCl_3$ were performed at 580 nm, where the spectral change is the largest, with the aim of evaluating the equilibrium constant, K_{app}, of the binding reaction (equation (5.21), charges omitted)

$$\text{12-MC-4} + \text{La} \overset{\text{L}}{\rightleftarrows} \text{15-MC-5} \qquad (5.21)$$

Note that a further ligand molecule is required in order the reaction can undergo. Experiments were performed at I = 0.1 M (KCl) and pH = 4.75. Figure 5.15A shows the obtained titration curve. Titrations were analyzed according to equation (5.22).

$$\frac{C_M C_L}{\Delta A} + \frac{\Delta A}{\Delta \varepsilon^2} = \frac{1}{K \Delta \varepsilon} + \frac{C_M + C_L}{\Delta \varepsilon} \qquad (5.22)$$

where $\Delta A = \varepsilon_L C_L$, $C_L = C_{12MC4}$ and $C_M = C_{La}$.

Intercept and slope of the straight line obtained according to equation (5.22) provide the equilibrium constant, K_{app}, together with the change in extinction coefficient, Δε (Figure 5.15B). The onset of an equilibrium between 12-MC-4 and 15-MC-5 is indicated by the positive intercept of the plot of Figure 5.12B.

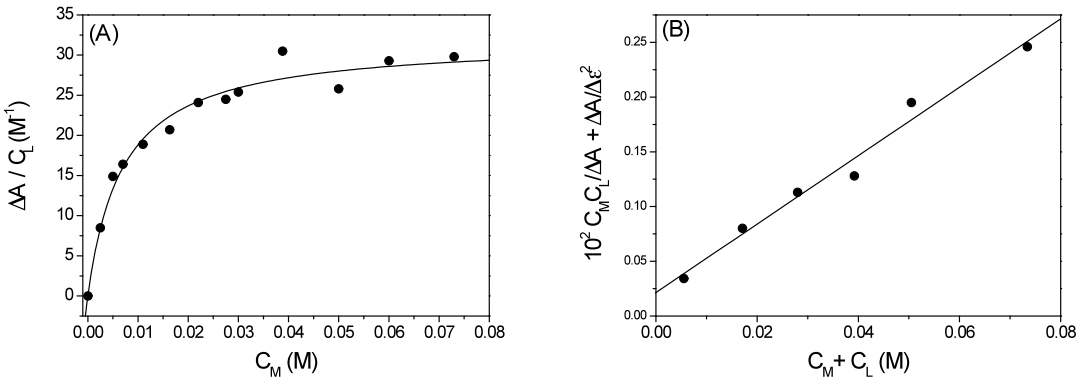

Figure 5.15 *Binding isotherm (A) and data plot obtained from equation 5.2 (B) for the reaction between 12-MC-4 and La(III).* $C_{12\text{-}MC\text{-}4}=2.7\times10^{-4}$ *M,* $C_{La}=1\times10^{-1}$ *M.* λ*= 580 nm; I=0.1 M; pH=4.5; T= 298 K.*

The K_{app} value is reported in Table 5.5.

Table 5.5 *Thermodynamic and kinetic parameters for the 12-MC-4/La(III) reaction. I=0.1 M; pH=4.5; T= 298 K.*

$K_{app}(M^{-1})$	$10\ k_{f,fast}(M^{-1}s^{-1})$	$10^3k_{d,fast}(s^{-1})$	$K_{fast}\ (M^{-1})$	$10^4k_{f,slow}(s^{-1})$	$10^4k_{d,slow}(s^{-1})$	K_{slow}
145±8.1[a]						
167±9.9[b]	1.9±0.1[b]	5.6±0.2[b]	33.2±0.3[b]	5.5±0.1[b]	1.4±0.1[b]	4.0±0.2[b]

[a]*Value obtained from spectrophotometric analysis.*

[b]*Values obtained from kinetic analysis.*

5.6 15-MC-5 self-assembly kinetics

Kinetics of 12-MC-4 interaction with La(III) to give the bigger 15-MC-5 metallacrown have been investigated under pseudo first-order conditions (C_{La}>>$10C_{12\text{-}MC\text{-}4}$). All the experiments have been performed at pH = 4.5, I = 0.1 M (KCl).

5.6.1 Rate dependence on La(III) concentration

A series of kinetic measurements at different La(III) concentrations has been performed using the classical spectrophotometric method. The required stoichiometric ratio for 15-MC-5 ($C_{Cu(II)}$:C_L = 1:1) has been used for all the experiments. The analyzed system displays two kinetic effects (Figure 5.16). Thus, the global process (5.19) actually consists of two reactive steps,that can be summed according to the sequence (5.23).

$$12\text{-MC-4} + La \overset{L}{\leftrightarrows} \text{Intermediate} \leftrightarrows 15\text{-MC-5} \qquad (5.23)$$

where the system passes through an intermediate species before giving the final $[LaCu_5L_5]^{3+}$ species, denoted as 15-MC-5.

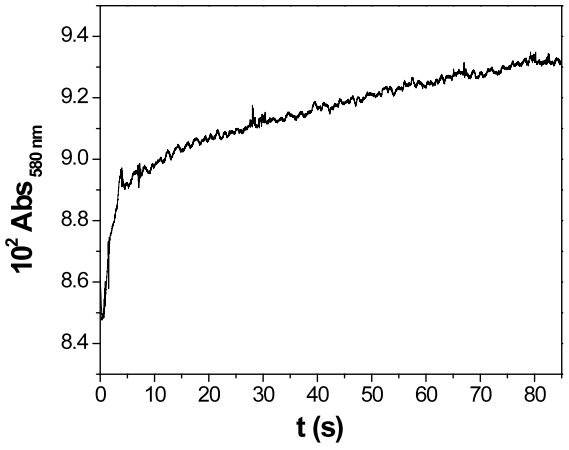

Figure 5.16 *Biphasic kinetic curve for the reaction of 12-MC-4 with La(III). C_{La} =3.9×10^{-2} M; C_{Cu} = C_L = 3×10^{-3} M; I = 0.1 M; pH = 4.75; λ = 580nm; T=298 K.*

The analysis of the recorded traces provided the amplitude and time constants, $1/\tau_{fast}$ and $1/\tau_{slow}$, of the two corresponding kinetic effects. Experiments carried out keeping constant the pH, the 12-MC-4 and the chloride concentration and varying the La(III) concentration show a good linearity of $1/\tau_{fast}$ versus C_M (Figure 5.17A), according to equation (5.24).

$$1/\tau_{fast} = k_{f,fast}C_M + k_{d,fast} \qquad (5.24)$$

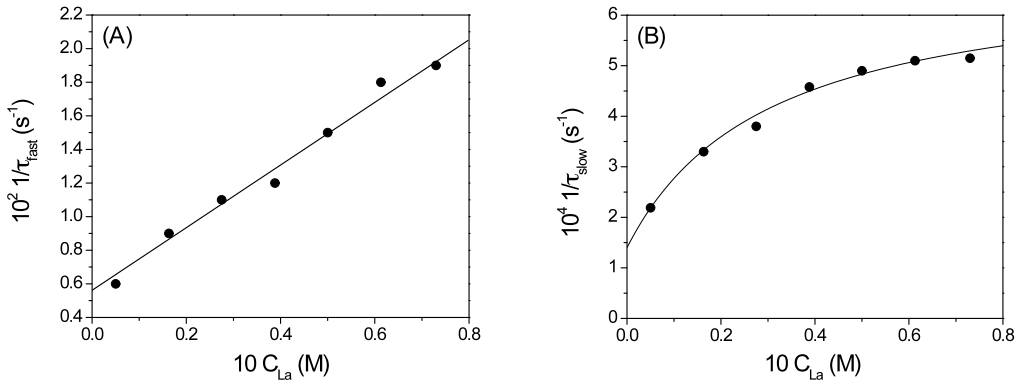

Figure 5.17 *Time constant dependence on La(III) concentration for the fast and slow kinetic effect observed for the 12-MC-4/La(III) reaction. pH = 4.5, I = 0.1 M; T = 298 K.*

Thus, a linear interpolation of the experimental data would provide the values of the direct ($k_{f,fast}$) and reverse ($k_{d,fast}$) rate constants for the first step of reaction (5.23). Values of the resulting parameters together with their ratio, $K_{fast} = k_{f,fast}/k_{d,fast}$ are reported in Table 5.5.Concerning the slow kinetic effect, the overall rate constants depend on La(III) concentration according to equation(5.25) that well represents the experimental behaviorof Figure 5.14B and that is derived in Appendix III.

$$\frac{1}{\tau_{slow}} = \frac{K_{app,fast}k_{f,slow}C_M}{1 + K_{app,fast}C_M} + k_{d,slow} \qquad (5.25)$$

According to sequence (5.23), the overall apparent equilibrium constant, K_{app}, should be a function of the rate constants of the two processes observed in the kinetic experiments, as shown in equation (5.26).

$$K_{app} = \frac{k_{f,fast}}{k_{d,fast}}\left(1 + \frac{k_{f,slow}}{k_{d,slow}}\right) \qquad (5.26)$$

The obtained value is in good accordance with that resulting from the spectrophotometric analysis, confirming that equation (5.23) well describes the reaction mechanism. Values of $k_{f,slow}$, $k_{d,slow}$, their ratio K_{slow} and K_{app} are collected in Table 5.5.

5.6.2 Rate dependence on (S)-α-Alaha concentration

The dependence of 15-MC-5 formation kinetics on (S)-α-Alaha (L) concentration has been investigated using the classical spectrophotometric method, in order to understand in which step of reaction scheme (5.23) the free ligand is involved. Biexponential kinetic curves have been recorded at different excess ligand concentrations, keeping constants the La(III) and Cu(II) concentrations, pH and ionic strength. The fastest time constant, $1/\tau_{fast}$, is independent of the ligand concentration (Figure 5.18A), while the slowest time constant, $1/\tau_{slow}$, increases as shown in Figure 5.18B.

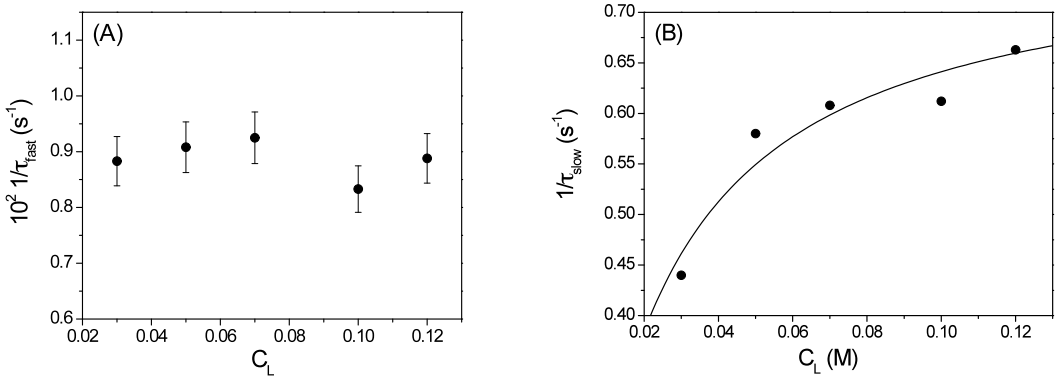

Figure 5.18 *Time constant dependence on (S)-α-Alaha concentration for the fast and slow kinetic effect observed for the 12-MC-4/La(III) reaction. pH = 4.5, I = 0.1 M; T = 298 K.*

Such a behavior can be justified by reaction scheme (5.27)-(5.29)

$$La + L \overset{K_{LaL}}{\leftrightarrows} LaL \qquad (5.27)$$

$$12\text{-MC-4} + LaL \leftrightarrows 12\text{-MC-4-LaL} \qquad (5.28)$$

$$12\text{-MC-4-LaL} \leftrightarrows 15\text{-MC-5} \qquad (5.29)$$

Independence of $1/\tau_{fast}$ on C_L is justified by assuming that K_{LaL} is high enough to make formation of LaL, according to reaction (5.27), almost complete. In such a way both reactions (5.27) and (5.28) only depend on La concentration, that in the performed experiments has been kept constant.

Concerning the slow step, it turns out that, according to Scheme (5.27)-(5.29), the dependence of $1/\tau_{slow}$ on C_L is given by equation (5.30), which well represents the experimental trend shown in Figure 5.18B.

$$\frac{1}{\tau_{slow}} = \frac{K_{LaL}K_1k_2C_{La}C_L}{1+K_{LaL}K_1C_{La}C_L} + k_{-2} \qquad (5.30)$$

5.6.3 Rate dependence on Cu(II) concentration

A series of kinetic experiments with different excess Cu(II) amounts has been performed in order to investigate the interaction of 12-MC-4 with La(III). The time course of the reaction has been measured at 580 nm by classical spectrophotometry. No excess ligand is present in solution, thus 15-MC-5 does not form and just one kinetic effect, corresponding to the fast one, has been detected (Figure 5.19).

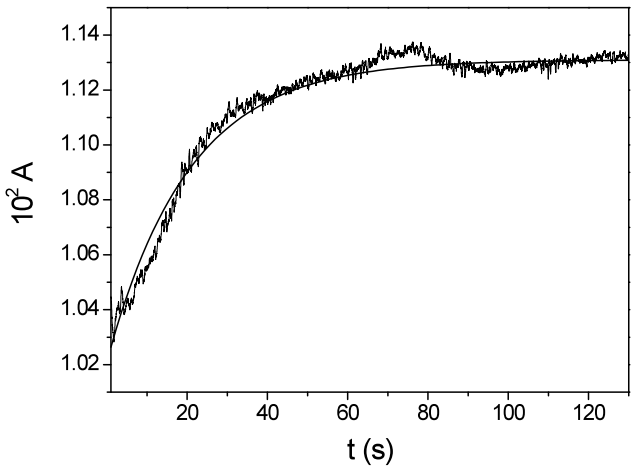

Figure 5.19 *Monophasic kinetic curve for the reaction of 12-MC-4 with La(III) and excess Cu(II); C_{La} =1.23×10^{-1} M C_{Cu} = 1×10^{-2} M; I = 0.1 M; pH = 4.5; λ = 580nm; T=298 K.*

The time constant values depend linearly on La(III) concentration for each excess C_{Cu}, as shown in Figure 5.20, thus relationship (5.24) is still valid. The slope and the intercept of each straight line correspond to $k_{f,fast}$ and $k_{d,fast}$, respectively. While $k_{f,fast}$ values remain practically constant for all the investigated series, because La(III) concentration does not change, $k_{d,fast}$ increases when raising the Cu(II) excess. This result provides evidence for the involvement of Cu(II) in the reverse reaction. In light of this finding, is reasonable to consider that, in the fast step of 12-MC-4 interaction with La(III), one copper ion, possibly the one present in the core of the metallacrown, is released.

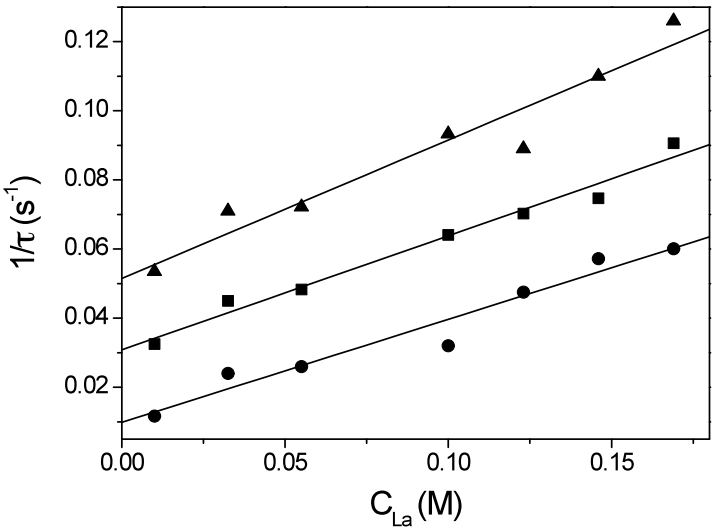

Figure 5.20 *Rate constants dependence on La(III) concentration for the fast kinetic effect observed for the 12-MC-4/La(III) reaction with different excess Cu(II) concentrations.* •C_{Cu} *= 1×10^{-2} M;*■ C_{Cu} *= 2.5×10^{-2} M;*▲ C_{Cu} *= 5×10^{-2} M; pH = 4.5, I = 0.1 M; T = 298 K.*

5.7 Discussion

Mechanisms of formation of both 12-MC-4 and 15-MC-5 self-assemblies have been determined by suitable combination of static and dynamic experiments. Concerning 12-MC-4 formation, it is worth of note that the macromolecule formation involves a dimeric species. Paniago and Carvalho already supposed the existence of such a compound in solution, proposing the structure D1 shown in Scheme 5.6 (Paniago and Carvalho, 1984). However, in 1989 Farkas and coworkers published a detailed work on the characterization of the Cu^{2+}/α-Alaha system in aqueous solution where they suggested the structure D2 (Scheme 5.6) for the dimer (Farkas et al., 1989). Both structures correspond to the same stoichiometry, but differ in the deprotonation site. Actually, more recent investigations by

Tegoni and coworkers (Tegoni et al., 2008) showed that all collected data assigned to the dimer are better attributable to the pentacopper species 12-MC-4, providing evidence of its presence in solution. On the contrary, they did not found any evidence for the existence the dimeric species in solution.

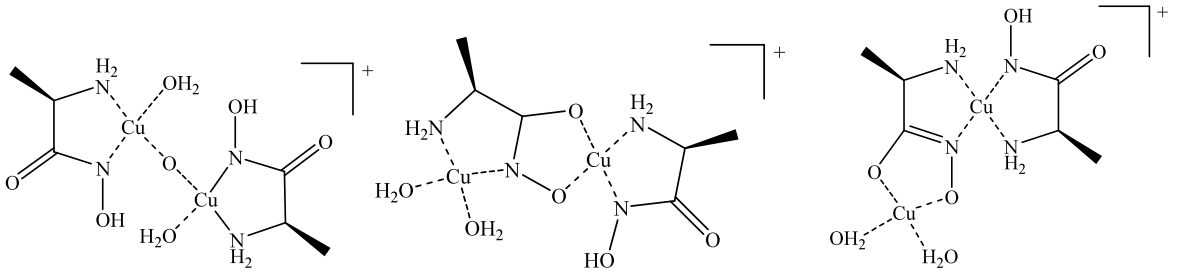

D1 **D2** **D3**

Scheme 5.6 *Possible structures for the Cu(II)/(S)-α-Alaha dimer.*

In this thesis work, for the first time, dimer formation is reconsidered as a intermediate species in the process that gives rise to the more stable 12-MC-4. In fact, although no evidence for dimer presence could be found in the equilibria studies or FAB-MS analysis, its formation is revealed by the kinetic investigation. According to the reaction mechanism worked out in this thesis, the dimer represents the half part of the 12-MC-4 ring. Therefore, it must necessarily correspond to structure D2, in order to own the typical O-Cu-N sequence of the 12-MC-4. In this way, the ambiguity between the proposed structures (D1 and D2) is resolved. Actually, another dimeric structure (D3, Scheme 5.6) should form with equal probability of structure D2. For 50% of the dimer molecules a conformational conversion from D3 to D2 is thus required in order to give rise to 12-MC-4. Such a rearrangement is slow and explains the low rate of the last reactive step of the mechanism, here proposed in Scheme 5.5. Finally it could be noticed that the slow effect observed for 12-MC-4 self-assembly could be composed of more than one step. In effect, hypotheses as that of the concerted collision of three species (two dimers and a Cu^{2+} ion) is scarcely probable.

Concerning the reaction of 12-MC-4 with La(III) to give the 15-MC-5, the kinetic study here performed provides interesting information on the reaction mechanism. Experimental results lead to the hypothesis of the expulsion of the core Cu(II) ion of 12-MC-4 induced by La(III). However, this first stage cannot be seen as a real replacement of Cu(II) by

La(III), as the 12-MC-4 cavity is still too small to host La(III) ion. Thus this process should be better considered as a side interaction.

However, further studies on this system still have to be performed, in order to better analyze some aspects of the 15-MC-5 formation mechanism induced by La(III) and to collect more quantitative information.

CHAPTER 6

Conclusions

This thesis focuses on thermodynamic and kinetic analysis of complexation reactions between transition metal ions and hydroxamic acids, mainly in aqueous solution, but also in micellar media. In particular, interactions of salicylhydroxamic and (S)-α-alaninehydroxamic acids with some of the most relevant and common cations in biological, industrial and environmental fields (Ni(II), Fe(III) and Cu(II)) are studied. Concerning (S)-α-alaninehydroxamic acid, investigations are performed focusing on the evolution of simple complexes which undergo self-assembly processes to give supramolecular compounds. A detailed reaction scheme is derived for all the analysed systems.

First, a combination of kinetic and thermodynamic methods is employed to investigate the mechanism of Ni(II) binding to salicylhydroxamic acid (SHA) in sodium dodecyl sulphate (SDS) micellar solution. As the ligand is fairly distributed between the aqueous and the micellar phase, we worked out a series of equations in order to evaluate the effective contributes of the reactions taking place in both phases. This method happens to be applicable not only to this particular case, but also to the thermodynamic and kinetic analysis of other systems partitioned between two phases. Despite the ligand amounts adsorbed on the micellar phase are not that high, the SDS micelles exert a strong accelerating effect on the complex formation step. Therefore further studies on stripping reactions of these systems, coupled with ultrafiltration technique, would be required to prove their effectiveness and applicability to metal extraction processes. Experimental evidence is provided for the rotation of the phenol ring of SHA, induced by chelation of

Ni(II). Such a rotation from *cis* to *trans* structure provides a site on the complex ML for allocating a second metal ion to give M_2L, but has not been observed in the case of Ni(II). On the contrary, such a binding site is found to be able to react with a second metal ion when the latter presents a higher charge, as Fe^{3+}. The kinetic study of the interaction of Fe(III) with benzohydroxamic acid and salicylhydroxamic acid required a rather complete knowledge of the hydrolysis and self-aggregation processes of Fe(III). In this work special attention is paid to clarify the features and the formation kinetics of a Fe(III) trimer, which is often neglected when considering the species present in Fe(III) solutions. The ambiguity existing about the structure of this species is solved through the elucidation of the mechanism of its formation/dissociation. The formation of a dinuclear complex (M_2L), formed by the reaction of Fe(III) with salicylhydroxamic acid (SHA), is demonstrated by spectrophotometric titrations, stopped-flow kinetics and FTIR experiments. The binding of the second Fe(III) atom involves the deprotonation of the SHA N-H site, and the formation of M_2L provides the rationale for the building of complex structures as metallacrowns. The results obtained in the kinetic study of formation/decomposition of M_2L enable us to describe for the first time the microscopic processes that are at the basis of the formation of the building blocks of the metallacrowns. The results presented here provide a valuable basis for further kinetic studies on Fe(III) based metallacrowns and represent a first step to describe the interactions involved in metallacrowns formation. The mechanism of these macromolecules self-assembly is also investigated in this thesis work, together with metallacrowns host-guest solution equilibria. A combined thermodynamic and kinetic approach has been used also in this case. The understanding of the equilibria and mechanisms of these processes is a key point for devising and isolating new metallacrowns as new materials and recognition agents.

Thermodynamic studies concerning Cu(II)/(S)-α-alaninhydroxamic acid 12-MC-4 and 15-MC-5 complexes have provided a valuable set of parameters that describe, with a good level of completeness, the origin and limits of the stability of metallacrowns and other Cu(II) complexes in aqueous solution, together with their dependence on pH, metal-to-ligand ratio, temperature and ionic strength. Kinetic analysis of both systems turned out to be fundamental to outline, for the first time, the reaction mechanisms of their self-assembly process.

Interestingly, this work gives evidence for the formation of a dimer as an intermediate species along the route leading to 12-MC-4 self-assembly. Only (S)-α-alaninhydroxamic acid has been used in the experiments performed for this thesis, but a mixture of different hydroxamic acids could be employed too, as the outlined reaction mechanism is independent of the nature of the ligand. The existence of such dimeric species could thus lead to the devising of mixed metallacrowns, made up of two dimers containing two different kinds of ligands. This is just one of the several applications of metallacrowns, whose importance in supramolecular chemistry is rapidly increasing. Nevertheless, a number of thermodynamic and kinetic investigations still have to be performed, in order to obtain a complete description of the assembly of metallacrowns in solution and of their related host-guest equilibria.

Concerning our investigation on metallacrowns, all the experiments have been performed in aqueous solution (see Chapter 5). However for a variety of applications metallacrowns need to be dissolved in non-aqueous media. Thus, the stability of metallacrowns and their formation/dissociation mechanisms in solvents different from water should be studied too, thus more data are desirable in the future.

Concerning 15-MC-5, kinetic studies on core metal ion exchange would be of great interest, in order to delineate and control the mechanism of this reaction that allows to use metallacrowns as selective sequestering agents.

In this thesis work, examples of three different modes of coordination of hydroxamic acids with metal ions have been reported and analyzed: from mononuclear complexes to supramolecular compounds, passing through a dinuclear complex. Actually the richness of hydroxamic acids chemistry stems from the assortment of their coordination modes and the wide range of transition metal ions that they are able to bind. Studies of hydroxamic acids continue to show potential uses of these ligands and their complexes in a wide variety of fields. Undeniably, there are several applications of hydroxamic acids coordination chemistry that still have to be revealed.

APPENDIX I

Determination of the first acid dissociation constant of SHA

The dissociation constant of a weak acid with a pK_A between 4 and 10 can not be determined spectrophotometrically by direct addition of a strong base to the weak acid because the hydrogen concentration at the equilibrium is very low and therefore not easily evaluable. Therefore it has been indirectly measured by titration of a proton exchange reaction with a weak acid which must have a pK_A value similar to the one under investigation.

The exchange reaction between SHA and Na_2HPO_4 (HA) can be expressed by the relationship

$$HL^- + H_2PO_4^- \leftrightarrows HPO4^{2-} + H_2L \qquad \text{(I.1)}$$

whose equilibrium constant is

$$K = \frac{[HPO_4^{2-}][H_2L]}{[HL^-][H_2PO_4^-]} = \frac{K_{H_2PO_4^-}}{K_{A2}} \qquad \text{(I.2)}$$

where K_{HA} is the acid dissociation constant of HA and K_{A2} the acid dissociation constant of SHA expressed by

$$K_{A2} = \frac{[HL^-][H^+]}{[H_2L]} \qquad \text{(I.3)}$$

If the Lambert & Beer law applies, for a wavelenght where the two species $[HL^-]$ and $[H_2L]$ only absorb and for a 1 cm path lenght cell, the overall absorbance is given by the equation

$$A = \varepsilon_{HL^-}[HL^-] + \varepsilon_{H_2L}[H_2L] \qquad \text{(I.4)}$$

The following mass balance equations also apply

$$C_{H2L} = [HL^-] + [H_2L] \qquad \text{(I.5)}$$

$$C_A = [A^-] + [HA] \quad \text{(I.6)}$$

If we now define

$$\Delta A = A - \varepsilon_{HL} C_{HL} \quad \text{(I.7)}$$

and

$$\Delta\varepsilon = \varepsilon_{H2L} - \varepsilon_{HL} \quad \text{(I.8)}$$

Introduction of equation (I.5) into (I.4) yields

$$\Delta A = \Delta\varepsilon[H_2L] \quad \text{(I.9)}$$

Introduction of equation (I.5) and (I.9)into (I.2) yields

$$\frac{C_{HL}}{\Delta Abs} = \frac{1}{\Delta\varepsilon} + \frac{1}{K\Delta\varepsilon}\frac{\left[A^-\right]}{\left[HA\right]} \quad \text{(I.10)}$$

which corresponds to equation (3.4) of chapter 3. A plot of $C_{HL}/\Delta A$ vs. $[A^-]/[HA] = (C_A - C_{HCl})/C_{HCl}$ yields a straight line whose slope and intercept are equal to $1/K\Delta\varepsilon$ and $1/\Delta\varepsilon$, respectively. Therefore, K is obtained as the intercept/slope ratio and, subsequently, K_{A2} is obtained as the K_{HA}/K ratio.

APPENDIX II

Determination of the equilibrium constant for formation of a 1:1 complex

The reaction between a metal, M, and a ligand, L, to form the ML complex can be expressed by the relationship

$$M_f + L_f \overset{K_{app}}{\rightleftarrows} ML_T \qquad \text{(II.1)}$$

where M_f and L_f are the total concentrations of uncomplexed metal and ligand respectively, whereas ML_T is the total complex concentration whose equilibrium constant is

$$K_{app} = \frac{[ML_T]}{[M_f][L_f]} \qquad \text{(II.2)}$$

The mass conservation equations are

$$C_L = [L_f] + [ML_T] \qquad \text{(II.3)}$$

$$C_M = [M_f] + [ML_T] \qquad \text{(II.4)}$$

where C_L and C_M the overall concentration of the ligand and metal respectively. If the Lambert & Beer law applies for a wavelength where the ligand and the complex only absorb, with a 1 cm path length cell the overall absorbance is given by the equation

$$A = \varepsilon_{L_f}[L_f] + \varepsilon_{ML_T}[ML_T] \qquad \text{(II.5)}$$

If also the metal absorbs at the used wavelength, equal amounts of metal solutions are added both to sample and reference cell at each stage of the spectrophotometric titration, in order to remove its contribution to the overall absorbance. Introduction of equation (II.3) in (II.5) yields

$$A = \varepsilon_{L_f}(C_L - [ML_T]) + \varepsilon_{ML_T}[ML_T] \qquad \text{(II.6)}$$

If we now define

$$\Delta A = A - \varepsilon_{L_f} C_L \qquad \text{(II.7)}$$

$$\Delta\varepsilon = \varepsilon_{ML_T} - \varepsilon_{L_f} \quad \text{(II.8)}$$

equation (II.6) becomes

$$\Delta A = \Delta\varepsilon[ML_T] \quad \text{(II.9)}$$

Introduction of equations (II.3) and (II.4) into (II.2) yields

$$K_{app} = \frac{[ML_T]}{(C_M - [ML_T])(C_L - [ML_T])} \quad \text{(II.10)}$$

Substituting $[ML_T]$ obtained from equation (II.9) into equation (II.10) and rearranging, one obtains

$$\frac{C_M C_L}{\Delta Abs} + \frac{\Delta A}{\Delta\varepsilon^2} = \frac{1}{K_{app}\Delta\varepsilon} + \frac{C_M + C_L}{\Delta\varepsilon} \quad \text{(II.11)}$$

which corresponds to equation (3.8) of chapter 3 and (5.22) of chapter 5. Such equation enables K_{app} and $\Delta\varepsilon$ to be obtained by an iterative procedure. That is, disregarding the $\Delta A/\Delta\varepsilon^2$ term on first approximation, $\Delta\varepsilon$ can be calculated from the reciprocal of the slope of the straight line interpolating the data of the $C_MC_L/\Delta A$ vs. (C_M+C_L). Then, introduction of this $\Delta\varepsilon$ value into equation (II.11) enables the $(C_MC_L/\Delta A + \Delta A/\Delta\varepsilon^2)$ term to be evaluated and new values of K_{app} and $\Delta\varepsilon$ to be obtained. The procedure is repeated until convergence is reached.

APPENDIX III

A. Derivation of the relaxation time equation for a reaction at the equilibrium

The reaction between M and L is represented by the first order reaction respect to each reagents

$$M_f + L_f \underset{k_d}{\overset{k_f}{\rightleftarrows}} ML_T \qquad \text{(IIIA.1)}$$

whose kinetic law can be written as

$$-\frac{d[L_f]}{dt} = k_f[M_f][L_f] - k_d[ML_T] \qquad \text{(IIIA.3)}$$

$$\delta[L]=[L_f]_{eq} - [L_f] \qquad \text{(IIIA.4)}$$

$$\delta[ML] = [ML_T]_{eq} - [ML_T] \qquad \text{(IIIA.5)}$$

and the (IIIA.2) becomes

$$\frac{d\left(\delta[L]-[L_f]_{eq}\right)}{dt} = k_f\left([M_f]_{eq}-\delta[M]\right)\left([L_f]_{eq}-\delta[L]\right) - k_d\left([ML_T]_{eq}-\delta[ML]\right) \qquad \text{(IIIA.6)}$$

or

$$\frac{d\delta[L]}{dt} = k_f[M_f]_{eq}[L_f]_{eq} - k_d[ML_T]_{eq} + k_f\delta[M]\delta[L] - k_f\left([M_f]_{eq}\delta L + [L_f]_{eq}\delta M\right) + k_d\delta[ML] \qquad \text{(IIIA.7)}$$

The mass conservations can be written in differential form as

$$\delta[M] + \delta[ML] = 0 \qquad \text{(IIIA.8)}$$

$$\delta[L] + \delta[ML] = 0 \qquad \text{(IIIA.9)}$$

Introduction of equations (IIIA.9) in (IIIA.7) reasonably assuming that product $\delta[M]\delta[L]$ is negligible and taking into account that $k_f[M_f]_{eq}[L_f]_{eq} = k_d[ML_T]_{eq}$ equation (IIIA.7) reduces to

$$-\frac{d\delta[L]}{\delta[L]} = \left\{k_f\left([M_f]_{eq} + [L_f]_{eq}\right) + k_d\right\}dt \qquad \text{(IIIA.10)}$$

Integration of equation (III.10) yields

$$\delta L = \delta L^0 e^{-t/\tau} \qquad \text{(IIIA.11)}$$

where $1/\tau$ (s^{-1}) is the time constant of reaction (IIIA.1) and is expressed by equation (IIIA.12)

$$\frac{1}{\tau} = k_f\left([M_f]_{eq} + [L_f]_{eq}\right) + k_d \qquad \text{(IIIA.12)}$$

For $C_M \geq 10C_L$ (pseudo first order conditions), equation (IIIA.12) becomes

$$\frac{1}{\tau} = k_f C_M + k_d \qquad \text{(IIIA.13)}$$

which corresponds to equations (3.13) of chapter 3, (4.16) of chapter 4 and (5.24) of chapter 5.

B. Derivation of the relaxation time equation for a dimerization reaction

The dimerization reaction for a complex ML can be described by the reaction

$$2ML \underset{k_d}{\overset{k_f}{\rightleftarrows}} M_2L_2 \qquad \text{(IIIB.1)}$$

where ML is the complex formed starting from M and L. In this case the kinetic law corresponds to

$$\frac{d[M_2L_2]}{dt} = k_f[ML]_{eq}^{\ 2} - k_d[M_2L_2]_{eq} \qquad \text{(IIIB.2)}$$

By using the same procedure described in eqs (IIIA.3)-(IIIA.7), relationship (IIIB.3) is obtained

$$\frac{d\delta[M_2L_2]}{dt} = 2k_f[ML]_{eq}\delta[ML] - k_d\delta[M_2L_2] \qquad \text{(IIIB.3)}$$

The mass conservation equation is

$$C_{ML}=[ML]_{eq}+[M_2L_2]_{eq} \qquad \text{(IIIB.4)}$$

whose differential form is given by eq (IIIB.5)

$$\delta ML + 2\delta M_2L_2 = 0 \qquad \text{(IIIB.5)}$$

Introduction of eq (IIIB.5) in eq (IIIB.3) reduces to

$$\frac{d\delta[M_2L_2]}{\delta[M_2L_2]} = \left\{4k_f[ML]_{eq} + k_d\right\}dt \qquad \text{(IIIB.6)}$$

that integrated yields

$$\delta[M_2L_2] = \delta[M_2L_2]^0 e^{-t/\tau} \qquad \text{(IIIB.7)}$$

where $1/\tau$ (s^{-1}) is the time constant of reaction (IIIB.1) and is expressed by equation (IIIB.8)

$$\frac{1}{\tau} = 4k_f[ML]_{eq} + k_d \qquad \text{(IIIB.8)}$$

that gives a straight line, whose slope and intercept correspond to $4k_f$ and k_d, respectively and that corresponds to eq (5.11) of chapter 5.

As the exact value of $[ML]_{eq}$ is not known, evaluation of $1/\tau$ must be performed by iteration: at the first step $[ML]_{eq}$ in eq (IIIB.8) is replaced by C_{ML}. Thus, dependence of $1/\tau$ on C_{ML} gives a first approximation of k_f and k_d, whose rate, k_f/k_d, corresponds to the apparent constant K_{app}.

Introduction of K_{app} in eq (IIIB.9) allows to determine the equilibrium concetration of the dimer, $[M_2L_2]_{eq}$.

$$[M_2L_2]_{eq} = \frac{\left(2C_{ML} + K_{app}^{-1}\right) - \sqrt{\left(2C_{ML} + K_{app}^{-1}\right)^2 - 4C_{ML}{}^2}}{2} \qquad \text{(IIIB.9)}$$

By using eq (IIIB.4) is possible to determine $[ML]_{eq}$, that can be reintroduced in eq (IIIB.8). This process can be iterated until convergence.

C. Derivation of the relaxation time equation for coupled reactions at the equilibrium

Consider reactions (IIIC.1) and (IIIC.2) (charges omitted) coupled by means of MH_2L:

$$M + H_2L \underset{k_{d1}}{\overset{k_{f1}}{\rightleftarrows}} MH_2L \qquad \text{(IIIC.1)}$$

$$MH_2L \underset{k_{d2}}{\overset{k_{f2}}{\rightleftarrows}} MHL + H \qquad \text{(IIIC.2)}$$

Mass conservation equations are:

$$C_M = M + MHL + MH_2L \qquad \text{(IIIC.3)}$$

$$C_L = H_2L + MHL + MH_2L \qquad \text{(IIIC.4)}$$

that in their differential form reduce to

$$\delta M + \delta MHL + \delta MH_2L = 0 \qquad \text{(IIIC.5)}$$

$$\delta H_2L + \delta MHL + \delta MH_2L = 0 \qquad \text{(IIIC.6)}$$

The reaction system (IIIC.1)-(IIIC.2) is characterized by two kinetic equations:

$$-\frac{d[H_2L]}{dt} = k'_{f1}\,[M]\,[H_2L] - k_{d1}\,[MH_2L] \qquad \text{(IIIC.7)}$$

$$\frac{d[MHL]}{dt} = k_{f2}\,[MH_2L] - k'_{d2}\,[MHL] \qquad \text{(IIIC.8)}$$

where $k'_{f1} = k_{f1}C_M$ e $k'_{d2} = k_{d2}\,[H^+]$.

The displacement of the concentration of each reactant from its equilibrium concentration is:

$$\delta H_2L = [H_2L]_{eq} - [H_2L] \quad \text{(IIIC.9)}$$

$$\delta MH_2L = [MH_2L]_{eq} - [MH_2L] \quad \text{(IIIC.10)}$$

$$\delta MHL = [MHL]_{eq} - [MHL] \quad \text{(IIIC.11)}$$

Introduction of equation (IIIC.9), (IIIC.10) and (IIIC.11) in (IIIC.7) and (IIIC.8) gives:

$$-\frac{d([H_2L]_{eq} - \delta H_2L}{dt} = k'_{f1}([H_2L]_{eq} - \delta H_2L) - k_{d1}([MH_2L]_{eq} - \delta MH_2L) \quad \text{(IIIC.12)}$$

$$\frac{d([MHL]_{eq} - \delta MHL)}{dt} = k_{f2}([MH_2L]_{eq} - \delta MH_2L) - k'_{d2}([MHL]_{eq} - \delta MHL) \quad \text{(IIIC.13)}$$

Equilibrium relationships can be written as in eqs (IIIC.14) and (IIIC.15)

$$k'_{f1}\,[H_2L]_{eq} = k_{d1}[MH_2L] \quad \text{(IIIC.14)}$$

$$k_{f2}\,[MH_2L]_{eq} = k'_{d2}\,[MHL]_{eq} \quad \text{(IIIC.15)}$$

Thus, equation (IIIC.12) and (IIIC.13) reduce to

$$-\frac{d\delta H_2L}{dt} = k'_{f1}\,\delta H_2L - k_{d1}\,\delta MH_2L \quad \text{(IIIC.16)}$$

$$-\frac{d\delta MHL}{dt} = -k_{f2}\,\delta MH_2L + k'_{d2}\,\delta MHL \quad \text{(IIIC.17)}$$

Introduction of equation (IIIC.4) in equations (IIIC.16) and (IIIC.17) gives:

$$-\frac{d\delta H_2L}{dt} = (k'_{f1} + k_{d1})\,\delta H_2L + k_{d1}\,\delta MHL \quad \text{(IIIC.18)}$$

$$-\frac{d\delta MHL}{dt} = k_{f2}\,\delta H_2L + (k_{f2} + k'_{d2})\,\delta MHL \qquad \text{(IIIC.19)}$$

By defining the following parameters:

$a_{11} = k'_{f1} + k_{d1}$

$a_{12} = k_{d1}$

$a_{21} = k_{f2}$

$a_{22} = k'_{d2} + k_{f2}$

equations (IIIC.18) and (IIIC.19) turn to

$$-\frac{d\delta H_2L}{dt} = a_{11}\,\delta H_2L + a_{12}\,\delta MHL \qquad \text{(IIIC.20)}$$

$$-\frac{d\delta MHL}{dt} = a_{21}\,\delta H_2L + a_{22}\,\delta MHL \qquad \text{(IIIC.21)}$$

Such a two-equation system can be solved by considering the eigen-values, λ_k, of the matrix having the coefficients a_{jk}, that is by setting the matrix determinat to zero:

$$\begin{vmatrix} a_{11} - \lambda_k & a_{12} \\ a_{21} & a_{22} - \lambda_k \end{vmatrix} = 0 \qquad \text{(IIIC.22)}$$

Equation (IIIC.22) gives the solutions:

$$\lambda_k = \frac{(a_{11} + a_{22}) \pm \sqrt{(a_{11} + a_{22})^2 - 4(a_{11} \cdot a_{22} - a_{12} \cdot a_{21})}}{2} \qquad \text{(IIIC.23)}$$

Eqs (IIIC.1) and (IIIC.2) constitute a system that can theoretically display two different relaxation effects, each one being characterized by its relaxation time $1/\tau_k = \lambda_k$.

We put k=1 for the fast step (IIIC.1) and k=2 for the slow step (IIIC.2). For the investigated Ni(II)/SHA system (Chapter 3) it results $\lambda_1 >> \lambda_2$. Thus, the equilibrium of reaction (IIIC.1) is not influenced by reaction (IIIC.2).

We can deduce from equation (IIIC.22) that

$$a_{11} + a_{22} = \lambda_1 + \lambda_2 \qquad \text{(IIIC.24)}$$

$$a_{11}\, a_{22} - a_{12}\, a_{21} = \lambda_1\, \lambda_2 \qquad \text{(IIIC.25)}$$

In the case of the Ni(II)/SHA system, being $\lambda_1 >> \lambda_2$ and $a_{11} >> a_{22}$, equation (IIIC.24) turns to

$$\lambda_1 = a_{11} \qquad \text{(IIIC.26)}$$

that is

$$\lambda_1 = k_{f1}\, C_M + k_{d1} \qquad \text{(IIIC.27)}$$

that describes the linear trend of $1//\tau_{fast}$ (= $1//\tau_1 = \lambda_1$) with C_M (Inset of Figure 3.10A of Chapter 3) . On the other hand, by applying the conditions $\lambda_1 >> \lambda_2$ and $a_{11} >> a_{22}$, equation (IIIC.25) reduces to

$$\lambda_2 = \frac{a_{11} \cdot a_{22} - a_{12} \cdot a_{21}}{a_{11}} = a_{22} - \frac{a_{12} \cdot a_{21}}{a_{11}} \qquad \text{(IIIC.28)}$$

by introducing definitions of the coefficients a_{jk} in equation (IIIC.28), we obtain

$$\lambda_2 = k_{f2} + k'_{d2} - \frac{k_{d1} \cdot kf_2}{(k'_{f1} + k_{d1})} \qquad \text{(IIIC.29)}$$

that can be written as

$$\lambda_2 = k'_{d2} + \frac{(k'_{f1}/k_{d1})\cdot k_{f2}}{1+k'_{f1}/k_{d1}} \qquad \text{(IIIC.30)}$$

By putting the definitions of k'_{f1} and k'_{d2} in equation (IIIC.30) and defining $K_1 = k_{f1}/k_{d1}$, equation (IIIC.31) is obtained

$$\lambda_2 = \frac{K_1 \cdot k_{f2} \cdot C_M}{1+K_1 \cdot C_M} - k'_{d2} \qquad \text{(IIIC.31)}$$

that describes the dependence of $1/\!/\tau_{slow}$ (= $1/\!/\tau_2 = \lambda_2$) on C_M (Inset of Figure 3.10B of chapter 3 and Figure 5.17 of chapter 5).

APPENDIX IV

Separation of contributions in aqueous and micellar media for two coupled reaction at the equilibrium.

The reaction between a metal, M, and a ligand, L, can be described by the two step mechanism

$$M + L \underset{k_{d1}}{\overset{k_{f1}}{\rightleftarrows}} (ML)_I \qquad \text{(IV.1)}$$

$$(ML)_I \underset{k_{d2}}{\overset{k_{f2}}{\rightleftarrows}} (ML)_{II} \qquad \text{(IV.2)}$$

Reactions (IV.1) and (IV.2) (charges omitted) are coupled by means of ML.

A surfactant containing solution is formed by two pseudo-phases (aqueous and micellar phases) that are homogeneously mixed. In such a solution, depending on the reactants affinity for each phase, a complexation reaction can take place only in water, in micelle or in both media. In the last case the overall concentrations can be expressed as

$$C_L^T = C_L^W + C_L^S \qquad \text{(IV.3)}$$

$$C_M^T = C_M^W + C_M^S \qquad \text{(IV.4)}$$

$$C_{ML}^T = C_{ML}^W + C_{ML}^S \qquad \text{(IV.5)}$$

where the superscripts “T”, “W” and “S” indicate the concentrations in the whole solution, in water and in micelle, respectively.

Differential forms of equilibrium concentrations for each species are given by eqs (IV.6)-(IV.8).

$$\delta[L]^T = \delta[L]^W + \delta[L]^S \qquad \text{(IV.6)}$$

$$\delta[M]^T = \delta[M]^W + \delta[M]^S \qquad \text{(IV.7)}$$

$$\delta[ML]^T = \delta[ML]^W + \delta[ML]^S \qquad \text{(IV.8)}$$

The relationship between the reactants concentrations in water and in micelle are expressed by the retention coefficients

$R_L = C_L^W/C_L^S$ (IV.9)

$R_M = C_M^W/C_M^S$ (IV.10)

$R_{ML} = C_{ML}^W/C_{ML}^S$ (IV.11)

that were already defined in chapter 3.

Retention coefficients can be expressed also by using the equilibrium concetrations differential forms:

$R_L = \delta[L]^W/\delta[L]^S$ (IV.12)

$R_M = \delta[M]^W/\delta[M]^S$ (IV.13)

$R_{ML} = \delta[ML]^W/\delta[ML]^S$ (IV.14)

When using pseudo-first order conditions ($C_M \geq 10C_L$), the kinetic law for step (IV.1), corresponding to the fast kinetic effect, can be expressed for both the aqueous and micellar medium as reported in eqs (IV.15)-(IV.16).

$$-\frac{d\delta L^W}{dt} = k_f^W C_M^W \delta L^W - k_d^W \delta[ML]^W \quad \text{(IV.15)}$$

$$-\frac{d\delta L^S}{dt} = k_f^S C_M^S \delta L^S - k_d^S \delta[ML]^S \quad \text{(IV.16)}$$

The mass conservations can be written in differential form, for both phases, as

$\delta[M] + \delta[ML] = 0$ (IV.17)

$\delta[L] + \delta[ML] = 0$ (IV.18)

Introduction of eq (IV.18) in eqs (IV.15) and (IV.16) gives

$$-\frac{d\delta L^W}{dt} = k_f^W C_M^W \delta L^W + k_d^W \delta[L]^W \quad \text{(IV.19)}$$

$$-\frac{d\delta L^S}{dt} = k_f^S C_M^S \delta L^S + k_d^S \delta[L]^S \quad \text{(IV.20)}$$

Thus, as already shown in Appendix IIIA, the rate constants for each phase can be

expressed as

$$\frac{1}{\tau_{fast}}^{W} = k_f^W C_M^W + k_d^W \quad \text{(IV.21)}$$

$$\frac{1}{\tau_{fast}}^{S} = k_f^S C_M^S + k_d^S \quad \text{(IV.22)}$$

Combination of eqs (IV.19)-(IV.22) gives

$$-\frac{d\left(\delta[L]^W + \delta[L]^S\right)}{dt} = \frac{1}{\tau_{fast}}^{W} \delta[L]^W + \frac{1}{\tau_{fast}}^{S} \delta[L]^S \quad \text{(IV.23)}$$

Introduction of eqs (IV.6) and (IV.12) in eq (IV.23) leads to

$$-\frac{d\delta[L]^T}{dt} = \frac{1}{\tau_{fast}}^{W} \frac{R_L}{(1+R_L)} \delta[L]^T + \frac{1}{\tau_{fast}}^{S} \frac{1}{(1+R_L)} \delta[L]^T \quad \text{(IV.24)}$$

Therefore the rate constant for the reaction in the overall solution corresponds to

$$\frac{1}{\tau_{fast}}^{T} = \frac{1}{\tau_{fast}}^{W} \frac{R_L}{(1+R_L)} + \frac{1}{\tau_{fast}}^{S} \frac{1}{(1+R_L)} \quad \text{(IV.25)}$$

Insertion of eqs (IV.21) and (IV.22) in eq (IV.25) allows to express $1/\tau_{fast}^T$ as a function of the metal concentration in each phase.

$$\frac{1}{\tau_{fast}}^{T} = \left(k_f^W C_M^W + k_d^W\right)\frac{R_L}{(1+R_L)} + \left(k_f^S C_M^S + k_d^S\right)\frac{1}{(1+R_L)} \quad \text{(IV.26)}$$

By introducing eqs (IV.7) and (IV.10) into eq (IV.26), one can obtain the $1/\tau^T$ dependence on the total metal concentration in solution, C_M^T.

$$\frac{1}{\tau_{fast}}^{T} = \left\{k_f^W \frac{R_M}{(1+R_M)}\frac{R_L}{(1+R_L)} + k_f^S \frac{1}{(1+R_M)}\frac{1}{(1+R_L)}\right\} C_M^T + \left\{k_d^W R_L + k_d^S\right\}\frac{1}{(1+R_L)} \quad \text{(IV.27)}$$

that corresponds to eq 3.14 of chapter 3.

Eq (IV.27) represents a straight line, whose slope and intercept depend on the forward and reverse kinetic constants both in water and in micellar solution. Being the kinetic constants in water (k_f^W and k_d^W) known from literature, it is possible to determine k_f^S and k_d^S.

Reactive step (IV.2) corresponds to the slow kinetic effect of the whole mechanism. As demonstrated in Appendix IIIC, the rate constant of the slower of two coupled reactions can be expressed as

$$\frac{1}{\tau_{slow}}^{T} = \frac{K_1 k_{f2} C_M^T}{1 + K_1 C_M^T} + k_{d2} \qquad \text{(IV.28)}$$

where K_1 represents the equilibrium constant of reaction (IV.1) and $1/\tau_{slow}^{T}$ is the rate constant of the slow step in the overall solution. The same equation can be used to describe the rate constants in aqueous and micellar phases:

$$\frac{1}{\tau_{slow}}^{W} = \frac{K_1^W k_{f2}^W C_M^W}{1 + K_1^W C_M^W} + k_{d2}^W \qquad \text{(IV.29)}$$

$$\frac{1}{\tau_{slow}}^{S} = \frac{K_1^S k_{f2}^S C_M^S}{1 + K_1^S C_M^S} + k_{d2}^S \qquad \text{(IV.30)}$$

The overall kinetic law for step (IV.2) can be expressed as the sum of the contributions in both the phases, in analogy with eq (IV.23).

$$-\frac{d\left(\delta[ML_I]^W + \delta[ML_I]^S\right)}{dt} = \frac{1}{\tau_{slow}}^{W} \delta[ML_I]^W + \frac{1}{\tau_{slow}}^{S} \delta[ML_I]^S \qquad \text{(IV.31)}$$

Introduction of eqs (IV.8) and (IV.14) in eq (IV.31) gives

$$-\frac{d\delta[ML]^T}{dt} = \frac{1}{\tau_{slow}}^{W} \frac{R_{ML}}{(1+R_{ML})} \delta[ML]^T + \frac{1}{\tau_{slow}}^{S} \frac{1}{(1+R_{ML})} \delta[ML]^T \qquad \text{(IV.32)}$$

and the rate constant for the slower reactive step in the overall solution is provided by eq (IV.33).

$$\frac{1}{\tau_{slow}}^{T} = \frac{1}{\tau_{slow}}^{W} \frac{R_{ML}}{(1+R_{ML})} + \frac{1}{\tau_{slow}}^{S} \frac{1}{(1+R_{ML})} \qquad \text{(IV.33)}$$

By introducing eqs (IV.29) and (IV.30) in eq (IV.33) it is possible to express $1/\tau_{fast}^{T}$ as a function of the metal concentration in water (C_M^W) and in micellar phase (C_M^S).

$$\frac{1}{\tau_{slow}}^{T} = \left[\frac{K_1^W k_{f2}^W C_M^W R_{ML}}{1+K_1^W C_M^W} + k_{d2}^W R_{ML} + \frac{K_1^S k_{f2}^S C_M^S}{1+K_1^S C_M^S} + k_{d2}^S\right]\frac{1}{(1+R_{ML})} \qquad \text{(IV.34)}$$

Insertion of eqs (IV.7) and (IV.10) in eq (IV.34) gives eq (IV.35), where $1/\tau_{slow}^{T}$ depends on the total metal concentration.

$$\frac{1}{\tau_{slow}}^{T} = \left[\frac{K_1^W k_{f2}^W R_M R_{ML}}{1+R_M+K_1^W R_M C_M^T} + \frac{K_1^S k_{f2}^S}{1+R_M+K_1^S C_M^T}\right]\frac{C_M^T}{(1+R_{ML})} + \left[k_{d2}^W R_{ML} + k_{d2}^S\right]\frac{1}{(1+R_{ML})} \qquad \text{(IV.35)}$$

Eq (IV.35) corresponds to eq (3.20) of chapter 3. All parameters in water are known from literature. Once known K_1^S, for instance from static experiments, it is possible to derive the kinetic constants of the slow effect in the micellar phase (k_{f2}^S and k_{d2}^S), without the contribution of the reaction in the aqueous phase.

APPENDIX V

Derivation of the equilibrium constants for hydrolysis, dimerization and trimerization of Iron(III).

The mass conservation for Iron(III) is expressed by equation (V.1) (charges omitted).

$$C_M = [Fe] + [FeOH] + 2[D] + 3[T] \qquad (V.1)$$

where D = $Fe_2(OH)_2^{4+}$ and T = $Fe_3(OH)_4^{5+}$ (see scheme (4.2) of chapter 4)
The equilibrium constants to be evaluated are defined as:

$$K_H = [FeOH]\frac{[H]}{[Fe]} \qquad (V.2)$$

$$K_D = \frac{[D]}{[FeOH]^2} \qquad (V.3)$$

$$K_T = \frac{[T][H]}{[FeOH][D]} \qquad (V.4)$$

The absorbance of the system is given by equation (V.5).

$$A = \varepsilon_{Fe}[Fe] + \varepsilon_{FeOH}[FeOH] + \varepsilon_D[D] + \varepsilon_T[T] \qquad (V.5)$$

Introduction of equations (V.2), (V.3) and (V.4) into equation (V.1) yields equation (V.6).

$$\frac{3K_TK_D[FeOH]^3}{[H]} + 2K_D[FeOH]^2 + \left(1 + \frac{[H]}{K_H}\right)[FeOH] - C_M = 0 \qquad (V.6)$$

Introduction of equations (V.2), (V.3) and (V.4) into (V.5) and division by equation (1.1) yields equation (V.7).

$$\frac{A}{C_M} = \frac{\left(\varepsilon_{Fe}\frac{[H]}{K_H} + \varepsilon_{FeOH}\right) + \varepsilon_D K_D [FeOH] + \varepsilon_T K_D K_T \frac{[FeOH]^2}{[H]}}{\left(1 + \frac{[H]}{K_H}\right) + 2K_D [FeOH] + 3K_T K_D \frac{[FeOH]^2}{[H]}} \qquad (V.7)$$

A first evaluation of [FeOH] is provided by the solution of equation (V.6), in which rough estimates of K_H, K_D and K_T are first introduced. The obtained [FeOH] values are then introduced in equation (V.7) and the values of the parameters are obtained by a non-linear least-square procedure. The so obtained values of K_H, K_D and K_T are reintroduced in equation (V.6) and the procedure is repeated to convergence. The final [FeOH] values are calculated solving for the cubic equation (V.6) and the molar fraction of FeOH is then obtained as $\alpha_{FeOH} = \frac{[FeOH]}{C_M}$.

APPENDIX VI

Derivation of the relaxation times for a system of coupled reactions using the Castellan's method

Consider the reaction scheme (charges omitted)

$$Fe \rightleftarrows FeOH + H \qquad \text{(VI.1)}$$

$$2\,FeOH \rightleftarrows D \qquad \text{(VI.2)}$$

$$D + FeOH \rightleftarrows T + H \qquad \text{(VI.3)}$$

Following an external perturbation of the system equilibrium, reaction (VI.1) reaches the equilibrium much faster than reactions (VI.2) and (VI.3), so the $\frac{[FeOH]}{[Fe]} = \frac{K_H}{[H]}$ ratio remains constant for each [H] value (in excess) considered. This fact has enabled us to reduce the reaction system to the simpler form

$$2M \underset{c_{-D}}{\overset{c_D}{\rightleftarrows}} D \qquad \text{(VI.4)}$$

$$D + M \underset{c_{-T}}{\overset{c_T}{\rightleftarrows}} T \qquad \text{(VI.5)}$$

where [M] = [Fe] + [FeOH].

Let's denote the exchange rates of reactions (VI.4) and (VI.5) as r_D and r_T, respectively.

$$r_D = c_D [M]^2 = c_{-D} [D] \qquad \text{(VI.6)}$$

$$r_T = c_T [D][M] = c_{-T} [T] \qquad \text{(VI.7)}$$

According to Castellan (Castellan, 1963), the coupling coefficients of the reaction system (VI.4)-(VI.5) are defined as:

$$g_{11} = \frac{4}{[M]} + \frac{1}{[D]} \tag{VI.8}$$

$$g_{12} = g_{21} = \frac{2}{[M]} - \frac{1}{[D]} \tag{VI.9}$$

$$g_{22} = \frac{1}{[M]} + \frac{1}{[D]} + \frac{1}{[T]} \tag{VI.10}$$

The two relaxation times, $1/\tau_k$, of the system of coupled reaction (VI.4)-(VI.5) depend on the equilibrium concentrations according to the determinant equation (VI.11)

$$\begin{vmatrix} r_D g_{11} - \frac{1}{\tau_k} & r_D g_{12} \\ r_T g_{21} & r_T g_{22} - \frac{1}{\tau_k} \end{vmatrix} = 0 \tag{VI.11}$$

which provides the expressions for $1/\tau_k$ in the form (VI.12)

$$\frac{1}{\tau_k} = \frac{TR \pm \sqrt{TR^2 - 4DET}}{2} \tag{VI.12}$$

where TR is the trace and DET is the determinant of equation (VI.11). The k = 1 value corresponds to $1/\tau_f$ (fast) and k = 2 corresponds to $1/\tau_s$ (slow). Instead of considering separately the two expressions (VI.12), we have applied the properties

$$\frac{1}{\tau_f} + \frac{1}{\tau_s} = TR \tag{VI.13}$$

$$\frac{1}{\tau_f} \times \frac{1}{\tau_s} = DET \tag{VI.14}$$

where $TR = r_D g_{11} + r_T g_{22}$ and $DET = r_D r_T (g_{11} g_{22} - g_{12} g_{21})$.

Introduction of equations (VI.6)-(VI.10) into equations (VI.13) and (VI.14) yields equations (VI.15) and (VI.16)

$$\frac{1}{\tau_f} + \frac{1}{\tau_s} = (4\chi_D + \chi_T)[M] + (\chi_{-D} + \chi_{-T}) \quad \text{(VI.15)}$$

$$\frac{1}{\tau_f} \times \frac{1}{\tau_s} = 6\chi_D\chi_T[M]^2 + 4\chi_D\chi_{-T}[M] + \chi_{-D}\chi_{-T} \quad \text{(VI.16)}$$

Since the concentration of the total monomer, [M] over the explored range of concentrations is much higher than that of the aggregated species, one can replace [M] by C_M.

Equations (VI.15) and (VI.16) are reported in the text (equation 4.7 and 4.8 of chapter 4) with this approximation.

APPENDIX VII

Derivation of the relaxation times for the complex formation between Iron(III) and SHA

Consider the reactions (charges omitted)

$$\begin{array}{ccc} FeOH + H_3L & \underset{k_{-1}}{\overset{k_1}{\rightleftharpoons}} & FeH_2L + H_2O \\ K_D \Big\Updownarrow FeOH & & K_C \Big\Updownarrow FeOH \end{array} \qquad \text{(VII.1)}$$

$$Fe_2(OH)_2 + H_3L \underset{k_{-2}}{\overset{k_2}{\rightleftharpoons}} Fe_2OHH_2L + H_2O \qquad \text{(VII.2)}$$

$$Fe_2OHH_2L \underset{k_{-3}}{\overset{k_3}{\rightleftharpoons}} Fe_2HL + H_2O \overset{1/K_{CH}}{\rightleftharpoons} Fe_2L + H \qquad \text{(VII.3)}$$

which are coupled to the hydrolysis and self aggregation reactions (S2.1), (S2.2) and (S2.3) though the common components FeOH and $Fe_2(OH)_2$ (≡ D). Note that K_{CH} = $[Fe_2HL]/([Fe_2L][H])$.

The derivation of the relaxation times shown below does imply that both the vertical steps of the above reaction scheme should be faster compared with the horizontal steps. Using the data of Tables 4.1 and 4.3, and accepting the (reasonable) assumption that the rate constant, k_C, of the vertical step corresponding to K_C, is similar to k_D, then we have estimated the ratios of the rates of the exchange reactions r_D/r_2 and r_C/r_1. Over the Iron(III) and SHA concentration range employed, it turns out that r_D/r_2 ranges between 43 M s^{-1} and 215 M s^{-1}, whereas r_C/r_1 ranges between 150 M s^{-1} and 1050 M s^{-1}. The hypothesis formulated to derive the expression for $1/t_{fast}$, that the vertical steps are fast compared to the horizontal steps, is thus reliable. Note that if the reverse were true, *i.e.* $r_C/r_1 \ll 1$, then the first-order term with respect to $FeOH^{2+}$ would not be observed in the fast process, in contrast with the experimental observation. On the other hand, if r_C and r_1 were the same order, the fast process would display a biexponential behavior, contrary to experiments as well.

The mass conservation with respect to the ligand is expressed, in differential form, by eq (VII.4)

$$\delta[H_3L] + \delta[FeH_2L] + \delta[Fe_2OHH_2L] + \delta[Fe_2L] + \delta[Fe_2HL] = 0 \qquad \text{(VII.4)}$$

The reacting system displays two relaxation effects well separated on the time scale, so the fast effect can be analyzed separately from the slow one.

Fast effect

Step (VII.3) is assumed to be slow compared to preceding steps, so the fast effect does involve only reactions (VII.1) and (VII.2). Under these circumstances eq (VII.4) reduces to eq (VII.5)

$$\delta[H_3L] + \delta[FeH_2L] + \delta[Fe_2OHH_2L] = 0 \qquad \text{(VII.5)}$$

Under pseudo-first order conditions ($C_M/C_L \geq 10$), the rate equation of the fast step, expressed as the rate of disappearance of the ligand, is given by eq (VII.6)

$$-\frac{d\delta[H_3L]}{dt} = k_1[FeOH]\delta[H_3L] + k_2[Fe_2(OH)_2]\delta[H_3L] - k_{-1}\delta[FeH_2L] - k_{-2}\delta[Fe_2OHH_2L] \qquad \text{(VII.6)}$$

Under the conditions in which the vertical equilibria characterized by K_D and K_C are fast with respect to the horizontal steps, eq (VII.6) becomes:

$$-\frac{d\delta[H_3L]}{dt} = (k_1[FeOH] + k_2K_D[FeOH]^2)\delta[H_3L] - \left(k_{-1} + k_{-2}\frac{\delta[Fe_2OHH_2L]}{\delta[FeH_2L]}\right)\delta[FeH_2L] \qquad \text{(VII.7)}$$

and eq (VII.5) becomes:

$$\delta[H_3L] = -\delta[FeH_2L](1 + K_C[FeOH]) \qquad \text{(VII.8)}$$

Introduction of eq (VII.8) into eq (VII.7) yields

$$-\frac{d\delta[H_3L]}{dt} = \left[k_1[FeOH] + k_2K_D[FeOH]^2 + \left(\frac{k_{-1} + k_{-2}K_C[FeOH]}{1 + K_C[FeOH]}\right)\right]\delta[H_3L] \qquad \text{(VII.9)}$$

Integration of eq (VII.9) provides the expression for the relaxation time of the fast effect in the form of eq (VII.10)

$$\frac{1}{\tau_{fast}} = k_1[FeOH] + k_2K_D[FeOH]^2 + \left(\frac{k_{-1} + k_{-2}K_C[FeOH]}{1 + K_C[FeOH]}\right) \qquad \text{(VII.10)}$$

Slow effect

Since steps (VII.1) and (VII.2) are much faster than the process (VII.3), the former reactions are now assumed to be described by their equilibrium constants, $K_1 = k_1/k_{-1}$ and $K_2 = k_2/k_{-2}$. The mass conservation is now expressed by eq (VII.4) which, taking into account that also the proton transfer step characterized by $1/K_{CH}$ is fast, yields eq (VII.11)

$$\left(\frac{1 + K_1[FeOH]}{K_2[Fe_2(OH)_2]} + 1\right)\delta[Fe_2OHH_2L] = -\left(\frac{1 + K_{CH}[H]}{K_{CH}[H]}\right)\delta[Fe_2HL] \qquad \text{(VII.11)}$$

The rate equation corresponding to the slow process can be written in the form of eq (VII.12)

$$\frac{d(\delta[Fe_2HL] + \delta[Fe_2L])}{dt} = k_3\delta[Fe_2OHH_2L] - k_{-3}\delta[Fe_2HL] \qquad \text{(VII.12)}$$

Introducing the expression for $1/K_{CH}$ and eq (VII.11) into eq (VII.12), one obtains eq (VII.13).

$$\frac{d\delta[Fe_2HL]}{dt} = \left(k_3\frac{K_2[Fe_2(OH)_2]}{1 + K_1[FeOH] + K_2[Fe_2(OH)_2]} + k_{-3}\frac{K_{CH}[H]}{1 + K_{CH}[H]}\right)\delta[Fe_2HL] \qquad \text{(VII.13)}$$

Expressing $[Fe_2(OH)_2]$ as $K_D[FeOH]^2$, integration of eq (VII.13) yields the expression for the relaxation time of the slow effect as eq (VII.14)

$$\frac{1}{\tau_{slow}} = \frac{k_3 K_D K_2 [FeOH]^2}{1 + K_1[FeOH] + K_2 K_D [FeOH]^2} + \frac{k_{-3} K_{CH}[H]}{1 + K_{CH}[H]} \qquad \text{(VII.14)}$$

Note that in complex dissociation kinetics the forward step could be neglected and the time constant denoted in chapter 4 as $1/t_{diss}$ becomes:

$$\frac{1}{\tau_{diss}} = \frac{k_{-3} K_{CH}[H]}{1 + K_{CH}[H]} \qquad \text{(VII.15)}$$

Appendix VIII

Derivation of the relationship between the apparent binding constant, K_{app}, and the individual binding constant, K

Consider the apparent reaction (VIII.1)

$$M_f + L_f \rightleftarrows ML_T \qquad \text{(VIII.1)}$$

whose equilibrium constant is defined according to eq (VIII.2)

$$K_{app} = \frac{[ML_T]}{[M_f][L_f]} \qquad \text{(VIII.2)}$$

In the case of the Iron(III)/BHA system, it runs out that, in the range of the investigated acidity

$$[ML_T] = [FeHL] \qquad \text{(VIII.3)}$$

$$[L_f] = [H_2L] \qquad \text{(VIII.4)}$$

$$[M_f] = [FeOH]/\alpha_{FeOH} \qquad \text{(VIII.5)}$$

Introduction of eqs (VIII.3), (VIII.4) and (VIII.5) in eq (VIII.2) yields

$$K_{app} = \frac{[FeHL]}{[FeOH][H_2L]}\alpha_{FeOH} \qquad \text{(VIII.6)}$$

The concentration ratio in eq (VIII.6) represents KML, the stability constant of the FeHL complex formed by reaction of FeOH with H_2L (reaction (12) of the text). Hence, eq (VIII.6) converts to:

$$K_{app} = K_{ML}\alpha_{FeOH} \qquad \text{(VIII.7)}$$

The derivation of α_{FeOH}, defined as α_{FeOH} = [FeOH]/[M_f] requires the solution of the cubic equation (VIII.8) to obtain [FeOH].

$$\frac{3K_T K_D}{[H^+]}[FeOH]^3 + 2K_D[FeOH]^2 + \left(1 + \frac{[H^+]}{K_H}\right)[FeOH] - [M_f] = 0 \qquad \text{(VIII.8)}$$

Since $C_M >> C_L$ it turns out that [M_f] ≅ C_M, so in eq (VIII.8) [M_f] has to be replaced by C_M .

APPENDIX IX

Derivation of the fast relaxation time at $[H^+] > 0.04$ M according to reactions (4.1)-(4.2)-(4.5) of Chapter 4

Let´s consider the reaction scheme (charges omitted)

$$Fe \overset{K_H}{\rightleftarrows} FeOH + H \qquad \text{(IX.1)}$$

$$2\,FeOH \overset{k_D}{\underset{k_{-D}}{\rightleftarrows}} D \qquad \text{(IX.2)}$$

$$FeOH + Fe \overset{k'_D}{\underset{k'_{-D}}{\rightleftarrows}} D + H \qquad \text{(IX.2')}$$

$$D + FeOH \rightleftarrows T + H \qquad \text{(IX.3)}$$

under conditions of relatively high acidity, step (IX.3) can be neglected, so the reacting system is represented by steps (IX.1), (IX.2) and (IX.2'). If the displacement of the equilibria is small, as it occurs in the case of a dilution jump, then the chemical relaxation analysis can be applied to the reacting system as follows. The mass conservation equation in differential form is given by:

$$\delta Fe + \delta FeOH + 2\delta D = 0 \qquad \text{(IX.4)}$$

The protonation transfer step (IX.1) is very fast with respect to the steps of dimer formation. Moreover, since the H^+ concentration is sufficiently high to buffering the system, the equilibrium expression for reaction (IX.1) can be written in differential form as eq (IX.5):

$$\delta Fe = \frac{[H]}{K_H}\delta FeOH \qquad \text{(IX.5)}$$

Introduction of eq (IX.5) into eq (IX.4) yields eq (IX.6):

$$\delta FeOH = -2\frac{K_H}{[H]+K_H}\delta D \qquad \text{(IX.6)}$$

Therefore, the rate of the dimer formation in differential from is given by eq (IX.7):

$$\frac{d\delta D}{dt} = 2k_D[FeOH]\delta FeOH + k'_D([Fe]\delta FeOH + [FeOH]\delta Fe) - k_{-D}\delta D - k'_{-D}[H]\delta D \qquad \text{(IX.7)}$$

Introduction of eqs (IX.5) and (IX.6) into eq (IX.7) yields eq (IX.8):

$$-\frac{d\delta D}{dt} = \left[4\left(k_D + k'_D\frac{[H]}{K_H}\right)\left(\frac{K_H}{[H]+K_H}\right) + \left(k_{-D} + k'_{-D}[H]\right)\right]\delta D \qquad \text{(IX.8)}$$

Integration of eq (IX.8) yields the expression for the fast relaxation time in the form of eq (IX.9)

$$1/\tau_f = 4\left(k_D + k'_D\frac{[H]}{K_H}\right)\left(\frac{K_H}{[H]+K_H}\right) + \left(k_{-D} + k'_{-D}[H]\right) \qquad \text{(IX.9)}$$

which corresponds to equation (4.6) of chapter 4.

References

- Albrecht-Gary, A.-M. and Crumbliss, A.L., Coordination chemistry of siderophores: Thermodynamics and kinetics of iron chelation and release. *Met. Ions Biol. Syst.* **1998**, 35, 239-327.

- Aniansson, E.A.G., Wall, S.N., Almgren, M., Hoffmann, H., Kielmann, I., Ulbricht, W., Zana, R., Lang, J. and Tondre, C., Theory of the kinetics of micellar equilibria and quantitative interpretation of chemical relaxation studies of micellar solutions of ionic surfactants. *J. Phys. Chem.* **1976**, 80(9), 905-922.

- Arnold, M., Brown, D.A., Deeg, O., Errington, W., Haase, W., Herlihy, K., Kemp, T.J., Nimir, H. and Werner, R., Hydroxamate-bridged dinuclear nickel complexes as models for urease inhibition. *Inorg. Chem.* **1998**, 37, 2920-2925.

- Artemenko, A.I., Anufriev, E.K. and Tikunova, I.V., Study of the structure of noncomplex salts of hydroxamic acids by an IR-spectroscopic method. *Zh. Prikl. Spektrosk.* **1980**, 32(4), 641-647.

- Baes, C.F. and Mesmer, R.E., The hydrolysis of cations, John Wiley & Sons, New York, **1976**.

- Beccia, M.R., Biver, T., García, B., Leal, J.M., Secco, F. and Venturini, M., Route to metallacrowns: The mechanism of formation of a dinuclear Iron(III)-salicylhydroxamate complex. *Inorg. Chem.* **2011**, 50(20), 10152-10162.

- Bechtler, A., Breitschwerdt, K.G. and Tamm, K., Ultrasonic relaxation studies in aqueous solutions of 2-2 electrolytes. *J. Chem. Phys.* **1970**, 52, 2975-2982.

- Berezin, I.V., Yatsimirski, A.K. and Martinek, K., *Dokl. Akad. Nauk SSSR* **1970**, 194, 840.

- Birus, M., Van, E.R., Gabricevic, M. and Zahl, A., NMR kinetic study of lanthanum(III) complexation with acetohydroxamic acid. *Eur. J. Inorg. Chem.* **2002**, 819-825.

- Biver, T., Ghezzi, L., Malvaldi, V., Secco, F., Tinè, M.R. and Venturini, M., Kinetics and equilibria of the interaction of 8-hydroxyquinoline with gallium(III) in water and sodium dodecyl sulfate solution. *J. Phys. Chem. B* **2009**, 113(6), 1598-1606.

- Brown, D.A., Googan, R.A., Fitzpatrick, N.J., Glass, W.K., Abukshima, D.e., Shiiels, L., Ahlgran, M., Smolander, K., Pakkanen, T.T., Pakkanen, T.A. and Perakyla, M., Conformational behavior of hydroxamic acids: Ab initio and structural studies. *J. Chem. Soc., Perkin Trans. 2* **1996**, 2673-2680.

- Burgess, J., Metal ions in solution. Ellis Horwood Ltd. , Chichester, U.K., **1979**.

- Burt, W.R., Underwood, A.L. and Appleton, G.L., Hydroxamic acid from histoplasma capsulatum that displays growth factor activity. *Appl. Environ. Microbiol.* **1981**, 42, 560-563.

- Buzatu, S. and Darie, V., Is the facilitated diffusion exclusively a passive membrane transport mechanism? *Roum. Biotechnol. Lett.* **2003**, 8, 1123-1128.

- Byers, B.R., Powell, M.V. and Lankford, C.E., Iron-chelating hydroxamic acid (schizokinen) active in initiation of cell division in bacillus megaterium. *J. Bacteriol.* **1967**, 93, 286-294.

- Careri, M., Dallavalle, F., Tegoni, M. and Zagnoni, I., Pentacopper(II) 12-metallacrown-4 complexes with α- and β-aminohydroxamic acids in aqueous solution: A reinvestigation. *J. Inorg. Biochem.* **2003**, 93, 174-180.

- Castellan, G.W., Calculation of the spectrum of chemical relaxation times for a general reaction mechanism. *Ber. Bunsen Phys. Chem.* **1963**, 67(9), 898-908.

- Chatlas, J. and Jordan, R.B., Complexation of the aqua-iron(III) dimer by tiron - kinetics of complex-formation and dissociation. *Inorg. Chem.* **1994**, 33(17), 3817-3822.

- Cöklen, K.E. and Hatton, T.A., Protein extraction using reverse micelles. *Biotechnol. Progr.* **1985**, 1(1), 69-74.

- Connick, R.E. and Fiat, D., Coordination numbers of beryllium and aluminum ions in aqueous solutions. *J. Chem. Phys.* **1963**, 39, 1349-1351.

- Dallavalle, F., Remelli, M., Sansone, F., Bacco, D. and Tegoni, M., Thermodynamics of self-assembly of copper(ii) 15-metallacrown-5 of Eu(III) or Gd(III) with (S)-α-alaninehydroxamic acid in aqueous solution. *Inorg. Chem.* **2010**, 49, 1761-1772.

- D'Amico, M.L., Paiotta, V., Secco, F. and Venturini, M., A kinetic study of the intercalation of ethidium bromide into poly(A)-poly(U). *J. Phys. Chem. B* **2002**, 106(48), 12635-12641.

- Davies, C.W., Ion association. Butterworths, London, **1962**.

- Dobosz, A., Dudarenko, N.M., Fritsky, I.O., Glowiak, T., Karaczyn, A., Kozlowski, H., Sliva, T.Y. and Swiatek-Kozlowska, J., N-bonding of the hydroxamic function in nickel(II) and copper(II) complexes with 2-(hydroxyimino)propanohydroxamic acid. *J. Chem. Soc., Dalton Trans.* **1999**, 743-750.

- Doulia, D. and Xiarchos, I., Ultrafiltration of micellar solutions of nonionic surfactants with or without alachlor pesticide. *J. Membr. Sci.* **2007**, 296(1-2), 58-64.

- Duan, J.J.W., Chen, L., Wasserman, Z.R., Lu, Z., Liu, R.-Q., Covington, M.B., Qian, M., Hardman, K.D., Magolda, R.L., Newton, R.C., Christ, D.D., Wexler, R.R. and Decicco, C.P., Discovery of γ-lactam hydroxamic acids as selective inhibitors of tumor necrosis factor α converting enzyme: Design, synthesis, and structure activity relationships. *J. Med. Chem.* **2002**, 45(23), 4954-4957.

- Eigen, M. and Tamm, K., Sound absorption in electrolytes as a consequence of chemical relaxation. I. Relaxation theory of stepwise dissociation. II. *Z. Elektrochem. Angew. Phys. Chem.* **1962**, 66, 107-121.

- Eigen, M. and Wilkins, R.G., The kinetics and mechanism of formation of metal complexes. *Adv. Chem. Ser.* **1965**, 49, 55-67.

- Engberts, J.B.F.N., Catalysis by surfactant aggregates in aqueous solutions. *Pure & Appl. Chem* **1992**, 64(11), 1653-1660.

- Exner, O., Hradil, M. and Mollin, J., Dissociation of hydroxamic acids: Solvent effects. *Collect. Czech. Chem. Commun.* **1993**, 58, 1109-1121.

- Exner, O. and Kakac, B., Acyl derivatives of hydroxylamine. VIII. A spectroscopic study of tautomerism of hydroxamic acids. *Collect. Czech. Chem. Commun.* **1963**, 28, 1656-1663.

- Farkas, E., Buglyó, P., Complex formation between transition metals and DL-Aspartic Acid-β-hydroxamic Acid (N-Hydroxyasparagine). *J. Chem. Soc., Dalton Trans.***1990**, 5, 1549-1551.

- Farkas, E., Enyedy, E.A., Micera, G. and Garribba, E., Coordination modes of hydroxamic acids in copper(II), nickel(II) and zinc(II) mixed-ligand complexes in aqueous solution. *Polyhedron* **2000**, 19, 1727-1736.

- Farkas, E., Szoke, J., Kiss, T., Kozlowski, H. and Bal, W., Complex-forming properties of l-α-Alaninehydroxamic acid (2-amino-n-hydroxypropanamide). *J. Chem. Soc., Dalton Trans.* **1989**, (11), 2247-2251.

- Ferrit, M.N., Del Valle, C. and Martinez, F., The study of the influence of surfactant charge on alkaline hydrolysis reactions of acetylsalicylic acid (Asa) and triflusal (TFL) using spectrophotometric methods. *Eur. J. Pharm. Sci.* **2007**, 31(3-4), 211-220.

- Fillipi, B.R., Scamehorn, J.F., Christian, S.D. and Taylor, R.W., A comparative economic analysis of copper removal from water by ligand-modified micellar-enhanced ultrafiltration and by conventional solvent extraction. *J. Membr. Sci.* **1998**, 145(1), 27-44.

- Fuoss, R.M., Parametric analysis of conductance data. *Proc. Natl. Acad. Sci. U. S. A.* **1974**, 71, 4491-4495.

- García, B., Ibeas, S., Hoyuelos, F.J., Leal, J.M., Secco, F. and Venturini, M., Hydroxamic acids as weak base indicators: Protonation in strong acid media. *J. Org. Chem.* **2001**, 66, 7986-7993.

- García, B., Secco, F., Ibeas, S., Munoz, A., Hoyuelos, F.J., Leal, J.M., Senent, M.L. and Venturini, M., Structural NMR and ab initio study of salicylhydroxamic and p-hydroxybenzohydroxamic acids: Evidence for an extended aggregation. *J. Org. Chem.* **2007**, 72, 7832-7840.

- Gazzaz, H.A. and Robinson, B.H., Kinetics involving divalent metal ions and ligands in surfactant self-assembly systems: Applications to metal-ion extraction. *Langmuir* **2000**, 16, 8685-8691.

- Ghezzi, L., Metal ions extraction and recovery by using micellar systems. PhD Thesis, University of Pisa, **2008**.

- Ghezzi, L., Robinson, B.H., Secco, F., Tinè, M.R. and Venturini, M., Binding of Pd(II) to PADA in water/micellar system: Complex formation, kinetics in water and DTAC solution. *Colloid Surface A* **2007**, 292(2-3), 139-147.

- Ghosh, K.K., Kinetic and mechanistic aspects of acid-catalyzed hydrolysis of hydroxamic acids. *Indian J. Chem., Sect. B: Org. Chem. Incl. Med. Chem.* **1997**, 36B, 1089-1102.

- Ghosh, K.K. and Tiwary, L.K., Influence of sodium bis (2-ethyl-1-hexyl) sulfosuccinate/isooctane/water microemulsions on the hydrolysis of salicylhydroxamic acid. *J. Mol. Liq.* **2003**, 102(1-3), 183-195.

- Gibney, B.R., Kessissoglou, D.P., Kampf, J.W. and Pecoraro, V.L., Copper(II) 12-metallacrown-4: Synthesis, structure, ligand variability, and solution dynamics in the 12-MC-4 structural motif. *Inorg. Chem.* **1994**, 33(22), 4840-4849.

- Gibney, B.R., Pecoraro, V.L., Huang, M., Coucouvanis, D., Blanton, W.B. and Gordon-Wylie, S.W., Synthesis of selected supramolecules. Use of salicyl- and naphthoyl-hydroxamate complexes in preparation of manganese and copper 12-metallacrown-4 complexes: Mn(II)(acetate)2[Mn(III)(salicylhydroxamate)]$_4$ and 2[Cu(II)$_5$(naphthoylhydroxamate)$_4$]. *Inorg. Synth.* **2002**, 33, 70-74.

- Gruen, D., The standard picture of ionic micelles surfactants, adsorption, surface spectroscopy and disperse systems. Lindman, B., Olofsson, G. and Stenius, P.,**1985**, Springer Berlin - Heidelberg. **70,** 6-16.

- Guntelberg, E., Untersuchungen uber ioneninteraktion. *Z. Phys. Chem,* **1926**, 123, 199-247.

- Hartley, G.S. and Roe, J.W., Ionic concentrations at interfaces. *Trans. Faraday Soc.* **1940**, 36, 101.

- Helm, L. and Merbach, A.E., Water exchange on metal ions: Experiments and simulations. *Coord. Chem. Rev.* **1999**, 187, 151-181.

- James, A.D. and Robinson, B.H., Micellar catalysis of metal-complex formation. Kinetics of the reaction between Ni(II) and pyridine-2-azo-p-dimethylaniline (PADA) in the presence of sodium dodecylsulphate micelles; a model system for the study of metal ion reactivity at charged interfaces. *J. Chem. Soc., Faraday Trans. 1: Physical Chemistry in Condensed Phases* **1978**, 74, 10-21.

- Jankolovits, J., Kampf, J.W., Maldonado, S. and Pecoraro, V.L., Voltammetric characterization of redox-inactive guest binding to Ln(III)[15-metallacrown-5] hosts based on competition with a redox probe. *Chem. Eur. J.* **2010**, 16, 6786-6796.

- Jobe, D.J., Reinsborough, V.C. and White, P.J., Solubilization sites in micellar sodium octylsulphate solutions by ultrasonic spectroscopy. *Can. J. Chem.* **1982**, 60(3), 279-284.

- Jones, M.N., Surfactants in membrane solubilisation. *Int. J. Pharm.* **1999**, 177(2), 137-159.

- Juang, R.-S., Xu, Y.-Y. and Chen, C.-L., Separation and removal of metal ions from dilute solutions using micellar-enhanced ultrafiltration. *J. Membr. Sci.* **2003**, 218(1-2), 257-267.

- Kaczor, A., Szczepanski, J., Vala, M. and Proniewicz, L.M., Matrix-isolation and computational study of salicylhydroxamic acid and its photochemical degradation. *Phys. Chem. Chem. Phys.* **2005**, 7(9), 1960-1965.

- Kehl, H., Chemistry and biology of hydroxamic acids, Karger, **1982**.

- Kim, C.K., Kim, S.S., Kim, D.W., Lim, J.C. and Kim, J.J., Removal of aromatic compounds in the aqueous solution via micellar enhanced ultrafiltration: Part 1. Behavior of nonionic surfactants. *J. Membr. Sci.* **1998**, 147(1), 13-22.

- Klepac, J., Simmons, D.L., Taylor, R.W., Scamehorn, J.F. and Christian, S.D., Use of ligand-modified micellar-enhanced ultrafiltration in the selective removal of metal ions from water. *Sep. Sci. Technol.* **1991**, 26(2), 165-173.

- Kroczewska, D., Kurzak, B., Jezierska, J., The role of the carboxylic group in the copper(II) mixed-ligand complexes of DL-aspartic acid- β-hydroxamic acid and polyamines. *Polyhedron* **2006**, 25, 678-686.

- Kurzak, B., Farkas, E., Glowiak, T. and Kozlowski, H., X-ray and potentiometric studies on a pentanuclear copper(II) complex with α-alaninehydroxamic acid. *J. Chem. Soc., Dalton Trans.* **1991**, 163-167.

- Kurzak, B., Kozlowski, H. and Farkas, E., Hydroxamic and aminohydroxamic acids and their complexes with metal ions. *Coord. Chem. Rev.* **1992**, 114, 169–200.

- Lah, M.S., Kirk, M.L., Hatfield, W. and Pecoraro, V.L., The tetranuclear cluster Fe(III)[Fe(III)(salicylhydroximato)(MeOH)(OAc)]$_3$ is an analog of M^{3+}(9-crown-3). *J. Chem. Soc., Chem. Commun.* **1989**, 1606-1608.

- Lah, M.S. and Pecoraro, V.L., Isolation and characterization of {Mn(II)[Mn(III)(salicylhydroximate)]$_4$(acetate)$_2$(DMF)$_6$}2DMF: An inorganic analog of M^{2+}(12-crown-4). *J. Am. Chem. Soc.* **1989**, 111, 7258-7259.

- Lang, J., Tondre, C., Zana, R., Bauer, R., Hoffmann, H. and Ulbricht, W., Chemical relaxation studies of micellar equilibriums. *J. Phys. Chem.* **1975**, 79(3), 276-283.

- Lente, G. and Fabian, I., Ligand substitution kinetics of the Iron(III) hydroxo dimer with simple inorganic ligands. *Inorg. Chem.* **2002**, 41(5), 1306-1314.

- Li, C.-W., Liu, C.-K. and Yen, W.-S., Micellar-enhanced ultrafiltration (MEUF) with mixed surfactants for removing Cu(II) ions. *Chemosphere* **2006**, 63(2), 353-358.

- Lim, C.-S., Cutland, V.N.A., Kampf, J.W. and Pecoraro, V.L., Assessing guest selectivity within metallacrown host compartments. *Eur. J. Inorg. Chem.* **2007**, 1347-1350.

- Marmion, C.J., Griffith, D. and Nolan, K.B., Hydroxamic acids - an intriguing family of enzyme inhibitors and biomedical ligands. *Eur. J. Inorg. Chem.* **2004**, 3003-3016.

- Martinek, K., Yatsimirski, A.K., Levashov, A.V. and Berezin, I.V., In micellization, solubilization and microemulsions, Plenum Press, New York, **1977**.

- Menger, F.M. and Portnoy, C.E., Chemistry of reactions proceeding inside molecular aggregates. *J. Am. Chem. Soc.* **1967**, 89(18), 4698-4703.

- Mentasti, E., Secco, F. and Venturini, M., Mechanism of complex formation equilibria and kinetics of Fe^{3+} and $FeOH^{2+}$ interactions with substituted salicylic acids. *Inorg. Chem.* **1982**, 21(2), 602-606.

- Mezei, G., Zaleski, C.M. and Pecoraro, V.L., Structural and functional evolution of metallacrowns. *Chem. Rev.* **2007**, 107, 4933-5003.

- Monteleone, G., Morroni, L., Robinson, B., Tiné, M.R., Venturini, M., Secco, F., Metal ion extraction in surfactant solution: Ni2+(aq) and Cd2+(aq) with the ligands PADA and PAR in SDS micellar systems. *Colloid Surf. A* **2004**, 243(1-3), 23-31.

- Monzyk, B. and Crumbliss, A.L., Mechanism of ligand substitution on high-spin iron(III) by hydroxamic acid chelators. Thermodynamic and kinetic studies on the formation and dissociation of a series of monohydroxamatoiron(III) complexes. *J. Am. Chem. Soc.* **1979**, 101, 6203-6213.

- Mulligan, C.N., Yong, R.N. and Gibbs, B.F., Heavy metal removal from sediments by biosurfactants. *J. Hazard. Mater.* **2001**, 85, 111-125.

- Nakahara, Y., Kida, T., Nakatsuji, Y. and Akashi, M., New fluorescence method for the determination of the critical micelle concentration by photosensitive monoazacryptand derivatives. *Langmuir* **2005**, 21, 6688-6695.

- Neilands, J.B., Siderophores: Diverse roles in microbial and human physiology. *Ciba Found. Symp.* **1976**, 107-124.

- Okada, H., Yamamoto, K., Tsutano, S. and Nakamura, S., A new group of antibiotics, hydroxamic acid antimycotic antibiotics. I. Precursor-initiated changes in productivity and biosynthesis of neoenactins NL1 and NL2. *J. Antibiot.* **1988**, 41, 869-874.

- Paniago, E.B. and Carvalho, S., The formation constants and structures of copper(II)-glycinehydroxamic acid complexes. *Inorg. Chim. Acta* **1984**, 92(4), 253-257.

- Parac-Vogt, T.N., Pacco, A., Nockemann, P., Yuan, Y.-F., Gorller-Walrand, C. and Binnemans, K., Mandelohydroxamic acid as ligand for copper(II) 15-metallacrown-5 lanthanide(III) and copper(II) 15-metallacrown-5 uranyl complexes. *Eur. J. Inorg. Chem.* **2006**, 1466-1474.

- Patist, A., Oh, S.G., Leung, R. and Shah, D.O., Kinetics of micellization: Its significance to technological processes. *Colloid Surf. A* **2001**, 176(1), 3-16.

- Pecoraro, V.L., Stemmler, A.J., Gibney, B.R., Bodwin, J.J., Wang, H., Kampf, J.W. and Barwinski, A., Metallacrowns: A new class of molecular recognition agents. *Prog. Inorg. Chem.* **1997**, 45, 83-177.

- Po, H.N. and Sutin, N., Kinetics and mechanism of dissociation of di-mu-hydroxo-octaaquodiiron(III). *Inorg. Chem.* **1971**, 10(2), 428-&.

- Porter, M.R., Handbook of surfactants, Springer, Berlin, **1994**.

- Prue, J.E., Ionic equilibria, Pergamon Press, Oxford, **1966**.

- Raymond, K.N., Biomimetic metal encapsulation. *Coord. Chem. Rev.* **1990**, 105, 135-153.

- Ricciu, A., Secco, F., Venturini, M., García, B. and Leal, J.M., Kinetics and equilibria of the interaction of indium(III) with pyrocathecol violet by relaxation spectrometry. *J. Phys. Chem. A* **2000**, 104, 7036-7043.

- Romsted, L.S., In Micellization, Solubilization and Microemulsions, Plenum Press, New York, **1976**.

- Rosen, M.J., Surfactants and interfacial phenomena, Wiley, New York, **1989**.

- Rossotti, F.J.C. and Rossotti, H., The determination of stability constants, Mc Graw-Hill Book Company Inc., New York, Toronto, London, **1961**.

- Santos, M.A., Gaspar, M., Simoes Gonçalves, M.L.S. and Amorim, M.T., Siderophores analogues. A new macrocyclic bis-(amine, amide, hydroximate) ligand. Synthesis, solution chemistry, electrochemistry and molecular mechanics calculations for the iron complex. *Inorg. Chim. Acta* **1998**, 278(1), 51-60.

- Scamehorn, J.F., Christian, S.D., El-Sayed, D.A., Uchiyama, H. and Younis, S.S., Removal of divalent metal cations and their mixtures from aqueous streams using micellar-enhanced ultrafiltration. *Separ. Sci. Technol.* **1994**, 29(7), 809-830.

- Scamehorn, J.F., Christian, S.D. and Ellington, R.T., Use of micellar-enhanced ultrafiltration to remove multivalent metal ions from aqueous streams. *Surfactant Sci. Ser.* **1989**, 33, 29-51.

- Secco, F. and Venturini, M., Complex formation between a dimer of iron(III) and 5-nitrotropolone. *Polyhedron* **1999**, 18(25), 3289-3293.

- Secco, F., Venturini, M. and Fanelli, N., Evidence for the reactivity of a metal dimer in the binding of iron(III) to tropolone. *Ann.Chim. (Rome)* **1999**, 89(1-2), 129-136.

- Seda, S.H., Janczak, J. and Lisowski, J., Synthesis and reactivity of copper(ii) metallacrowns with (S)-phenylalanine and 2-picolinehydroxamic acids. *Inorg. Chim. Acta* **2006**, 359(4), 1055-1063.

- Shinoda, K. and Hutchinson, E., Pseudo-phase separation model for thermodynamic calculations on micellar solutions. *J. Phys. Chem.* **1962**, 66(4), 577-582.

- Smissman, E.E. and Warner, V.D., Specificity in enzyme inhibition. 2. Aminohydroxamic acids as inhibitors of histidine decarboxylase and 3,4-dihydroxyphenylalanine decarboxylase. *J. Med. Chem.* **1972**, 15, 681-682.

- Sommer, B.A. and Margerum, D.W., Kinetic study of hydroxoiron(III) dimer. *Inorg. Chem.* **1970**, 9(11), 2517-&.

- Stalikas, C.D., Micelle-mediated extraction as a tool for separation and preconcentration in metal analysis. *Trends Anal. Chem.* **2002**, 21(5), 343-355.

- Stemmler, A.J., Kampf, J.W., Kirk, M.L., Atasi, B.H. and Pecoraro, V.L., The preparation, characterization, and magnetism of copper 15-metallacrown-5 lanthanide complexes. *Inorg. Chem.* **1999**, 38, 2807-2817.

- Stemmler, A.J., Kampf, J.W. and Pecoraro, V.L., A planar [15]metallacrown-5 that selectively binds the uranyl cation. *Angew. Chem., Int. Ed. Engl.* **1997**, 35, 2841-2843.

- Tegoni, M., Furlotti, M., Tropiano, M., Lim, C.S. and Pecoraro, V.L., Thermodynamics of core metal replacement and self-assembly of Ca^{2+} 15-metallacrown-5. *Inorg. Chem.* **2010**, 49, 5190-5201.

- Tegoni, M., Remelli, M., Bacco, D., Marchio, L. and Dallavalle, F., Copper(II) 12-metallacrown-4 complexes of α-, β- and γ-aminohydroxamic acids: A comparative thermodynamic study in aqueous solution. *J. Chem. Soc., Dalton Trans.* **2008**, (20), 2693-2701.

- Tegoni, M., Remelli, M., Metallacrowns of copper(II) and aminohydroxamates: Thermodynamics of self assembly and host–guest equilibria. *Coord. Chem. Rev.* **2012**, 256(1-2), 289-315.

- Tegoni, M., Tropiano, M. and Marchio, L., Thermodynamics of binding of carboxylates to amphiphilic Eu^{3+}/Cu^{2+} metallacrown. *J. Chem. Soc., Dalton Trans.* **2009**, 6705-6708.

- Tondre, C., Surfactant-based colloidal particles as the extracting phase for the removal of metal ions from aqueous environments: Kinetic and applied aspects. *ACS Symp. Ser.* **2000**, 740, 139-157.

- Tondre, C. and Zana, R., On the kinetics of the micelle dissolution-formation equilibrium in solutions of cationic detergents: A comparison between temperature-jump and stopped-flow data. *J. Colloid Interface Sci.* **1978**, 66(3), 544-558.

- Wilkins, R.G., Kinetics of formation of some bivalent transition metal-dye complexes, studied by the temperature-jump relaxation method. *Inorg. Chem.* **1964**, 3, 52O-52.

- Zamora, R., Grzesiok, A., Weber, H. and Feelisch, M., Oxidative release of nitric oxide accounts for guanylyl cyclase stimulating, vasodilator and anti-platelet activity of Piloty's acid: A comparison with Angeli's salt. *Biochem. J.* **1995**, 312 333-339.

- Zaghbani, N., Hafiane, A. and Dhahbi, M., Separation of methylene blue from aqueous solution by micellar enhanced ultrafiltration. *Sep. Purif. Technol.* **2007**, 55(1), 117-124.

- Wendt, H., *Inorg. Chem.* **1969**, 8, 1527-1528.